Masters                                                                 Science

2004-01-01

# Non Linear Electronic and Optical Processes in Fullerene Thin Films

Siobhan Phelan
*Technological University Dublin*

## Recommended Citation

# Non linear electronic and optical processes in Fullerene thin films

## By

## Siobhán Phelan

**A thesis submitted to the Dublin Institute of Technology, for the degree of Master of Philosophy (MPhil)**

**Focas/ School of Physics,
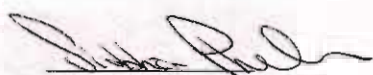Dublin Institute of Technology,
Kevin Street,
Dublin 8**

**2004**

**Declaration**

I certify that this thesis which I now submit for examination for the award of M.Phil. is entirely my own work and has not been taken from the work of others save and to the extent that such work has been cited and acknowledged within the text of my work.

This thesis was prepared according the regulations for postgraduate study by research of the Dublin Institute of Technology and has not been submitted in whole or in part for an award in any other Institute or University.

The institute has permission to keep, to lend or copy this thesis in whole or in part, on condition that any such use of the material of the thesis be duly acknowledged.

Siobhán Phelan

## Acknowledgements

Firstly I would like to thank my supervisors Dr. Hugh Byrne and Dr. Gordon Chambers for providing me with the opportunity to carry out this research, their advice and help throughout has been much appreciated.

I would also like to thank all the other students and members of staff, especially those involved in the Physics of Molecular Materials Group that have helped me and given me advice throughout the project.

Finally I would like to thank my family and friends, especially Peter for your support and my Parents for your patience and guidance.

## Abstract

In this study the current voltage characteristics of $C_{60}$ thin film sandwich structures fabricated by vacuum deposition on indium tin oxide (ITO) with an aluminium top electrode are presented and discussed. A strongly non-linear behavior and a sharp increase in the device conductivity was observed at relatively low voltages, at both room and low temperatures (30K). At room temperature the system is seen to collapse. In situ Raman measurements indicate that the collapse is the result of a solid state reduction of the fullerene thin film to a polymeric state. The high conductivity state was seen to be stable at elevated voltages and low temperatures. This state is seen to be reversible with the application of high voltages. At these high voltages the $C_{60}$ film was seen to sporadically emit white light at randomly localized points analogous to the much-documented electroluminescence in single crystals. Moreover the evidence suggests that this highly conducting species maybe similar in nature to a high intensity optically excited species.

# Table of Contents

# Chapter 4: Spectroscopy

# Chapter 5: Optically Excited States and Their Spectroscopy

## Chapter 6: Transport Processes in Molecular Solids

# Chapter 7: Insulator to Metal Transitions

# Chapter 8: Conclusions

# Appendix 1: Presentations and Journals

**Chapter 1**

**Introduction**

**1.1.    General Background**

Buckminsterfullerene or $C_{60}$ was discovered in 1985 by a group of British and American scientists [1]. In an attempt to simulate the chemistry of a carbon star, Harry Kroto, Bob Curl and Richard Smalley set up a mass spectrometer experiment to study the plasma produced by focusing a pulsed laser on solid graphite. During these experiments they stumbled across a reproducible unanticipated 720 amu peak. They proposed that this peak maybe the result of a cluster of 60 carbon atoms, which was later christened Buckminsterfullerene or $C_{60}$. The serendipitous discovery of this unique and curious molecule ranks as one of the most important moments in material science and illustrates the importance of interdisciplinary research.

It was proposed that this carbon cluster has a closed caged carbon structure of a truncated icosahedron (a football). It was named Buckminsterfullerene because of the resemblance to geodesic dome concepts, pioneered by the architect Buckminster Fuller, which played an important part in arriving at the solution for its structure. Kroto et al [1], suggested that when a carbon atom is placed at each vertex of this football type structure, as shown in figure 1.1, its valences can be satisfied by two single bonds and one double bond. Each carbon has a $sp^2$ type hybridised bonding arrangement, which gives rise to 60 delocalised $\pi$-electrons around the carbon cage.
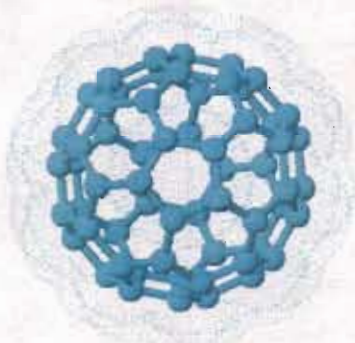


**Figure 1.1.** The proposed truncated icosahedral structure of the Buckminsterfullerene ($C_{60}$). Note a popular representation of this structure is a football.

Buckminsterfullerene generated huge interest but due to the unavailability of the material in large quantities, research was restricted to just theoretical models predicting properties. In 1990, five years after the initial discovery of the Buckminsterfullerene, IR and NMR [3,4] spectroscopy confirmed the structure originally proposed by Kroto and Smalley, which was of a perfectly symmetrical molecule, consisting of 60 carbon atoms arranged in hexagons and pentagons. The material had become more widely available in 1990 when Wolfgang Krätschmer and Donald Huffman succeeded in producing, and separating bulk samples of fullerene material [2] from arc- processed (in an inert gas atmosphere) carbon deposits. From then onwards, fullerene research continued and still proceeds at an exhilarating pace. This research has given rise to the realisation that $C_{60}$ was merely one molecule of a family of molecules known collectively as the fullerenes [1]. Examples of other types of these carbon clusters include $C_{70}$, carbon nanotubes and carbon onions. Figure 1.2 shows examples of these fullerenes where $C_{60}$ is the archetype.



| (a) | (b) |
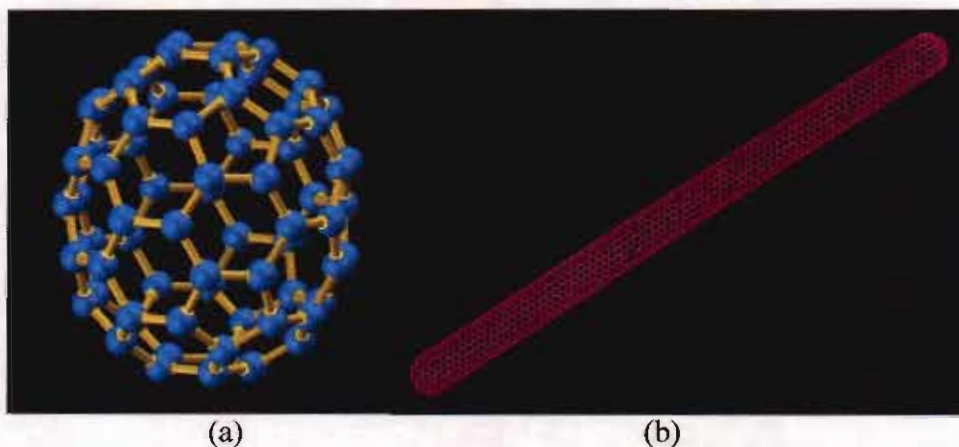
**Figure 1.2.** Examples of carbon clusters in the Fullerene family (a) $C_{70}$ (b) a single walled nanotube.

## 1.2. Defining a fullerene

In general a fullerene can be defined as a closed caged carbon molecule in which the atoms are arranged at the vertices of hexagonal and pentagonal rings. For such a structure to exist there must be at least 12 pentagonal faces and an arbitrary number of hexagonal faces [5]. In conjunction with the pentagon isolation rule one can arrive at this conclusion from Euler's theorem [6], describing the relationship between the number of edges, faces, and vertices in a closed polyhedron.

$C_{60}$ consists of 20 hexagons and 12 pentagons, $C_{70}$ consists of 25 hexagons and 12 pentagons and $C_{84}$ consists of 32 hexagons and 12 pentagons. The relative location of the pentagons in these structures creates different shapes, and consequently there can be a wide range of structures for each of these clusters, each with its unique properties. The range of structures extends beyond that of the single-shell fullerene structures and encompasses large multishelled structures, such as Multi Wall nanotubes and carbon onions [7,8]. The common structural element in all the fullerenes is a pentagon which is surrounded by hexagons. Mathematically, using Euler's Law, for closed shell polyhedra:

$$v + f = e + 2 \qquad\qquad\qquad Eq.1.2.1.$$

where v is the number of vertices, f is the number of faces, and e is the number of edges in the polyhedron. In fullerenes only pentagons (p) and hexagons (h) are considered, so therefore the number of faces should equal:

$$f = p + h \qquad\qquad\qquad Eq.1.2.2.$$

The number of bonds in this molecule will be equal to the number of edges (e) and since each edge joins two faces:

$$2e = 5p + 6h \qquad\qquad\qquad Eq.1.2.3.$$

The number of edges is equal to $3v/2$, so therefore:

$$3v = 5p + 6h \qquad\qquad\qquad Eq.1.2.4.$$

$$e = \frac{(5p+6h)}{2} = \frac{3v}{2} \qquad\qquad\qquad Eq.1.2.5.$$

These equations lead to:

$$6(f + v - e) = p = 12 \qquad\qquad\qquad Eq.1.2.6.$$

So it can be said that for each fullerene with only pentagonal and hexagonal faces there must be 12 pentagons and an arbitrary number of hexagons. Thus the smallest fullerene is $C_{20}$, built up of 12 pentagons and no hexagons. However, when two pentagons are adjacent to each other, there is a high local curvature and so a high strain [5] in these carbon structures. Such a situation is not energetically favourable.

There is an "isolated pentagon rule" which says that all the pentagons must be separated from each other. $C_{60}$ is the smallest fullerene obeying the isolated pentagon rule (i.e. no two adjacent pentagons) [9]; the next one is $C_{70}$. This fact has prompted some to suggest that $C_{60}$ is the smallest possible stable fullerene. Smaller pure carbon cage molecules formed from hexagons and pentagons must, due to geometric constraints, contain adjacent pentagons which gives rise to large strain energies and hence instabilities. While the exceptional stability of $C_{60}$ is undisputed, the impossibility of stable lower order fullerene like molecules is by no means a foregone conclusion. Recent theoretical and experimental work [10,11,12] has shown that $C_{36}$ is a stable carbon cage molecule When you add one hexagon to a fullerene you increase the number of carbons by 2, so all fullerenes have an even number of carbon atoms, based on the archetype of $C_{60}$.

## 1.3. Uses and Applications of $C_{60}$

Presently the research of fullerenes and their possible uses and applications is still ongoing. So far they have not been put to use on a commercial scale. However many possible uses for them have been suggested, and these applications cover many fields. As a flavour, in this section some novel applications which have been proposed are introduced. Much of the physics underlying the applications potential will be outlined in subsequent chapters.

### 1.3.1. HIV Protease Inhibitor

$C_{60}$ and its derivatives, because of their large size, stability, and hydrophobic character, may prove to have value as diagnostic or therapeutic agents in medicine. For example, derivatives of $C_{60}$ have been investigated as potential inhibitors of the protease enzyme specific to the human immunodeficiency virus protease (HIVP) [13,14]. The active site of this enzyme can be roughly described as an open-ended cylinder, which is lined almost exclusively by hydrophobic amino acids. Notable exceptions to this hydrophobic trend are two catalytic aspartic acids, which catalyse the attack of water on a peptide bond of the substrate. Because a $C_{60}$ molecule has approximately the same radius as the cylinder that describes the active site of HIVP and since $C_{60}$ and its derivatives are primarily hydrophobic, an opportunity exists for a strong hydrophobic van der Waals interaction between the nonpolar active-site surface and the $C_{60}$ surface. In addition, however, there is an opportunity for

4

increasing binding energy by the introduction of specific electrostatic interactions. One obvious possibility involves salt bridges between the catalytic aspartic acids on the floor of the HIVP active site and basic groups such as amines introduced on the $C_{60}$ surface. The key to exploiting this promising system will be the development of organic synthetic methodology to derivatise the $C_{60}$ surface in highly selective ways.

### 1.3.2 Optical Limiting.

The unique structure and properties of $C_{60}$ suggests that it has large and fast non-linear optical responses, which may have numerous applications in optical data processing, optical communications and for the protection of the human eye and optical sensors for high intense laser fields [15]. The development of these devices is based on various mechanisms such as non-linear absorption and refraction in semiconductors, optical breakdown induced scattering in carbon particle suspensions, thermal refractive beam spreading and excited state absorption.

Optical limiters are devices that strongly attenuate optical beams at high intensities. Optical limiting is accomplished through a saturation of the transmitted light intensity with increasing incident intensity. Transient excited state measurements [16] provide supporting evidence that reverse saturable absorption is the main mechanism for optical limiting properties of $C_{60}$. Inverse saturable absorption derives from the presence of an excited state absorption, which is larger than ground state. This commonly occurs in materials with (quasi) forbidden ground state absorption and large excited state absorption [17]. In fullerenes optical limiting has been shown to derive from ~100% population of the triplet state via the forbidden singlet ground state absorption [16,18]. This result implies that $C_{60}$ could be used as an optical limiter, to protect delicate or sensitive equipment from intense flashes of light, like that produced by a laser, by limiting the intensity of transmitted light to a maximum value, where the excess light is converted to heat.

### 1.3.3. Fullerene-Based Sensors

Fullerene-based inter-digitated capacitors have been developed to explore sensor applications [16]. The reasons why fullerenes and their films are attractive for the creation of sensor devices can be formulated as follows; the spherical shape and large size of fullerene molecule provide a substantial volume of empty intermolecular space

in a face-centred cubic lattice of solid fullerite (solid state of $C_{60}$). As a consequence, this material is easily intercalated by different impurities, changing its properties. Novel solid state design is based on the electron accepting properties of fullerene films and the changes that occur when planar molecules react with the film surface. Fullerene chemistry provides a high degree of selectivity and sensitivity, which can be increased by modifying the fullerene chemically or physically. Fullerenes in solid fullerite form can under go definite action, for example with intercalating substances, with high pressure, temperature or UV irradiation. Further research for new sensor materials based on the films of fullerene compounds is necessary but it undoubtedly holds great potential in sensor technology.

### 1.3.4. Conductivity and Superconductivity

Pure $C_{60}$ is a molecular insulator but it can change its properties in the solid state, from insulating to conducting or even superconducting as a result of a number of factors. Exposure to oxygen has been shown to have a detrimental effect on both the dark and photo-conductive behaviour [19]. Thermal annealing has been shown to induce a transition from a thermally activated transport mechanism to a more "metallic-like" temperature independent behaviour [20]. It is clear that the electronic properties of solid state fullerenes are critically dependent on local environment and crystal packing.

When solid state $C_{60}$ is doped with alkali metals, such as Potassium, Rubidium and/or Caesium the dopants find the voids between the large $C_{60}$ molecules and form a very stable structure. With a stoichiometry of 1:1, a metallic-like conducting salt can be achieved i.e. $A_1C_{60}$ [21]. Similarly if the stoichiometry is changed to 3:1 i.e. $A_3C_{60}$, then a superconducting state is obtainable. For example using Potassium as the dopant i.e. $K_3C_{60}$, the $C_{60}$ complex is shown to be superconducting below a transition temperature ($T_c$) of 18K [22]. The record high transition temperatures for these superconducting $C_{60}$ complexes doped with alkali metals is 33 K for $RbCs_2C_{60}$ [23] and 43K for $Rb_3C_{60}$ [24]. Metal alkali fullerenes show all the characteristic signs of a superconductor such as exhibiting diamagnetic properties to the total exclusion of all magnetic fields and zero resistance to electrical current. However the current densities are much lower than in other superconductors.

Much of the interesting physics of the superconducting molecules arises from the population of the lowest unoccupied molecular orbital (LUMO), by electron transfer from the dopant metal [25]. Although the detailed mechanism of superconductivity in alkali metal fullerides remains to be established, the simplicity of the materials and the progress already made suggest a definitive resolution of this question may be achieved. Such a population of the LUMO state is also obtainable without doping via optical excitation or by electron injection [26]. In the solid state, a stoichiometric 100% optical excitation of this upper state results in the formation of a metallic state [21]. When the population of this state is obtainable by optical excitation from the ground state, the metastable metallic state is highly luminescent and evolves non-linearly [27]. Similarly when produced by electron injection a broad band intense luminescence is produced with the additional interest that the current characteristics of the material become highly non-linear [28].

There is much potential for $C_{60}$ due to its ability to readily accept electrons via electron injection. In more recent work, high densities of electrons and holes where induced by gate doping in a field effect transistor geometry. $C_{60}$ crystal devices were prepared by vacuum deposition of gold source and drain electrodes on the crystal surface. An aluminium oxide dielectric layer and a gate electrode complete the FET structure. Using the field effect doping technique [29,30,31], superconductivity was demonstrated by injecting a high concentration of charge carriers, where $T_c$ changes systematically with carrier concentration. A complete switching between an insulating and superconducting state was achieved. When intercalated with $CHCl_3$ and $CHBr_3$ in order to expand the lattice, the dependence of $T_c$ on the lattice parameter follows the general trend of alkali metal doped $C_{60}$. Since the publication of the work by Schön et al [29,30,31], the scientific community has had difficulty in reproducing the results. Within the context of a broader body of work, the authenticity of the work presented has been brought into question. While allegations of scientific misconduct were upheld in many instances, the authenticity of the original observation of reversible superconducting transitions in $C_{60}$ crystals could not be disproved [32], and any judgement on the existence or not of fluctuations in any superconducting transition in $C_{60}$ was deferred to the appropriate scientific community. The inability to reproduce the effect is most likely down to the complex issues relating to growth of $C_{60}$ single crystals and the crystallinity of thin films.

In this work the main objective is to explore electron injection in thin films of $C_{60}$ and to try and elucidate the true nature of any conducting species produced by characterising them spectroscopically, comparing these electronically excited states in thin films to already well characterised optically excited states in thin films. A lot of previous studies were conducted in single crystals, however fabrication of single crystal devices is difficult and ultimately thin film technology is desirable. For this purpose, electronic processes of $C_{60}$ thin film sandwich structures fabricated by vacuum deposition on indium tin oxide (ITO) with an aluminium top electrode are presented and discussed. It will be shown that $C_{60}$ films undergo a reversible and cycleable transition from an insulating to a highly conducting state, and that in- situ spectroscopy will prove a valuable probe in identifying these electronic states.

## 1.4.    Thesis Outline

Initially in chapter 2 the structure of $C_{60}$ will be discussed and comparisons between the properties of the isolated molecule and the solid state will be drawn. This chapter also introduces the molecular symmetry and its significance to $C_{60}$. Similarly the electronic structure is examined through the use of the Hückel molecular orbital theory. Chapter 3 explains the methodology used throughout the study. It explains how $C_{60}$ was originally produced and fabricated into film form. The techniques and instruments used in this study are also discussed, in particular the electronic injection technique. Chapter 4 discusses the various spectroscopic techniques used in the examination of the vibrational and electronic spectra of $C_{60}$. Chapter 5 discusses the optically excited states and their spectroscopy, including a brief introduction to the excited triplet state, photochemical processes in $C_{60}$, and the large body of work previously done on the optically generated species in $C_{60}$ thin films. Chapter 6 discusses the transport mechanisms of organic semiconductors, with particular emphasis on the transport processes in solid $C_{60}$. Chapter 7 shifts away from the optical generation of transient species, and turns to the electrical generation of these species. This involves the use of electronic injection techniques to generate the species of interest, and in-situ spectroscopic analysis of such species. Chapter 8 discusses some conclusions of results obtained and suggests ideas for further investigation into these conducting species.

## 1.5. References

1    H.W. Kroto, J.R. Heath, S.C. O'Brien, R.F. Curl, and R.E. Smalley, *Nature* **318,** 162-163 (1985).

2    W. Krätschmer, L.D. Lamb, K. Fostiropoulos and D.R. Huffman, *Nature*, **347,** 354-358 (1990).

3    W. Krätschmer., K. Fostiropoulos and D.R. Huffman, *Chem. Phys. Lett.*, **170,** 167-170 (1990)

4    H. Ajie, M.A. Marcos, J.A. Samir, B.D. Rainer, and W. Krätschmer, *J .Phys. Chem.*, **94**, 8630-8633 (1990).

5    M.S. Dresselhaus, G. Dresselhaus, P.C. Eklund, '*Science of fullerenes and carbon nanotubes' Academic Press Inc. london* (1995).

6    K.L. Akers, Ph.D dissertation, University of Toronto (1994)

7    S. Iijima, *Nature*, **354**, 56-58 (1991)

8    D. Ugarte, *Nature*, **359**, 707 (1992)

9    H.W. Kroto, *Nature*, **329**, 529 (1987)

10    J.C. Grossman, M. Côté, S.G. Louie, M.L. Cohen, *Chem. Phys. Lett.*,**284**,344 (1998)

11    C. Piskoti, J. Yarger, A. Zettl, *Nature*, **393**, 771, (1998)

12    J.C. Grossman, S.G. Louie, M.J. Cohen, *Phys. Rev. B,* **60**, 10, R6941 (1999)

13    T. Pradeep, *Current Science*, **72**, 124-137 (1997).

14    S.H. Freidman, D.L. DeCamp, R.P. Sijbesma, G. Srdanov, F. Wudl, and G.L. Kenyon, *J.Am.Chem.Soc.*, **115**, 6506-6509 (1993).

15    L.W. Tutt and A. Kost, *Nature*, **356**, 225-226 (1992).

16    J.C. Withers, R.O. Loufty, T.P.Lowe, *Fullerene Science and Technology*, **5**(1), 1-31 (1997).

17    W. Blau, H. Byrne, W.M. Dennis and J.M. Kelly, *Opt. Commun.*, **56**, 25 (1985)

18    L.W. Tutt and A. Kost, *Nature*, **356**, 225-226 (1992).

19    M. Kaiser, W.K. Maser, H.J. Byrne, A. Mittelbach and S. Roth, *Solid State Commun.*, **87**, 281, (1993)

20    M.Kaiser, Dr. der Natur. Thesis, Univ. Karlsruhe (1993)

21    R.C. Haddon, A.F. Hebard, M.J.Rosseinsky, D.W. Murphy and S.J. Duclos, *Nature*, **350**, 320-322 (1991)

22    A.F. Hebard, M.J. Rosseinsky, R,C. Haddon, D.W. Murphy, S.H. Glarum, T.T.M. Palstra, A.P. Ramirez and A.R. Kortan, *Nature*, **350**, 600-601 (1991).

23    R. Komori, T. Naguosa, T.Hatae and Y. Miyamoto, *Jpn. J. Appl. Phys.,* **36,** 5600-5604 (1997)

24    M.J. Rosseinsky, A.P. Ramirez, S.H. Glarum, D.W. Murphy, R.C. Haddon, A.F. Hebard, T.T.M. Palstra, A.R. Korton, *Am. Phys, Soc.*, **60**, 2830-2832 (1991)

25    R.M. Fleming, A.P. Ramirez, M.J. Rossrinsky, D.W. Murphy and R.C. Haddon, *Nature*, **352**, 787-788 (1991).

26    R.C. Haddon, L.E. Brus and K. Raghavachari, *Chem. Phys. Lett.*, **125**, 459-464 (1986).

27    H.J. Byrne, W.K. Maser, M. Kaiser, W.W.Rühle, L. Akselrod, A.T. Werner, J. Anders, X.Q. Zhou, G. Mahler, T. Kuhn, A. Mittelbach and S. Roth, *Appl. Phys. A,* **57**, 303 (1993)

28    A.T. Werner, H.J. Byrne, D. O'Brien and S. Roth, *J. Mol. Crys.*, **256,** 795 (1994)

29    J.H. Schön, Ch. Kloc and B. Batlogg, *Science*, **293**, 2432-2434 (2001)

30    J.H. Schön, Ch. Kloc and B. Batlogg, *Nature*, **408**, 549-552 (2000)

31    J.H. Schön, Ch. Kloc, R.C. Haddon and B. Batlogg, *Science*, **288**, 656-658 (2000)

32    http://www.lucent.com/news_events/researchreview.html,    page    E-65    (Date Feb,2003)

**Chapter 2**

**Structure and Symmetry**

## 2.1.    Structure of $C_{60}$

Prior to the discovery of fullerenes [1], the most common forms of pure carbon were graphite and diamond, both of which are crystalline materials. By contrast the materials formed from fullerenes are molecular solids [2], and their structure and properties are of considerable interest both in the solid form (fullerite) and isolated molecular form. Considerable advances in research into their structural properties have been made over the past decade [2,3,4], and in this chapter both the internal structure of the molecule as well as the intermolecular structure of the solid are discussed.

The sixty carbon atoms in the $C_{60}$ molecule are arranged at the vertices of twenty hexagonal and twelve pentagonal rings. Each carbon molecule is in an $sp^2$ hybridised bonding arrangement which gives rise to sixty delocalised $\pi$- electrons around the closed carbon cage. These electrons are of particular interest when considering the electronic and optical properties of $C_{60}$.

### 2.1.2.    The Isolated Molecule

The structure of $C_{60}$ was determined theoretically and experimentally as an icosahedral structure. Since a carbon atom occupies each vertex of the truncated icosahedral, and each carbon atom has its valence requirements fully satisfied, all the carbon atoms are said to be chemically equivalent. This is consistent with the single peak in the NMR spectrum of $C_{60}$ [5]. Each carbon atom is connected to three other carbon atoms in a $sp^2$ hybridised bonding arrangement. Although each carbon atom is equivalent, the three bonds emanating from each atom are not equivalent, two being electron deficient single bonds, and one being an electron rich double bond. This effects the length of the bonds, making single bonds around each pentagon longer than the double bonds at the edge of each pair of adjacent hexagons. Every pentagon is surrounded by five hexagons (isolated pentagon rule). The double bonds are located at the junctions of the hexagons, there are no double bonds in the pentagons. The bond lengths are 1.40 Å for a hexagon edge and 1.46 Å for a pentagon edge [6]. The

bond angles on the hexagonal and pentagonal faces are $120.0^0$ and $108.0^0$ respectively. Table 2.1 shows a list of important physical constants for $C_{60}$ molecule. The sp$^2$ bonding arrangement gives rise to 60 delocalised electrons located around the fullerene sphere. Figure 2.1. shows a cross section of their distribution. As previously mentioned these electrons are of particular interest when considering the electronic and optical properties of $C_{60}$. These properties have been the subject of much research over the past decade [7,4].

| Quantity | Reference Value [8] |
|---|---|
| Average C-C distance | 1.44Å |
| C-C bond length on a pentagon | 1.46Å |
| C-C bond length between adjacent hexagon | 1.40Å |
| $C_{60}$ mean ball diameter | 7.10Å |
| $C_{60}$ diameter including electron cloud | 10.34Å |
| fcc Lattice constant | 14.17Å |
| $C_{60} - C_{60}$ centre to centre distance | 10.02Å |
| $C_{60} - C_{60}$ cohesive energy | 1.6eV |

**Table 2.1.** Physical Constants for $C_{60}$ molecules and crystalline $C_{60}$ in solid state
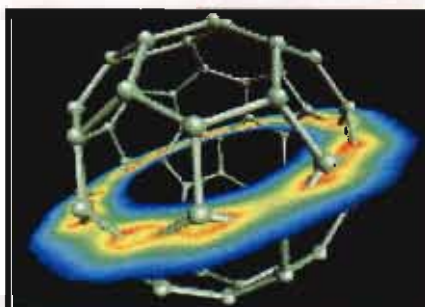


**Figure 2.1.** A 2-D slice through the electronic distribution of $C_{60}$

## 2.2.  Symmetry

### 2.2.1.  Introduction

The high symmetry of the Buckminsterfullerene has a strong influence on the numerous unique properties of this molecule, and hence must be considered when discussing and elucidating the structural aspects of $C_{60}$. Molecular symmetry makes it possible to classify molecules according to their geometrical shape (point group). Through the use of group theory the significance of molecular symmetry becomes much more evident, as it can influence the number of energetically distinguishable phonon modes and on the selection rules in spectroscopic experiments.

### 2.2.2.  $C_{60}$ Symmetry and point group

The $C_{60}$ molecule is highly symmetric, that means one can find many transformations that map the molecule onto itself. All such symmetry operations for a molecule are rotations around an axis, reflections in a plane, and sometimes inversions. All symmetry operations must leave the centre of mass of the molecule in place, so all rotation axes and mirror planes must go through that point. For the $C_{60}$ molecule there are three kinds of rotation axes. The most obvious ones are the 5-fold axes through the centres of two facing pentagons. Look down on one of the pentagons and you see that the molecule is symmetric under rotations of $360/5 = 72$ degrees. Next there are rotation axes through the centre of two facing hexagons. Observe that these axes are only 3-fold, i.e. it takes a rotation of 120 degrees to map the molecule onto itself. Finally there are 2-fold axis through the centres of the edges between two hexagons. Since there are 12 pentagons, there are 6 different 5-fold axes, each axis passes through two pentagons. Likewise, since there are 20 hexagons, there are 10 different threefold axes. To find the number of different two-fold axes, each hexagon is neighboured by three other hexagons. Hence there are 30 edges between two hexagons, i.e. 15 different 2-fold axes. The reflections symmetries are also related to the edges between adjacent hexagons: The mirror planes contain two such edges, hence there are also 15 different mirror planes. Finally, the $C_{60}$ molecule is invariant under the inversion with respect to the centre of mass. This means that if you replace each point with co-ordinates (x,y,z) by (-x,-y,-z), the molecule is mapped onto itself. Combining all those transformations, one finds 120 different symmetry operations. They form the icosahedral group, which is the point group with the largest number of

elements. Hence $C_{60}$ can be called the most symmetric molecule. The $C_{60}$ molecule is a regular truncated icosahedron, with a point group $I_h$. The symmetry operations of which consists of the identity operation, 12 five-fold axes through the centre of the pentagonal faces, 20 three-fold axes through the centres of the hexagonal faces, 15 two-fold axes through centres of the edges joining two hexagons. Each of the 60 rotational symmetry operations can be compounded with the inversion operation, resulting in 120 symmetry operations in the icosahedral point group $I_h$. Figure 2.2, shows the rotational symmetries of the $C_{60}$ molecule.



2-fold          3-fold          5-fold
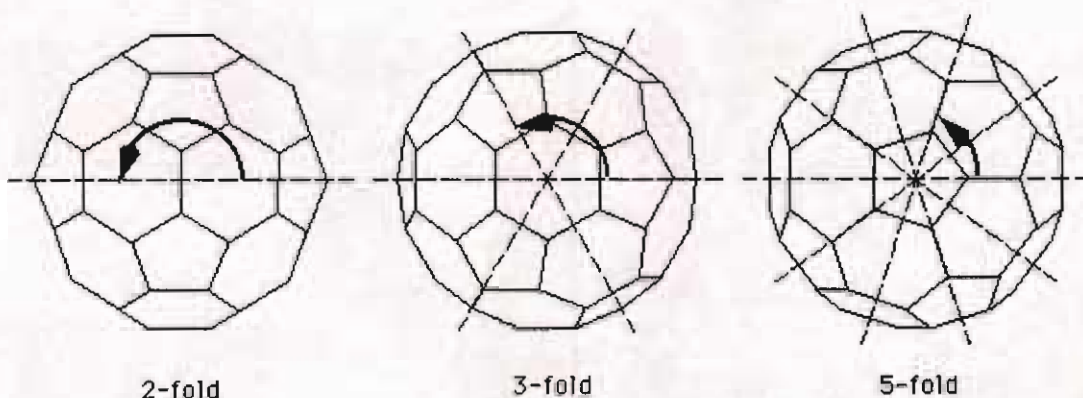
**Figure 2.2.** Rotational symmetries of the $C_{60}$ molecule. (a) Twofold axes pass through opposing pairs of hexagon-hexagon edges, (b) threefold axes connect midpoints of hexagonal faces related by inversion, (c) fivefold axes connect midpoints of the pentagonal faces related by inversion [9].

Molecules with $I_h$ symmetry, of which $C_{60}$ is the most prominent member, have the highest degree of symmetry of any known molecule. The character table of the $I_h$ is shown in table 2.2. and displays the 120 symmetry elements for molecular $C_{60}$. Using the table and group theory it is possible to obtain an expression for molecular $C_{60}$ known as irreducible representation,

$$\Gamma = 2A_g + 3F_{1g} + 4F_{2g} + 6G_g + 8H_g + 1A_u + 4F_{1u} + 6G_u + 7H_u \qquad \text{Eq.2.2.1}$$

# THE MULTIPLICATION TABLE OF THE GROUPS I AND I_h

| $I/I_h$ | E | $12C_5$ | $12C_5^2$ | $20C_3$ | $15C_2$ | $i$ | $12S_{10}$ | $12S_{10}^3$ | $20S_6$ | $15\sigma$ | III | IV |
|---|---|---|---|---|---|---|---|---|---|---|---|---|
| $A_g$ | 1 | 1 | 1 | 1 | 1 | 1 | 1 | 1 | 1 | 1 | | |
| $T_{1g}$ | 3 | $\frac{1}{2}(1+\sqrt5)$ | $\frac{1}{2}(1-\sqrt5)$ | 0 | -1 | 3 | $\frac{1}{2}(1-\sqrt5)$ | $\frac{1}{2}(1+\sqrt5)$ | 0 | -1 | $(R_x, R_y, R_z)$ | |
| $T_{2g}$ | 3 | $\frac{1}{2}(1-\sqrt5)$ | $\frac{1}{2}(1+\sqrt5)$ | 0 | -1 | 3 | $\frac{1}{2}(1+\sqrt5)$ | $\frac{1}{2}(1-\sqrt5)$ | 1 | -1 | | |
| $G_g$ | 4 | -1 | -1 | 1 | 0 | 4 | -1 | -1 | 1 | 0 | | |
| $H_g$ | 5 | 0 | 0 | -1 | 1 | 5 | 0 | 0 | -1 | 1 | | $(2z^2-x^2-y^2)$, $x^2-y^2$, $xy,yz,zx$ |
| $A_u$ | 1 | 1 | 1 | 1 | 1 | -1 | -1 | -1 | -1 | -1 | | |
| $T_{1u}$ | 3 | $\frac{1}{2}(1+\sqrt5)$ | $\frac{1}{2}(1-\sqrt5)$ | 0 | -1 | -3 | $-\frac{1}{2}(1-\sqrt5)$ | $-\frac{1}{2}(1+\sqrt5)$ | 0 | 1 | $(x,y,z)$ | |
| $T_{2u}$ | 3 | $\frac{1}{2}(1-\sqrt5)$ | $\frac{1}{2}(1+\sqrt5)$ | 0 | -1 | -3 | $-\frac{1}{2}(1+\sqrt5)$ | $-\frac{1}{2}(1-\sqrt5)$ | 0 | 1 | | |
| $G_u$ | 4 | -1 | -1 | 1 | 0 | -4 | 1 | 1 | -1 | 0 | | $(x^3,y^3,z^3)$ |
| $H_u$ | 5 | 0 | 0 | -1 | 1 | -5 | 0 | 0 | 1 | -1 | | $[x(z^2-y^2),y(z^2-x^2),$ $z(x^2-y^2),xyz]$ |

Table 2.2: The $I_h$ character table for $C_{60}$

There are 3N –6 vibrational modes for molecules with N atoms. Due to the high icosaheral symmetry ($I_h$), the 174 [=(60x3)-6] normal modes are reduced to 46 fundamental vibrational modes [10]. Each normal mode of vibration forms a basis for an irreducible representation of the point group of the molecule. A vibration will be spectroscopically active if its normal mode is contained within the irreducible representation. Due to selection rules only the modes of $A_g$ and $H_g$ symmetry are Raman-active, while only the $F_{1u}$ modes are IR-active [4]. The remaining 32 modes are silent in the isolated $C_{60}$ molecule. The Raman spectrum of the isolated molecule should therefore consist of ten lines while the Infrared spectrum should consist of four lines. Vibrational measurements of fullerenes have shown this to be the case [11].

## 2.3.    Electronic Structure of $C_{60}$

The structural and symmetrical properties of $C_{60}$ can be attributed to the arrangement of the σ electrons of the single bonds, which form the icosahedral cage. However it is the π electrons which dictate the electronic and optical properties of $C_{60}$. The σ and π orbitals of the fullerene are not pure, but may be treated as approximately so. The σ-π interaction which exists is relatively weak, they are not completely decoupled because of the curved molecular surfaces, but it is still a good approximation to consider only the 60 delocalised π electrons when considering the electronic structure.

The simplest model is the atomic orbital model, where the π electrons orbit around the carbon cage in Bohr like orbitals, with corresponding discrete orbital levels. The orbital levels of a spherical shell, whose energies are proportional to the product $\lambda(\lambda+1)$, where $\lambda$ is an orbital angular momentum quantum number. The corresponding atomic orbitals s,p,d,f,g,h,i… are $2\lambda+1$ fold degenerate. A schematic of this energy level system is shown in Figure 2.3, which also shows the correlation between the molecular orbitals of $I_h$ and the atomic orbitals which belong to the full rotational group $R_3$, in accordance with the description of Braga et al [12]. As stated before, although the σ and π orbitals of the fullerene are not pure, they may be treated as approximately so because the σ - π interaction which exists in this nonplanar system is relatively weak. The $R_3$-$I_h$ orbital correlations in Figure 2.3 are to the π orbitals of the latter. $I_h$ orbitals such as $3h_u$ and $6h_g$ in Figure 2.5 are σ molecular orbitals. The degeneracies of the atomic orbitals are conserved in the correlation e.g.

$$\lambda=3, \Rightarrow 4g_u 4t_{2u}$$
$$\lambda=5, \Rightarrow 5t_{2u}+5t_{1u}+4h_u$$
$$\lambda=6, \Rightarrow 2t_{1g}+5t_{2u}+2t_{2g}$$

The symmetric ground state $1^1A_g$ of $C_{60}$ [13] due to the closed $\pi$ electron configuration is

$$\ldots 3a_g^{(2)}4t_{1u}^{(6)}4h_g^{(10)}4t_{2u}^{(6)}4g_u^{(8)}4g_g^{(8)}7h_g^{(10)}4h_u^{(10)}\ldots\ldots 1^1A_g.$$

For this non-alternate species, the first three excited configurations, and corresponding state symmetries are

$$\ldots 7h_g^{(10)}4h_u^{(9)}5t_{1u}^{(1)} \quad \ldots\ldots {}^{1,3}T_{1g}, {}^{1,3}T_{2g}, {}^{1,3}G_g, {}^{1,3}H_g$$
$$\ldots 7h_g^{(9)}4h_u^{(10)}5t_{1u}^{(1)} \quad \ldots\ldots {}^{1,3}T_{1u}, {}^{1,3}T_{2u}, {}^{1,3}G_u, {}^{1,3}H_u$$
$$\ldots 7h_g^{(10)}4h_u^{(9)}2t_{1u}^{(1)} \quad \ldots\ldots {}^{1,3}T_{1u}, {}^{1,3}T_{2u}, {}^{1,3}G_u, {}^{1,3}H_u$$

Transitions from the ground state configuration to these excited configurations correspond to HOMO to LUMO, HOMO-1 to LUMO and HOMO to LUMO+1 respectively. The lowest excitation from the Highest Occupied Molecular Orbital (HOMO) to the Lowest Unoccupied Molecular Orbital (LUMO) i.e. $H_u$ to $t_{1u}$ gives a value of 1.897eV as the energy gap ($E_g$) of $C_{60}$ in solution. In $C_{60}$ the closed shell icosahedral symmetry renders the HOMO – LUMO transition dipole forbidden [12]. Transitions can occur weakly via Hertzberg-Teller vibrational coupling or Jahn-Teller distortions [14]. It is the occupation of the LUMO, which is of interest for chemical doping, optical processes and electronic processes. Singlet –triplet transitions, which are spin forbidden, can similarly appear, although extremely weak, due to spin orbit coupling effects.

# Electronic Structure of C₆₀
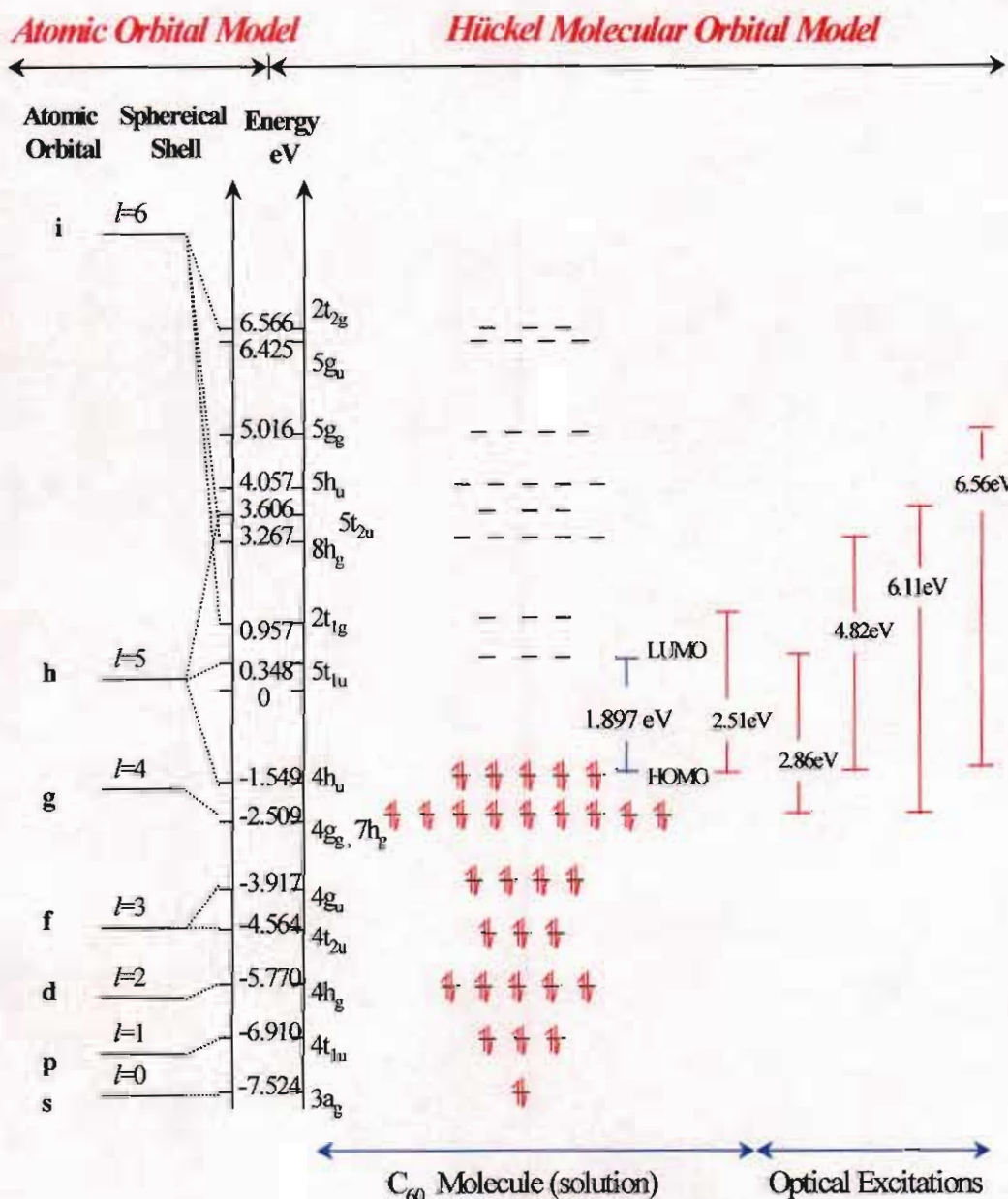


**Figure 2.3.** Electronic structure of $C_{60}$. On the left of the diagram is the Atomic Orbital model with the energy levels of a spherical shell. The black dotted lines connect these orbitals to the pi type molecular orbitals of the Huckel molecular orbital (HMO) model on the right. The HMO model also displays the energy of some optical transitions associated with the molecule.

## 2.4.    The Solid State Structure of $C_{60}$

So far the molecular structure of $C_{60}$ has been considered, i.e., the atomic connectivity and molecular shape. However, it is also important to consider the solid-state structure, i.e., the way in which $C_{60}$ molecules pack together in the bulk solid state. Bulk solid $C_{60}$ is sometimes referred to as "fullerite" in analogy to graphite. At room temperature X-ray powder diffraction has shown that fullerite adopts the face-centred cubic (fcc) close-packed structure with lattice constant a = 14.17 Å, a centre to centre $C_{60}$-$C_{60}$ distance of 10.02Å and a density of 1.72g/cm$^3$ (corresponding to 1.44 x 10$^{21}$ $C_{60}$ molecules/cm$^3$). As shown in figure 2.4, a fcc close-packed structure can be constructed by placing close- packed layers on top of one another. Spheres sit at the eight corners and at the centres of the six sides of the cubic unit cell, which has an edge length ("lattice constant") of a. The distance between nearest neighbours is 3.5Å.
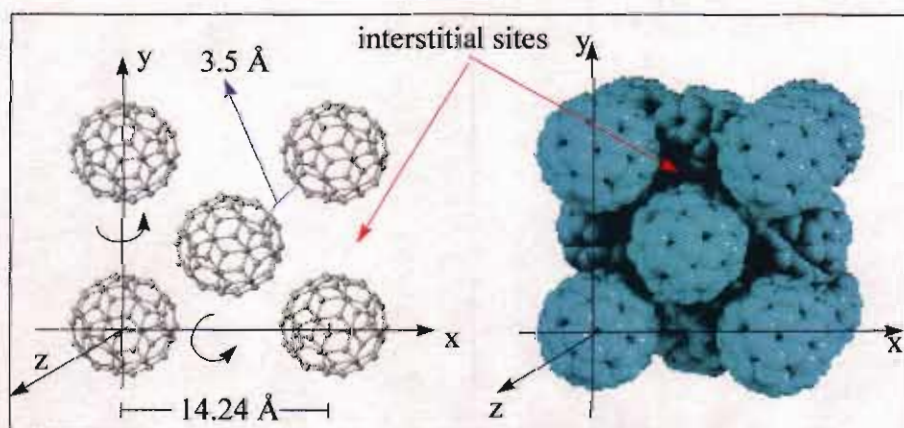


**Figure 2.4.** Solid State Structure of $C_{60}$

The molecules spin freely around the lattice positions at room temperature, and the fcc phase is referred to as the rotary phase due to the rotation of the molecules. This rotation decreases or 'freezes out' at temperatures below 249K and the molecules which had been in the fcc arrangement change to that of a simple cubic (sc) arrangement [15]. Above 249K the molecules can rotate freely around their lattice positions, and hence the 60 delocalised electrons would seem to be uniform around the molecule. However below this temperature of 249K the 'freezing out' of the molecular rotation is driven by the electron deficient pentagonal face aligning opposite to the reactive (electron rich) hexagonal double bond. As a result the

alignment of the $C_{60}$ molecules at the lattice positions are no longer equivalent, the x-ray diffraction pattern becomes that of a simple cubic lattice, and the lattice constant decreases. Figure 2.5 demonstrates this phase change in two dimensions.
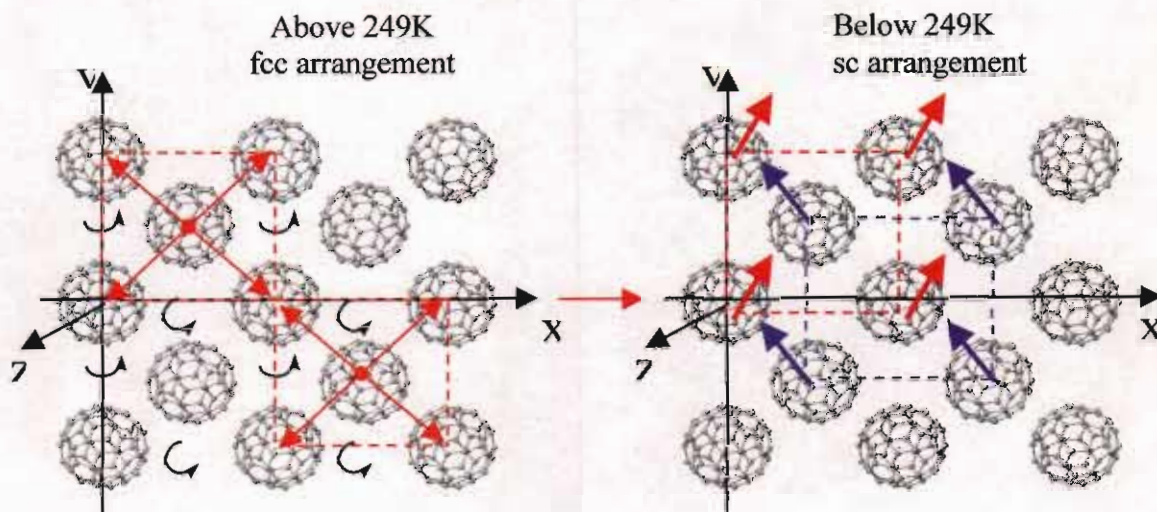


**Figure 2.5.** Above 249K, the molecules are rapidly spinning, giving rise to a fcc type lattice arrangement. However below 249K the spinning motion is frozen out and a simple cubic type lattice results.

Vibrational measurements are predominantly performed in the solid state at room temperature. The vibrational spectrum mostly retains its molecular character. The symmetry of the molecule is however effected by its interaction within the fcc lattice [16]. The symmetry is reduced to point group symmetry of $T_h$. Below the phase rotation of 249K [17] where the rotation of the balls is hindered and finally frozen out below 90K, significant symmetry reduction due to crystal field effects are predicted [18,11]. In fact crystal field effects are evident only very weakly in experimental measurements [15] (e.g. Raman spectroscopy) suggesting that the molecule largely retains its $I_h$ character in the solid confirming the importance of the icosahedral symmetry and structure to the $C_{60}$ molecule and its derivatives. The vibrational spectroscopy of $C_{60}$ will be discussed in chapter 4 and 5, as it was seen to be a useful probe of the electronic properties of $C_{60}$.

Of particular interest for this study is the degree of intermolecular interaction in the solid state, which might contribute to conductivity. $C_{60}$ forms a molecular solid but although molecules weakly interact, there is not a huge change to the electronic structure of the molecule. However, as outlined in chapter 4, an additional excited state specific to the solid is identified. This state is proposed to be characteristic of intermolecular electronic interactions in the crystal lattice.

Although fullerenes in themselves are highly stable, the solid fullerite is weakly bound and any perturbation causes increased interaction and collapse of the system. chapter 5 will show that the $C_{60}$ lattice is unstable to the addition of electrons and is prone to polymerisation above ~249K [19].

It has been shown that solvent inclusion and thermal annealing can be used to control lattice structure. Effects on the enhancement of the stability of the $C_{60}$ lattice, in order to reduce the chance of polymerisation, at ambient temperatures has been reported. The first is the formation of clathrate compounds of $C_{60}$, that is the inclusion of solvent molecules into the fcc lattice [19]. The electronic properties of solid state fullerenes can be modified by the control of the relative contributions of intra- and inter- molecular interactions via the incorporation of solvent molecules into the lattice [8]. When thin films are exposed to solvent vapour, the solvent molecules can be included into the lattice and providing the molecules are neutral i.e. no electronic interaction, they should inhibit any lattice collapse, by behaving like 'molecular spacers'. The second method is thermal annealing, which involves the structural reordering of the lattice [20,21]. Thermal annealing is essentially where thin films are heated at a temperature sufficiently below the sublimation temperature of the vacuum deposited sample. A number of studies on annealed films have been reported [20,21] where it was seen that UV/Vis and IR spectra show no indication of any chemical alteration of the sample but rather an apparent structural change is observed [20].

## 2.5. Summary

The structural and symmetrical properties of $C_{60}$ can be attributed to the arrangement of the $\sigma$ electrons of the single bonds, which form the icosahedral cage. The $C_{60}$ molecule is highly symmetric, with an icosahedral point group $I_h$. There are also sixty delocalised $\pi$- electrons around the closed carbon cage and it is the $\pi$- electrons which

dictate the electronic and optical properties of $C_{60}$. Of particular interest is the degree of intermolecular interaction in the solid state. The molecules are held together by weak Van der Waals interactions, where the molecules are free to rotate around their lattice positions at room temperature in a face centred cubic (fcc) arrangement. This rotary phase is frozen out below 249K and the fcc arrangement changes to that of a simple cubic (sc). As a result the $C_{60}$ molecules in the lattice are no longer equivalent, hence it might be expected this to influence how these molecules interact electronically. Spectroscopy will be used to probe and elucidate the changes that occur due to changes in temperature, changes due to polymerisation and changes due to annealing in solid state $C_{60}$.

## 2.6. References

1    H.W. Kroto, J.R. Heath, S.C. O'Brien, R.F. Curl, and R.E. Smalley, *Nature* **318,** 162-163 (1985).

2    W. Krätschmer, L.D. Lamb, K.Fostiropoulos and D.R. Huffman, *Nature*, **347**, 354-35 ,(1990)

3    K. Kuzmany, M.Matus, T.Picher and J. Winter. *Physics and Chemistry of Fullerenes*, K. Prassides ed., Klewer Academic, Dordrecht (1994).

4    G. Dresselhaus, M.S. Dresselhaus and P.C. Eklund, *Phys. Rev. B.*, **45**,6923 (1992)

5    H. Ajie, M.A. Marcos, J.A. Samir, B.D. Rainer and W. Krätschmer etal., *J. Phys. Chem.*, **94**, 8630-8633 (1990)

6    W. Krätschmer, K. Fostiropoulos and D.R.Huffman, *Chem. Phys. Lett.*, **170**,167-170 (1990)

7    H. Kuzmany, M. Matus, T. Pichler and J. Winter, *Physics and Chemistry of the Fullerenes*, K.Prassides ed., **443,** 287-309, Kluwer Academic, Dordrecht (1994)

8    **M.S. Dressel**haus, P.C Eklund, *Science of Fullerenes and Carbon Nanotubes*, Academic Press Inc. London (1995)

9    A.T. Werner, J. Anders, H.J. Byrne, W.K. Maser, M. Kaiser, A. Mittelbach and S. Roth, *Appl. Phys. A,* **57**, 157. **(1993)**

10    H.J. Byrne, in *Physics and Chemistry of Fullerenes and Derivatives*, H.Kuzmany, J.Fink, M. Mehring and S. Roth eds., World Scientific Sinapore, **183** (1995)

11    D. Betune, G. Meijer, W.C. Tang, H.J. Rosen, W.G. Golden, H. Seki, C.A. Brown and M.S. de Vries, *Chem. Phys. Lett..,* **179**, 181. (1991)

12    M. Braga, S. Larsson, A. Rosén, and A. Volosov. *Atron. Astrophys.* **245,** 232-238 (1991)

13    S. Leach, M. Vervloet, A. Després, E. Bréheret, J.P. Hare, T.J. Dennis, H.W. Kroto, R. Taylor, and D.R.M. Walton, *Chem. Phys.,* **160**, 451 (1992)

14    S.Leach, M.Vervloet, A. Després, E. Bréheret, J.P. Hare, T.J. Dennis, H.W. Kroto, R.Taylor and D.R.M Walton, *Chem. Phys.,* **160**, 451-466 (1992).

15    H.Kuzmany, M.Matus, B. Burger, J. Winter, *Adv. Mater.* **10**, 731-745. (1994)

16    P.H.M. van Loosdrecht, P.J.M. van Bentum, M. Verheijen and G. Meijer, *Chem. Phys. Lett.,* **198**,587 (1992)

17    J.E. Fisher, P.A. Heiney, D.E. Luzzi and D.E. Cox, *Fullerenes: Synthesis, Properties and Chemistry of Large Carbon Clusters,* from the American Chemical Society Symposium Series, **481**,55 (1992)

18    Y.P Sun, P. Wang and N.B. Hamilton, *J. Am. Chem. Soc.,* **115**, 6378 (1993)

19    A.M. Rao, P. Zhou, K.A. Wang and P.C. Eklund. *Science,* **259**, 955. (1993)

20    L. Akselrod, H.J. Byrne, T.E. Sutto, S. Roth, *Chem. Phys. Lett.,* **233**, 436 (1995)

21    M. Kaiser, W.K. Maser, H.J. Byrne, A. Mittelbach and S. Roth, *Solid State Commun.,* **87**, 281. (1993)

# Chapter 3

## Experimental

### 1.1.    Fullerene Synthesis and Purification

The first method of production of fullerenes by Kroto and Smalley used laser vaporisation of carbon in an inert atmosphere, but this produced microscopic amounts of fullerenes [1]. In 1990, apparatus using an arc to vaporise graphite was adapted in Germany by Krätschmer and Huffmann, to produce fullerenes [2]. This process gave 10% yields of $C_{60}$ but in larger quantities, it was now possible to produce in the order of 100mg of the purified material per day, making it a more likely and cost efficient production method for fullerenes.
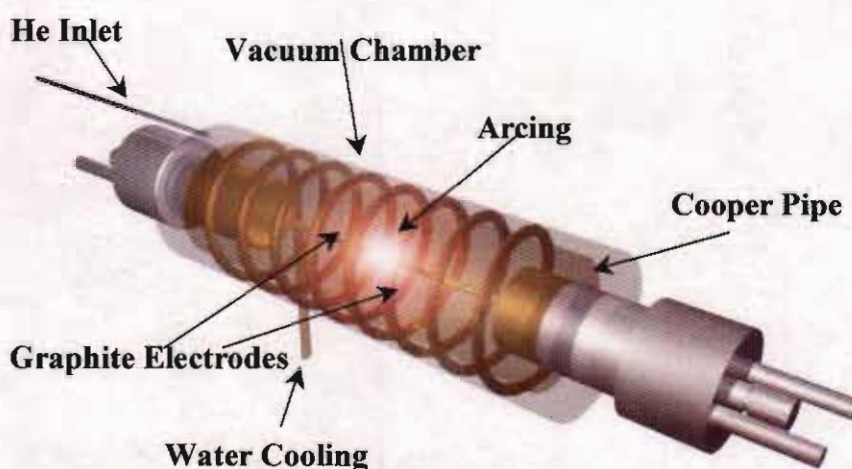


**Figure 3.1.** Schematic of a Krätschmer and Huffmann Fullerene Generator for the production of large quantities of fullerenes

In the Krätschmer-Huffman (KH) generator experiment, carbon radicals are produced simply by the slow evaporation of the surface of resistively heated graphite rods. A graphite rod is heated to vaporisation in an inert atmosphere (Helium) and the process yields visible fullerene soot on the inner casing. This high temperature process revolves around the ability to produce gaseous carbon atoms, and provide annealing

for clustering of the carbon atoms into linear carbon chains and monocyclic rings of $C_2$ to $C_{18}$ which assemble into fullerene molecules $C_n$ where n=60, 70, 84 etc.[3].

To date, most commercially available mechanisms to synthesise fullerenes are by this Arc vaporisation of graphite, shown schematically in figure 3.1. In the Krätschmer and Huffmann method graphite electrodes are brought into close contact. The system is pumped down to about 100 Torr of helium gas is introduced into the chamber. An Arc discharge is struck in this environment, sustained by a voltage of ~20V [4]. After several minutes there is a resulting black soot like material produced inside the bell jar. After a 5-10 min cool down period the bell jar is filled to atmospheric pressure, and the material collected, on average under certain conditions 10 % of the soot is $C_{60}$. The fullerenes in the soot are extracted by solvation in a small amount of organic solvent such as benzene, toluene or other benzene derivatives [5].

After extraction, the organic solvent is removed using a rotary evaporator, leaving behind a solid mixture of mostly $C_{60}$ with small amounts of larger fullerenes. Pure $C_{60}$ is obtained by liquid chromatography. The mixture is dissolved in toluene and pumped through a column of activated charcoal mixed with silica gel. The magenta colour $C_{60}$ solution comes off first, followed by the red $C_{70}$. The different colour solutions are collected separately and the organic solvent removed using a rotary evaporator.

The $C_{60}$ sample used in this project was supplied by SES Research, Houston, Texas, USA, and was 99.5% pure. The sample had residues of, Toluene 0.0089%, Acetone 0.051%, and Diemethylether 0.46%.

## 3.2. Preparation of solutions of $C_{60}$ for Spectroscopy

A concentrated solution of $C_{60}$ (3g/l) was made up in 50ml volumetric flask with chlorobenzene. Subsequent dilutions of this concentrated solution where made up to the following concentrations 1.5g/l, 0.75g/l, 0.375g/l, and 0.1875g/l diluted with chlorobenzene. These solutions where placed in quartz cuvettes (1cm) for spectroscopic measurements. All solutions where stored in the dark and in the fridge at ~4$^0$C.

### 3.3.    $C_{60}$ Film Preparation

Films of $C_{60}$ were prepared by vacuum sublimation onto indium tin oxide (ITO) substrates ($12mm^2$), used as the bottom electrode of a sandwich type geometry with aluminium as the top electrode. Merck (Darmstadt, Germany) supplied 14" square sheets (100nm) of ITO and UQG (Cambridge, UK) cut them into 12mm square substrates (12mm x 12 mm = $144mm^2$).

### 3.3.1.    Experimental Set-up for Evaporated Films

The $C_{60}$ was vapour deposited, using an Edwards Auto-305 evaporator, by resistively heating a molybdenum boat containing $C_{60}$ powder (~5mg), with the evaporation chamber evacuated to$10^{-6}$ mbar.
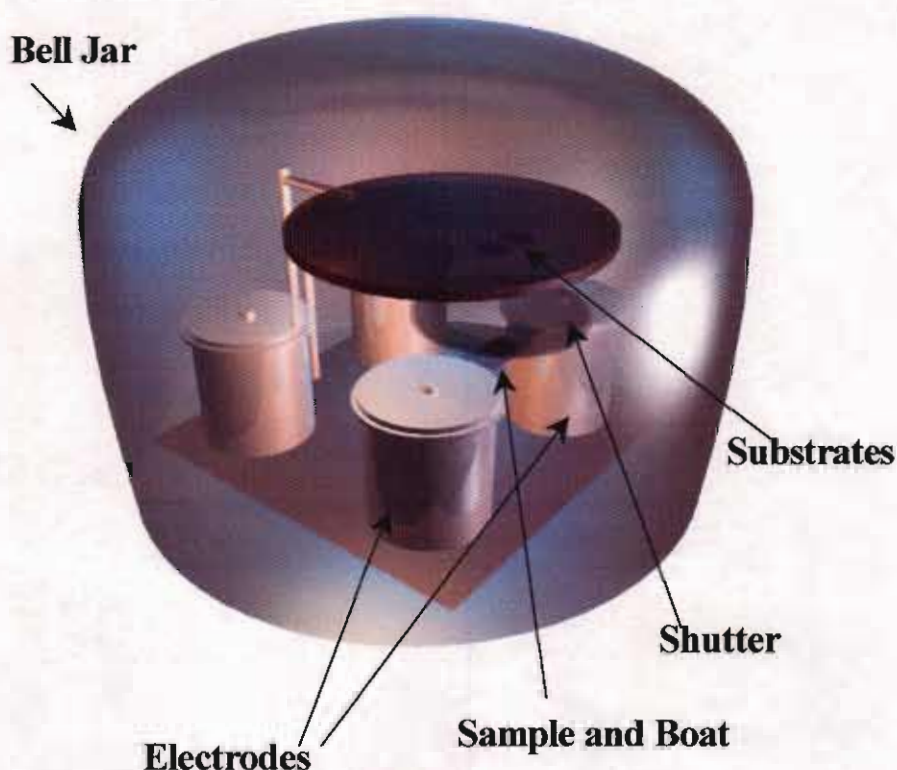


**Figure 3.2.** Experimental set-up for film preparation

The experimental set-up as shown in figure 3.2, consisted of two heating electrodes across which the molybdenum boat containing the $C_{60}$ is placed. The substrates are ITO on glass ($12mm^2$) (12mm x 12 mm = $144mm^2$) and are placed above the boat with a shutter in between, which can open and close to expose or protect the substrate

from evaporated material. The molybdenum boat is heated gently by passing a current through it, which is controlled by a built in power supply. The shutter is kept closed while the boat is heating and initially when $C_{60}$ starts to sublime, allowing impurities to evaporate off first. The shutter is then opened for approximately 10-30 minutes to give a film thickness ranging between 0.5-2.0 μm. The evaporation time and substrate height were varied in accordance with a set of calibration curves for the system, previously obtained [6] thereby allowing films of specific thickness to be obtained. Film thickness were subsequently verified as discussed in section 3.3.3. The system was allowed to cool under vacuum before the films where removed and stored in the dark and at room temperature. For evaporation of aluminium layers the molybdenum boat is replaced by tungsten wire and the process repeated.
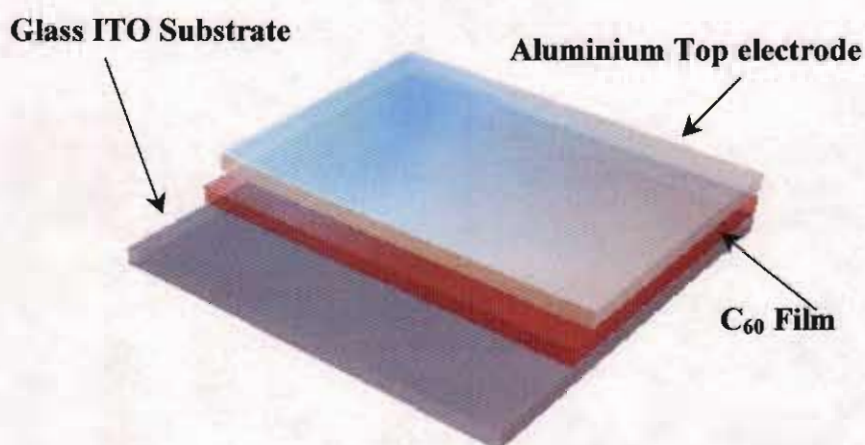


**Figure 3.3.** Sandwich structure device of $C_{60}$ thin film on Glass ITO substrate with Aluminium Top Electrode

The sandwich structures are chosen over in plane geometries as the films are polycrystalline with crystalline sizes of ~ 0.5μm. Planar geometry inter electrode spacings are typically of 1μm or more, and so transport is limited by crystallite domain boundaries. In the sandwich grain inter electrode spacings are governed by the film thickness which is ~0.1-0.5 μm.

27

### 3.3.2.   Thermal Annealing of $C_{60}$ Films

Chapter 4,6 and 7 will show evidence that the evaporated thin films can be annealed during deposition. Annealing can have an effect on film structure [7], so it is important that this effect can be controlled. By varying both the height of the substrate above the evaporation boat and the length of time of evaporation the effect of thermal annealing during film deposition can be reduced in order to achieve a true molecular insulator. Annealed films where deposited for an evaporation time of 30 minutes with the substrates as close to the shutter as possible (~4cm). Unannealed films where deposited for an evaporation time of 10 minutes with the substrates at the maximum distance from the shutter as the set-up would allow (~15cm). The absorption spectra of the films were recorded to monitor the changes caused by the annealing.

### 3.3.3. Determination of Film Thickness

The average thickness of the films used was 1μm, measured using the Veeco Dektak V350 Stylus Profiler System. This system can be used for measuring step-height repeatability, surface planarity and roughness. Alternatively film thickness can be determined from the absorption of the films and a set of published calibration curves of absorbance against film thickness at 610nm and 436nm [8,9]. Absorption spectra were recorded using a Perkin Elmer Lamda 900 UV/VIS/NIR Spectrometer.

According to the Beer-Lambert law [9], absorbance can be defined as,

$$A = \varepsilon.c.d \qquad \text{Eq.3.1.}$$

where A is the absorbance at a specific wavelength, $\varepsilon$ is the corresponding extinction co-efficient for that wavelength, c is the concentration, or density and d is the path length. For two absorbances, $A_1$ and $A_2$, of a solid material at the same wavelength then it can be said that

$$\frac{A_1}{d_1} = \varepsilon.c \qquad\qquad \frac{A_{12}}{d_2} = \varepsilon.c$$

and hence
$$\frac{A_1}{d_1} = \frac{A_2}{d_2} = \varepsilon.c$$

Therefore if $d_1$, $A_1$ and $A_2$ are known than $d_2$ can be easily found from equation 3.2, and known calibration curves.

$$d_2 = \frac{A_2}{A_1} d_1 \quad \text{Eq. 3.2}$$

### 3.4. Spectroscopic Methods

Spectroscopic methods used during this study are as follows

### 3.4.1. Raman Spectroscopy

Raman measurements were taken using an Instruments S.A. Labram 1B spectroscopic microscope (10 x objective, spot radius ~10μm) with a spectral resolution of $1cm^{-1}$ per pixel, using an internal Helium-Neon laser (632.8nm).

The Labram system is a confocal Raman imaging microscope system. Both Helium-Neon (632.8nm,11mW) and Argon ion (514.5nm, 50mW) are available as sources. Both are polarised, enabling measurement of depolarisation ratios and studies of orientation in materials. The light is imaged to a diffraction limited spot (typically 1-10 microns) via the objective of an Olympus BX40 microscope. The scattered light is collected by the objective in a confocal geometry, and is dispersed onto a electrically cooled CCD array by one of two interchangeable gratings, 1800 lines/mm or 600lines/nm, allowing the range from $150cm^{-1}$ to $4000cm^{-1}$ to be covered in a single image, or with greater resolution in a combination of images. With the former, a spectral resolution of $1cm^{-1}$ per pixel is achievable. The confocal, microscopic system allows measurement of powdered samples with no further sample preparation, direct measurement of liquids and solutions, as well as thin films. Spectral X-Y mapping may be performed with a precision of 0.1 μm. The system is furthermore equipped with a remote head, which is fibre coupled to the spectrometer.

### 3.4.2. IR Spectroscopy

All IR measurements were taken using a Perkin Elmer Spectrum GX FT-IR and AutoIMAGE Microscope. The spectrometer is a single-beam, Michelson interferometer based, Fourier transform infra-red spectrometer. It has a dual level optical module that is sealed and desiccated. The system is configured with a mid-

infra-red single source. MIR and FIR beamsplitters and DTGS detector kits allow the range 7000 to 50cm$^{-1}$ to be covered with a maximum resolution of 0.3cm$^{-1}$. The Spectrum GX is a modular system and can accommodate up to four equivalent output beams. The spectrometer is configured with the AutoIMAGE microscope system, which can operate in transmission or reflectance modes. All manual microscope operations including adjustments to aperture, focus and illumination are fully automated and controlled from the PC. It includes built-in 35W tungsten halogen illuminator, a motorised stage and a CCD video camera. The medium MCT detector covers the range from 5500 to 550 cm-1. An ATR attachment with a micro germanium crystal with a range from 5500 to 600 cm-1 can be used for micro samples and ATR mapping for surface studies.

### 3.4.3. UV / Vis / NIR

All UV / Vis measurements were taken using a Perkin Elmer Lamda 900 UV/VIS/NIR Spectrometer. Solution spectra were taken in a 1cm quartz cell with the solvent system as reference whereas solid samples were mounted in the cell compartment and run against a blank substrate as reference.

The Perkin Elmer Lamda 900 UV/VIS/NIR spectrometer is a double-beam, double monochromator ratio recording system with pre-aligned tungsten-halogen and deuterium lamps as sources. The wavelength range is from 175 to 3300nm with an accuracy of 0.08 nm in the UV-Visible region and 0.3nm in the NIR region guaranteed. It has a photometric range of +/-6 in absorbance. Accessories available include a 60mm Spectralon coated integrating sphere with a range from 200 to 2500 nm for measurement of samples of high optical density. A Common-beam depolariser for measurements with depolarised light in the 190 to 2600 nm range is also available.

### 3.5.   Solid State Electronic Measurements

The electrical properties of device structures, figure 3.3, were monitored at both room and low temperatures using a Keithley 237 programmable electrometer and current/voltage power source. Initially an Oxford CCC1204 Cryostat, Figure 3.4 was used for the low temperature measurements to reach 22K and also to provide shielding for the IV measurements at room temperature.

For low temperature in-situ Raman measurements, a Linkam microscope cooling stage with a liquid nitrogen purge was used to reach 77K (Figure 3.5). The film was contacted inside the cooling stage and allowed to equilibrate at 77K for 15 min before IV measurements and in situ Raman measurements were taken.



**Electrical Contacts**

**Sample Holder**

**Cold Finger**
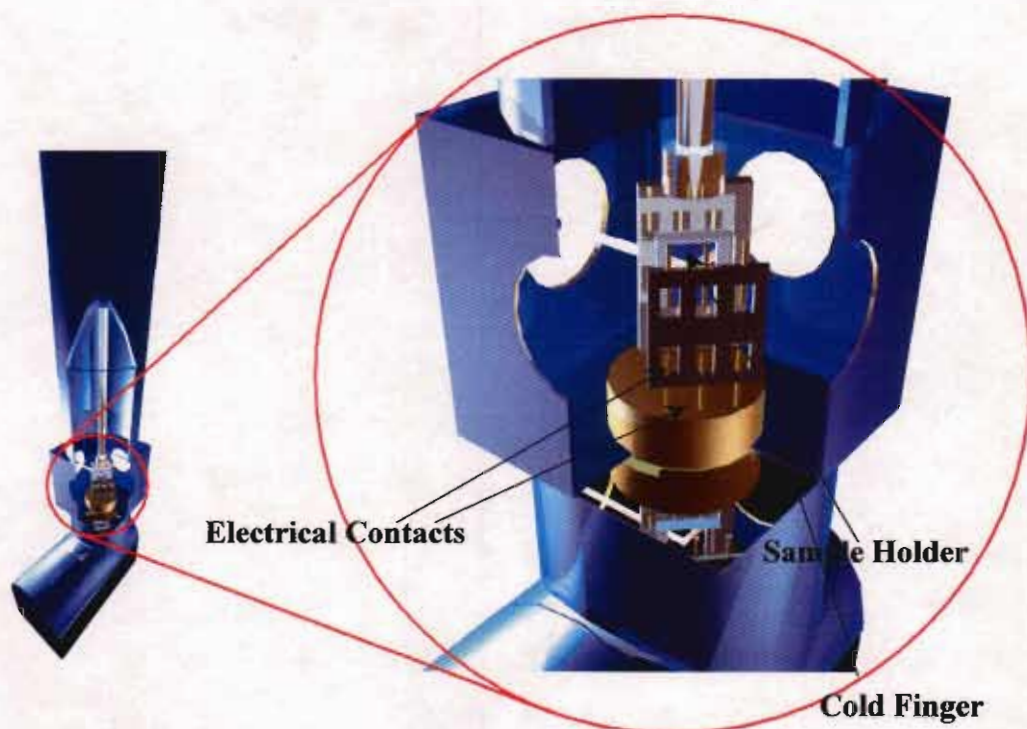
**Figure 3.4.** Experimental set-up showing Oxford CCC1204 Cryostat and sample holder for films.
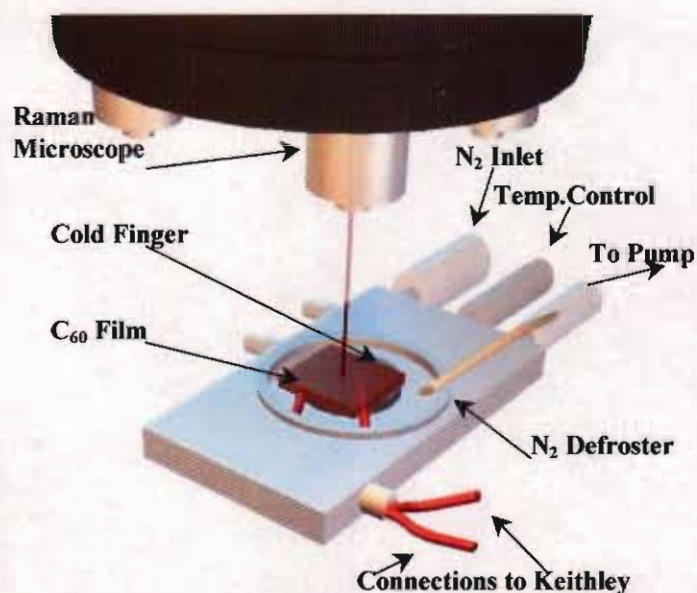
**Figure 3.5.** Experimental set-up showing in-situ Raman Spectroscopy on fullerene thin films at low temperatures using Linkam Cooling Stage.

### 3.6. Summary

This chapter dealt with the broad range of experimental techniques utilised throughout this project. Fullerene synthesis and purification where described, and also preparation of solutions of $C_{60}$ for spectroscopy and $C_{60}$ thin films for electrical and spectroscopic measurements.

The various spectroscopic methods described will be used to characterise both the isolated $C_{60}$ molecule and solid state $C_{60}$. Vibrational spectroscopy (IR and Raman) will give information on the structural and symmetrical properties of the molecule. Electronic spectroscopy (UV/Vis) will give information on the electronic configuration and reveal features specific to the solid. Further information will be derived from these spectroscopic techniques by varying the intensity of the light used or wavelength, to yield information on excited state species formed.

Solid state measurements are also described, in which electronically produced excited states are formed through electron injection. Raman spectroscopy will again be utilised to identify these excited species, through in situ measurements.

## 3.7. References

1    H.W. Kroto, J.R. Heath, S.C. O'Brien, R.F. Curl, and R.E Smalley, *Nature*, **318**, 162-163 (1985).

2    W. Krätschmer, L.D. Lamb, K. Fostiropoulos and D.R. Huffman, *Nature*, **347**, 354-358 (1990).

3    J.R. Heath, *Am. Chem. Soc. Symposium Series*, **481**, 1 (1992).

4    J.C Withers, R.O. Loufty, T.P. Lowe, *Fullerene Science and Technology*, **5**(1), 1-31 (1997).

5    R.Taylor, J.P. Hare, A.K. Abdul-Sada and H. Kroto, *Chem. Soc. Chem. Commun.*, **201**, 1423-1425 (1990).

6    A. Casey, Final Year BSc project (FT225) Dublin Institute of Technology, Kevin St. 2003.

7    L. Akselrod, H.J. Byrne, T.E. Sutto, S. Roth, *Chem. Phys. Lett.*, **233**, 436 (1995)

8    L. Akselrod, MSc disesertation, University of Dublin, Trinity College. (1993)

9    L. Akselrod, H.J. Byrne, J. Callaghan, A. Mittelbach and S. Roth, *Electronic Properties of Fullerenes,* H. Kuzmany, J. Fink, M. Mehring and S. Roth eds., Springer Series in Solid State Sciences, Springer Verlag Heidelberg, **117,** 219. (1993).

10   P.W. Atkins, *Physical Chemistry,* Oxford University Press, 426-531 (1990).

**Chapter 4**

**Spectroscopy**

## 4.1. Introduction

Spectroscopy is the theory of the interaction of electromagnetic radiation and matter and its practical interpretation in order to deduce the nature of the matter. To analyse the optical and electronic properties of fullerenes an array of spectroscopic techniques were used. Matter and radiation interact in three basic ways. Matter absorbs, transmits or scatters energy. It does these in precise measures determined by the laws of quantum mechanics, and it is this precision that makes interaction at particular energies characteristic of particular substances. Hence spectroscopy is useful as an analytical technique, as it is a powerful tool which can provide incontrovertible evidence for the charaterisation of the Buckminsterfullerene, as in initially proving $C_{60}$ had the icosahedral structure [1]. The vibrational and electronic spectra of $C_{60}$ should be comparatively simple due to the high symmetry of the molecule, as outlined in Chapter 2.

## 4.2. Vibrational Spectroscopy

### 4.2.1. Introduction

One of the most common spectroscopy techniques in fullerene research is Raman Spectroscopy. Using this technique it is possible to probe molecular vibrations of $C_{60}$. Raman Spectroscopy is based on radiation scattering as it passes through a medium. The scattering process can be either Rayleigh scattering (elastic) or Raman scattering (inelastic). Rayleigh scattering is a two photon process having a net effect of changing the direction of, or scattering light, while keeping frequency constant. The retention of the frequency indicates it is an elastic scattering process. Raman scattering is a two photon process having net effects of scattering photons but changing their frequency. This change in frequency is characteristic of inelastic scattering and provides the basis for this form of spectroscopy [2]. Incoming photons will shift their frequencies, up and down, by amounts equal to certain vibrations of the molecules.

Another important tool in the elucidation of fullerene properties is Infrared Spectroscopy. Infrared radiation is part of the electromagnetic spectrum between the

34

visible and microwave region. Infrared radiation is absorbed by organic molecules and converted into energy of molecular vibrations, either stretching or bending. IR is closely related to Raman since both result from the same type of quantised vibrational changes. There are however differences between the modes of vibration that are Raman active and IR active, as discussed in section 4.2.2. IR spectroscopy does not generate any excited states and hence it is a true representative of the ground state properties of a molecule. Raman on the other hand can generate excited states if a molecule is resonant at the particular wavelength used.

### 4.2.2.  Vibrational Spectroscopy of $C_{60}$

The vibrational interactions in fullerenes where investigated both in its isolated form and also in the solid state. As discussed in Chapter 2, there are 3N-6 vibrational modes for molecules with N atoms. $C_{60}$ has 174 [=(60x3)-6] normal modes which are reduced to 46 fundamental vibrational modes [3] because molecules with $I_h$ symmetry, which $C_{60}$ is the most predominant member have the highest degree of symmetry. These modes are described by the irreducible representation

$$\Gamma = 2A_g + 3F_{1g} + 4F_{2g} + 6G_g + 8H_g + 1A_u + 4F_{1u} + 6G_u + 7H_u \qquad \text{Eq.4.2.1}$$

The relevance of this expression predicts the bands that are Raman and IR active. Using this expression and a set of selection rules [4], the 46 non-degenerate modes can be further reduced. The selection rules are as follows,

1) For a vibration to IR active there must be a change in the dipole moment of the molecule i.e. $d\mu/dr$ is non-zero where r is the bond length and $\mu$ is the dipole moment.

2) For a vibration to be Raman active there must be a change in the polarisability tensor $\alpha$ i.e. $d\alpha/dr$ is non-zero.

Due to these selection rules the isolated $C_{60}$ molecule has 4 infrared active modes. They are of $F_{1u}$ symmetry and are located at 527, 576, 1183, and 1429 cm$^{-1}$. These modes are calculated based on the isolated molecule, but it must be noted that measurements of the vibrational spectroscopy of fullerenes are predominately done in the solid state [5,6,7]. Table 4.1 shows the referenced and observed values for the IR modes.

| Reference Value for IR Spectrum of $C_{60}$ Thin Films [8] | Observed Value for IR Spectrum of $C_{60}$ Thin Films | Assignment[9,10] |
|---|---|---|
| $528cm^{-1}$ | $526.70cm^{-1}$ | $F_{1u}(1)$ |
| $577cm^{-1}$ | $576.03cm^{-1}$ | $F_{1u}(2)$ |
| $1183cm^{-1}$ | $1182.46cm^{-1}$ | $F_{1u}(3)$ |
| $1429cm^{-1}$ | $1428.57cm^{-1}$ | $F_{1u}(4)$ |

**Table 4.1.** IR Modes and their Assignment
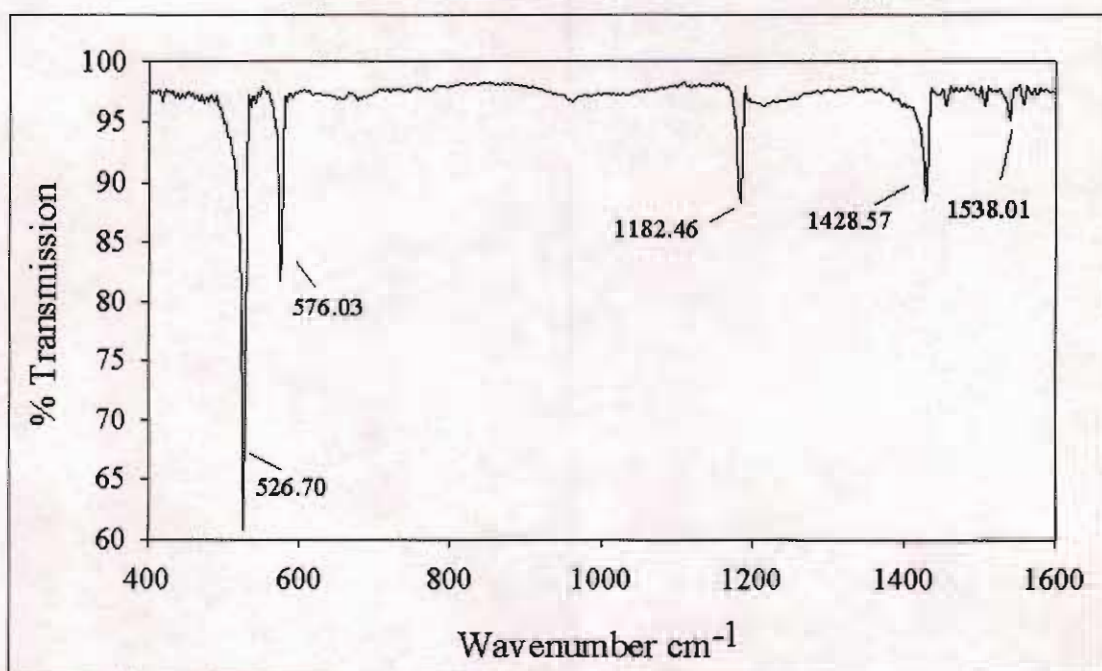


**Figure 4.1.** IR spectra for $C_{60}$ in solid state (KBr disc)

The IR active modes have 4 distinct frequencies, dictated by the molecule's icosahedral symmetry and so 4 main peaks would be expected in the IR spectrum of $C_{60}$. The observed spectrum, figure 4.1 shows these 4 allowed modes **at 526.70,** 576.03, 1182.46, and 1428.57cm$^{-1}$. In addition an extra mode is seen at 1538.01cm$^{-1}$, this mode is attributed to higher order effects discussed by Eklund [12]. The observed infrared (IR) spectrum (usually taken in the solid form), also displays a broad range of silent peaks, clearly indicating the influence of the solid state environment enhancing

the strength of forbidden lines by an increase in symmetry breaking. The most obvious symmetry-breaking mechanism is the isotope effect [13]. Most carbon atoms in nature are $^{12}$C, but there is naturally about 1.08% of the isotope $^{13}$C present in the $C_{60}$ molecule. The presence of $^{13}$C atoms in a $C_{60}$ molecule lowers the icosahedral symmetry creating a softening of the allowed fundamental modes and hence contributing to the vibrational spectra.

| Reference value for Raman Spectrum of $C_{60}$ Thin Films [5] | Observed value of Raman Spectrum of $C_{60}$ Thin Films at 300K | Observed value of Raman Spectrum of $C_{60}$ Thin Films at 77K | Assignment[9,10,11] |
|---|---|---|---|
| 497.5cm$^{-1}$ | 429.6cm$^{-1}$ | 429.6cm$^{-1}$ | $A_g(1)$ |
| 1470.0cm$^{-1}$ | 1469.4cm$^{-1}$ | 1469.4cm$^{-1}$ | $A_g(2)$ |
| 273.0cm$^{-1}$ | 267.1cm$^{-1}$ | 267.1cm$^{-1}$ | $H_g(1)$ |
| 432.5cm$^{-1}$ | | 428.2cm$^{-1}$ | $H_g(2)$ |
| 711.0cm$^{-1}$ | 709.8cm$^{-1}$ | 709.8cm$^{-1}$ | $H_g(3)$ |
| 775.0cm$^{-1}$ | 768.7cm$^{-1}$ | 768.7cm$^{-1}$ | $H_g(4)$ |
| 1101.0cm$^{-1}$ | | 1100.0cm$^{-1}$ | $H_g(5)$ |
| 1251.0cm$^{-1}$ | 1250.2cm$^{-1}$ | 1250.2cm$^{-1}$ | $H_g(6)$ |
| 1426.5cm$^{-1}$ | 1430.5cm$^{-1}$ | 1430.5cm$^{-1}$ | $H_g(7)$ |
| 1577.5cm$^{-1}$ | 1563.6cm$^{-1}$ | 1563.6cm$^{-1}$ | $H_g(8)$ |

**Table 4.2.** Raman Modes and their Assignment

Due to the selection rules the isolated $C_{60}$ molecule has 10 Raman active vibrations; two nondegenerate modes with $A_g$ symmetry and eight fivefold degenerate modes

with $H_g$ symmetry. At room temperature the two $A_g$ modes are the radial-breathing mode at $493cm^{-1}$ and the pentagonal pinch mode at $1469cm^{-1}$. The $H_g$ modes are observed at 267, 428, 710, 769, 1100, 1250, 1431, and 1564 $cm^{-1}$. Table 4.2 shows the referenced and observed Raman modes.
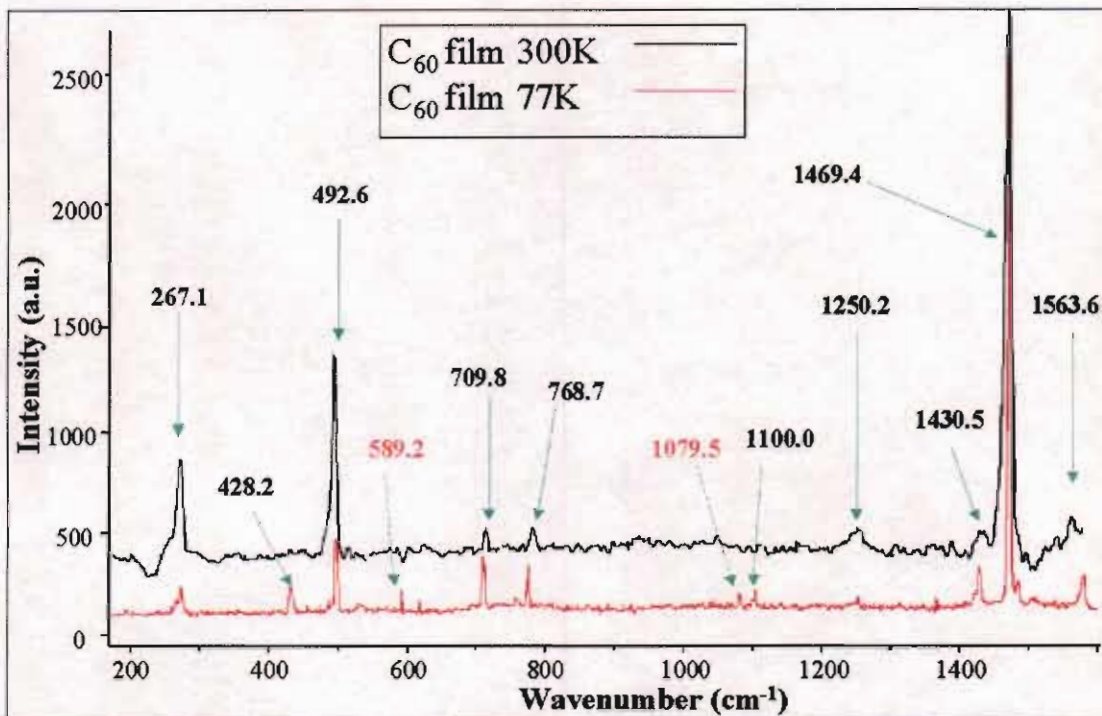


**Figure 4.2.** Raman Spectra of $C_{60}$ thin film at 300K and 77K

Figure 4.2 shows the solid state Raman spectrum at both 300K and 77K. In thin film form at room temperature eight modes of vibrations were detected with only, the $H_g(2)$ and $H_g(5)$ modes not distinguishable. However at low temperatures (77K) the ten allowed modes of vibration are clearly visible. The two $A_g$ modes present at approximately $493cm^{-1}$ ($A_g(1)$) and $1469cm^{-1}$ ($A_g(2)$) are the strongest peaks present in the ground state $C_{60}$ Raman spectrum, and is one of the reasons the $A_g(2)$ mode will be used in the characterisation of $C_{60}$. The $A_g(2)$ represents the contraction of the pentagons (i.e. the pentagonal pinch mode) whereas the $A_g(1)$ mode is representative of the expansion of the hexagonal rings (i.e. hexagonal breathing mode).

As discussed in Chapter 2, the vibrational spectrum of the solid state remains mostly molecular in character. The symmetry however of the molecule is affected by its interaction with the fcc lattice [14], and reduced slightly to the point group symmetry $T_h$. Below the phase transition of 249K [15] the rotation of the balls is hindered and

eventually frozen out below 90K, there is significant symmetry reduction due to crystal field effects at low temperatures. Hence the symmetry of the molecule is reduced to $T_h$, resulting in a lifting of the degeneracy. This is evident by the splitting of the $H_g$ modes into two lines $E_g$ and $F_g$ at room temperature and eight lines at temperatures below the phase transition of 249K [15]. Van Loosdrecht et al. [16] have reported the appearance of a significant number of new Raman lines in the low temperature spectrum of a $C_{60}$ crystal and have assigned them all only to the activation of the silent *gerade* fundamentals. Two such modes can be seen in figure 4.2 positioned at 589.2cm$^{-1}$ and 1079cm$^{-1}$, and can be assigned to the silent gerade fundamentals $F_{2g}(1)$ and $F_g(4)$ respectively (highlighted in red in figure 4.2). The reduction in symmetry of the $C_{60}$ molecule is implicit in the activation of these silent modes, as well as the splitting of some of these modes, has been ascribed solely to the effects of the crystal-field [16].

Experiments show that spectra taken of solid $C_{60}$ match the aforementioned calculated modes and the spectra obtained for isolated mode in gas form, inviting the conclusion that the effect of the solid state on the vibrational spectrum is very weak, and although $C_{60}$ is slightly resonant at laser wavelength used (633nm), the effect is small and therefore Raman can be taken to be a representative of the ground state.

## 4.3. Electronic Spectroscopy

### 4.3.1. Introduction

The energy states of electrons in atoms and molecules are quantised. The exact pattern of quantisation (spacing between energy levels, number of states available to electrons) is related to the chemical nature of the atom or molecule. Electronic spectroscopy probes directly the quantisation of electronic energy. The technique is based on the interaction between the electrons in the sample and electromagnetic radiation. For a system in a low energy state, energy from a photon will be absorbed, raising the systems energy to a higher quantum mechanical allowed state. This process is called absorption. Conversely, a system in a high energy state may decay to a low energy state by emission of a photon, whose energy corresponds to the difference in the energy allowed quantum states. This process is called emission. In

both cases the photon energy must be precisely equal to the energy difference between the electronic levels.

The relationship between chemical structure and the wavelength of light emitted or absorbed from a material is very specific which makes electronic spectroscopy a very powerful technique to describe the structure of low and high energy states of atoms and molecules.

### 4.3.2. Electronic Spectroscopy of $C_{60}$

As in the case in the vibrational spectroscopy, the high degree of symmetry of the fullerenes plays an important role in the electronic spectroscopy of the molecules. In $C_{60}$ the closed shell icosahedral symmetry renders the HOMO-LUMO transition dipole forbidden [17], as discussed in Chapter 2.
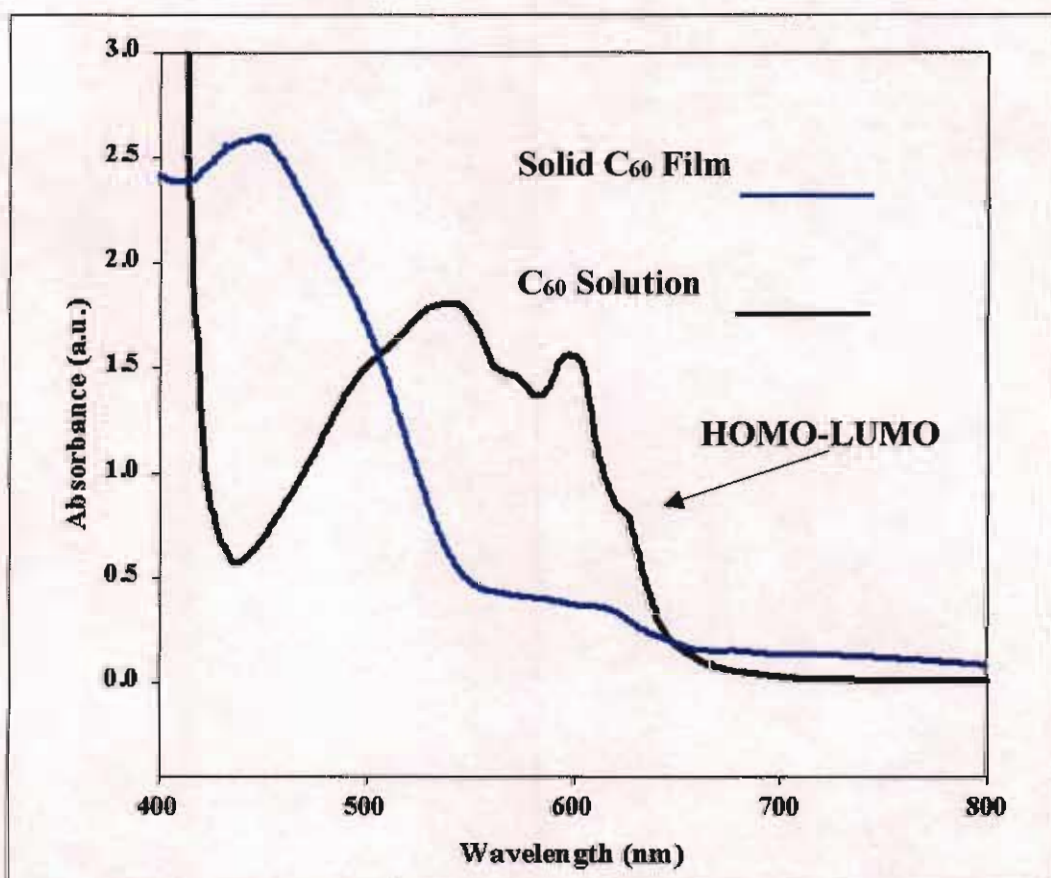


**Figure 4.3.** Absorption spectra of $C_{60}$ in Solution (chlorobenzene 3g/l) and $C_{60}$ Film

40

Transitions can occur weakly via Hertzberg-Teller vibrational coupling or Jahn-Teller distortions. Singlet- triplet transitions, which are spin forbidden, can similarly appear, although weakly due to spin orbit coupling effects. Figure 4.3 shows the UV absorption spectrum of $C_{60}$, both in solution and in solid film form. For $C_{60}$ in solution the spectrum is divided into 4 sections as described by Leach et al [18]. Between 190 and 350nm, not shown in figure 4.3, there exists three strong bands, and these, in addition to weaker, vibronically structured bands in the region of 359-430nm, are assigned to nine orbitally allowed singlet-singlet transitions (HOMO-LUMO+1 etc.). The vibrational structure has been assigned to the effects of Jahn-Teller distortions. A broad feature is observed in the spectral region between 450-640nm. This absorption is very weak and possesses a rich vibrational structure. The features of this region have been ascribed to the HOMO-LUMO transition whose forbiddeness has been partially lifted by Herzberg-Teller interactions as well as Jahn-Teller distortions. Although not apparent in figure 4.3, Leach also identified four extremely weak bands between 627 and 690nm and assigned them to vibronic features of the spin forbidden singlet to triplet transition.

Figure 4.4 shows a set of absorption spectra of $C_{60}$ in chlorobenzene at different concentrations (the peaks in the 3g/l plot at ~550nm are due to the high concentration of the solution and the saturation of the detector). The features discussed for $C_{60}$ in a solution are clearly visible for all concentrations. It is possible to calculate the extinction coefficient of $C_{60}$ by using the Beer- Lambert law [4] and by plotting a graph of Absorbance at 532nm against concentration as in figure 4.5. As can be seen from the graph a linear response is seen and by calculating the slope and using equation 3.1 extinction coefficient can be calculated.

$$A = c.\varepsilon.d \qquad\qquad\qquad Eq.3.1.$$

A=absorbance(a.u.) $\qquad\qquad$ $\varepsilon$=extinction coefficent $(mol^{-1}cm^{-1})$

c=concentration (mol/l) $\qquad\qquad$ d=path length (1cm)
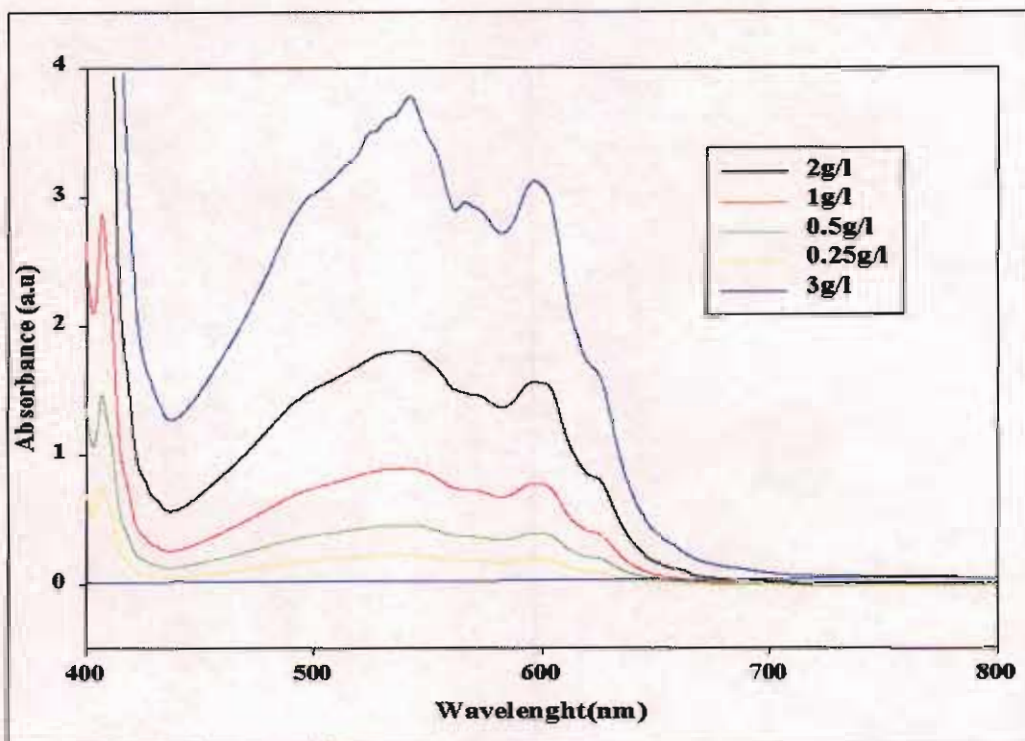
**Figure 4.4.** Absorption spectra of $C_{60}$ in Chlorobenzene at various concentrations
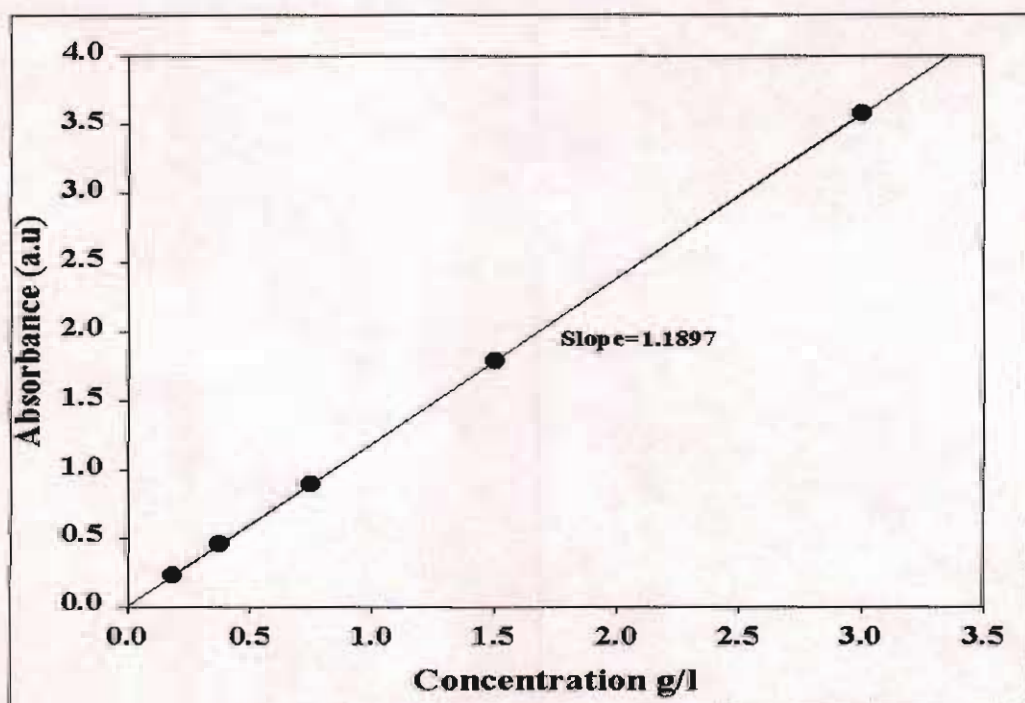


**Figure 4.5.** A plot of absorbance at 532nm against concentration.

The linear response also supports the notion that the absorption spectrum of $C_{60}$ solution is that of the isolated molecule, since the Beer-Lambert law assumes no

aggregation of the molecules in solution. The slope of the graph was calculated as $1.1897g^{-1}/l$, hence giving an extinction coefficient at 532 nm of $C_{60}$ to be 857 mol$^-$ $^1$cm$^{-1}$, which is in good agreement to the literature values [19].

Figure 4.3 also shows a comparison of the absorption spectrum of $C_{60}$ in solution (isolated molecule) and a solid $C_{60}$ film. An examination of the spectrum shows that the lowest energy transition in the solid state which has a maximum at 630nm is still present, but slightly red shifted. All the higher order allowed molecular transitions also appear in the solid state (shown in figure 4.6) but are also slightly red shifted. This shows that the solid state of $C_{60}$ appears to behave like a classical molecular solid. However, there is one feature that is different. The relatively strong absorption in the range 420-500nm with maximum at ~450nm is not present in the solution spectrum. It is widely accepted that this feature [3] is in fact the solid state's influence on the electronic properties of the molecule. Hence is not molecular in character but is the result of an intermolecular charge transfer excited state [21].
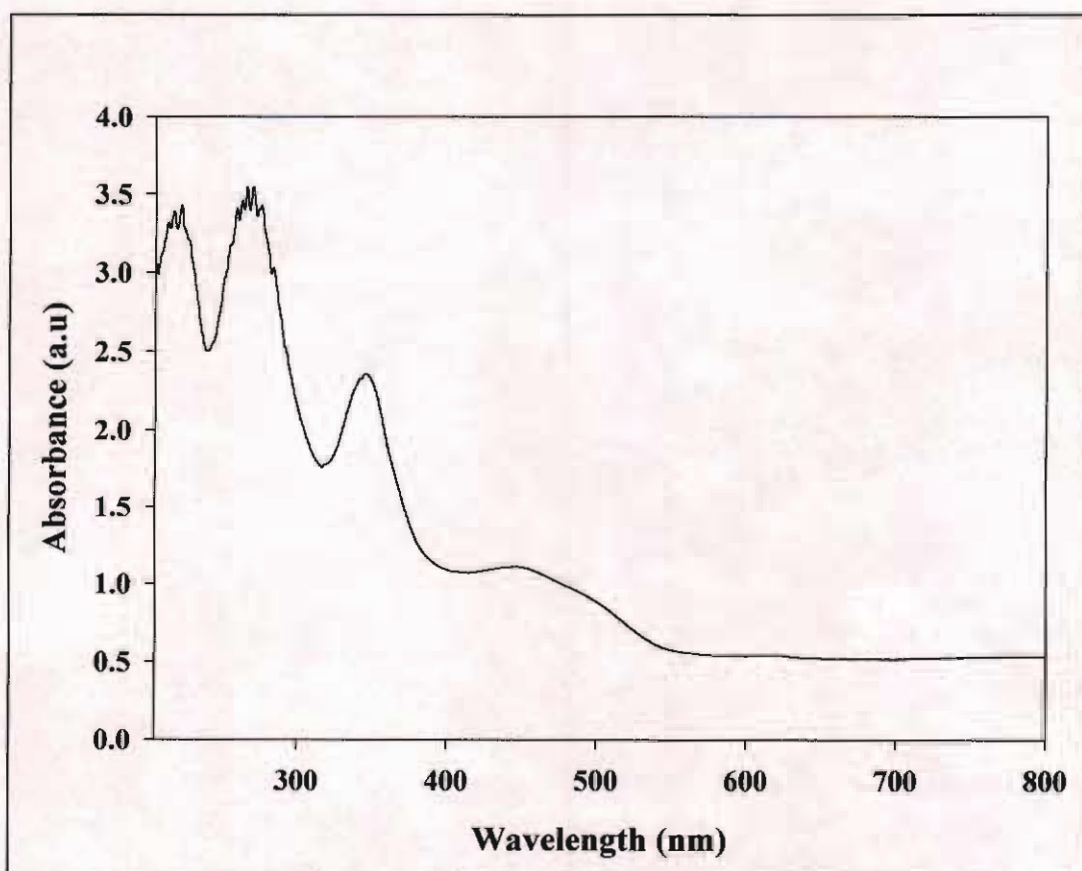


**Figure 4.6.** Absortion spectra of Solid $C_{60}$ Film evaporated onto Quartz substrate.

The intermolecular interactions do not change the low energy features of the absorption spectrum significantly. The absorption spectrum of the solid $C_{60}$ and the isolated molecule are very close, suggesting that the optical excited state of $C_{60}$ is governed by Frenkel exciton states. The Frenkel exciton picture is valid if the exciton binding energy (the energy required to take an electron from a molecule and to put it on a different molecule in the solid), is much larger than the energy of exciton transfer between molecules. In solid $C_{60}$ this condition is well satisfied. However intermolecular charge transfer (CT) excitations become possible in addition to Frenkel Excitons. A charge transfer excitation corresponds to a creation of an electron and the hole on different molecules. If an electron and a hole are situated on nearest neighbour molecules and are bound to each other, then they are called a CT exciton. However, this does not mean that they are localised on two molecules. In the fcc lattice of $C_{60}$, the electron can be located on any one of the twelve equivalent nearest neighbour molecules around the molecule occupied by the hole, and vice versa. A CT exciton exists once the electron and hole are separated by one or more lattice distances but are still correlated to each other.

### 4.3.3. Modifying Crystal Packing

As discussed in chapter 2, thermal annealing is one approach to modifying/stabilising the $C_{60}$ lattice. A number of spectroscopic analyses [22,23,24] of annealed $C_{60}$ films have lead to the conclusion that structural reordering of the lattice has occurred. Figure 4.7 is taken from a previous study [24], and shows a comparison of the absorption spectra taken for a $C_{60}$ thin film annealed as a function of time.

The unheated film shows the well accepted pristine solid $C_{60}$ spectrum. After measurement of this spectrum the film was transferred into a vacuum oven and heated over different time periods and a spectrum taken after each period. With increasing annealing time, significant changes where visible. Firstly there was a dramatic selective loss in intensity in the features at 470nm and 520nm. Secondly there is a continuous red shift of these solid features while the HOMO-LUMO absorption at 620nm appears to remain constant. This apparent shifting accompanied by the loss in intensity can be attributed to closer packing of the molecules in the solid state. This absorption spectrum of the annealed film indicates a structural change as opposed to a chemical or thermal change.
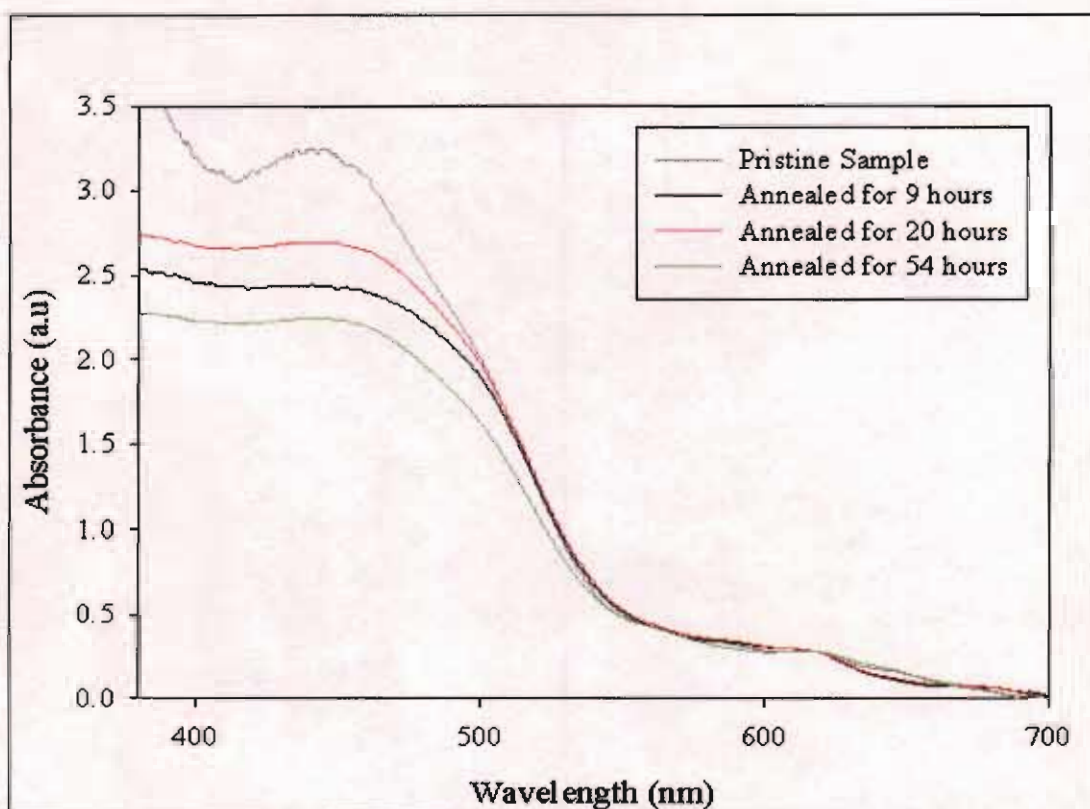
**Figure 4.7.** Absorption spectra as a function of time for annealed $C_{60}$ film.[24]

Within this study, samples were annealed in situ. Annealed films were prepared by having the distance between the substrates and the evaporation boat at a minimum, with an evaporation time of 30 minutes, which corresponds to the total annealing time. Pristine films were prepared by having the distance between the substrates and the evaporation boat at a maximum, with an evaporation time of 10 minutes. The thickness of the $C_{60}$ films is dependent upon the amount of sample, the substrate distance and the evaporation time. In this study the amount of $C_{60}$ placed in the evaporation boat was kept constant (5mg). The evaporation time and height were varied in accordance with a set of calibration curves for the system, previously obtained [25].

An absorption spectrum of both the annealed and pristine films where taken, figure 4.8. As can be seen from figure 4.8 in the annealed film there is a small loss of intensity and a small red shift in the solid state features at 470nm and 520nm of a few nm while the HOMO-LUMO absorption at 620nm appears to remain constant. This seems to show that an annealing effect can be produced during deposition. The differences seen due to annealing during deposition are small compared to previous

studies but this may be due to the relative annealing times 30 minutes to 54 hours respectively. The changes observed in the absorption spectrum for the annealed films has been well characterised in literature [9] and is known not to be due to any variation in film thickness. It is not possible at this stage to determine the point at which the effects of annealing begin to dominate over the effects of film thickness during the evaporation process. However changes observed due to variations in the range of film thickness used in this study result in a linear change in intensity of all the bands without any observable shifts in position [25] whereas the spectra shown in figure 4.7 clearly shows the effects of annealing and not a thickness dependence.
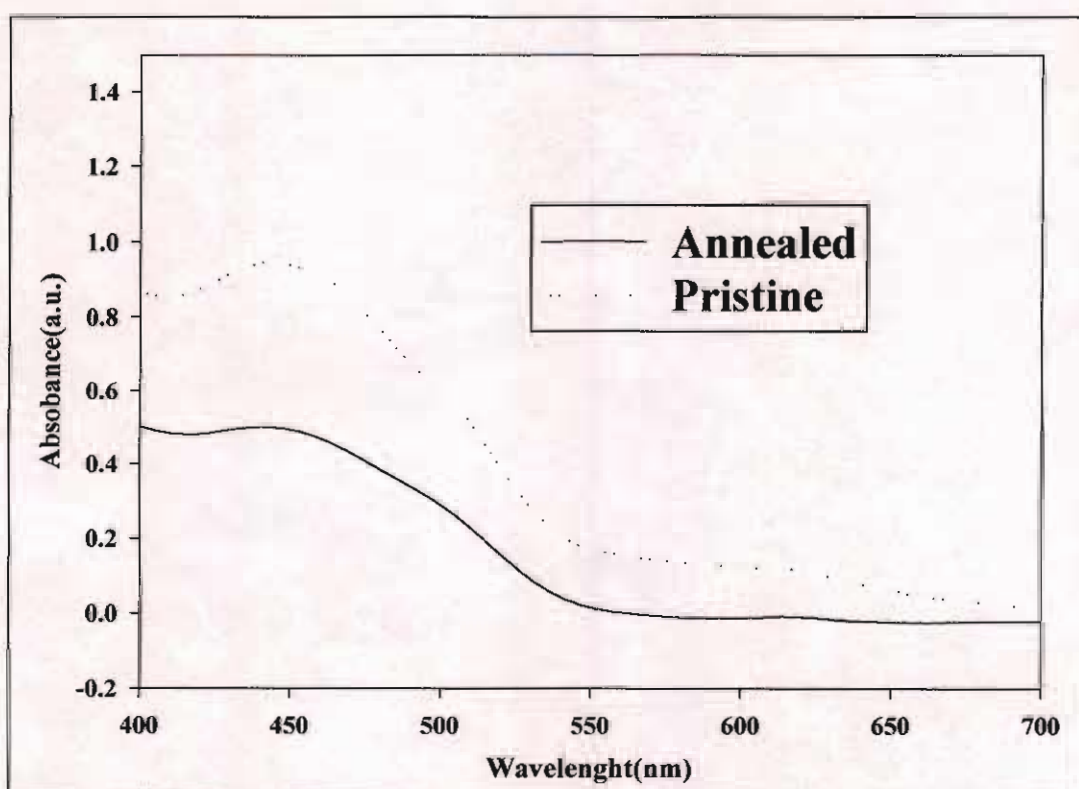


**Figure 4.7.** Absorption spectra of Unannealed and Annealed $C_{60}$ Film.

### 4.4. Summary

In this chapter spectroscopy is shown to be a useful tool into the characterisation of $C_{60}$. The spectroscopic properties of $C_{60}$ can be seen to be very much influenced by its high degree of symmetry. In vibrational spectroscopy, the isolated $C_{60}$ molecule has been calculated to have 10 Raman active modes, and 4 IR active modes. Measurements are taken in the solid state, and since these peaks match those calculated for the isolated molecule it can be concluded that the effect of the solid

state on the vibrational spectrum is very weak, showing very little ground state–ground state interaction. Electronic spectroscopy however reveals features that are specific to the solid. Intermolecular charge transfer excitons, in which charge is separated between molecules in adjacent sites, has turned out to be an important process in fullerene solids, the significance of which shows the first sign of communication of the pi electrons of neighbouring molecules. It was shown by absorption spectroscopy that thermal annealing could be used to control the lattice structure, identified by a loss of intensity and red shifting in the solid state features when film was annealed. Furthermore it was seen that this annealing effect can also be achieved during deposition of the $C_{60}$ film.

## 4.5 References

1.  H.W. Kroto, J.R. Heath, S.C. O'Brien, R.F. Curl, and R.E. Smalley, *Nature* **318,** 162-163 (1985).

2.  C.V. Raman and K.S. Krishan, *Nature*, **121**, 501 (1928)

3.  H.J. Byrne, in *Physics and Chemistry of Fullerenes and Derivatives*, H. Kuzmany, J. Fink, M. Mehring and S. Roth eds., World Scientific Sinapore, 183 (1995)

4.  P.W. Atkins, *Physical Chemistry*, 426-531 (Oxford University Press 1990)

5.  W. Krätschmer, L.D. Lamb, K. Fostiropoulos and D.R. Huffman, *Nature*, **347**, 345-358 (1990)

6.  H. Kuzmany, M. Matus, B. Burger, J. Winter, *Adv. Mater*, **10**, 731-745 (1994)

7.  D.S. Bethane, G. Meijer, W.C. Treacy and H.J. Rosen, *Chem. Phys. Lett.*, **174**, 219-222 (1990)

8.  W. Krätschmer, L.D. Lamb, K. Fostiropoulos and D.R. Huffman, *Nature*, **347**, 6271,pp 345-358 (1990)

9.  L.Akselrod PhD dissertation, University of Dublin, Trinity College. 1993

10. Z-H. Dong, P. Zhou, J.M. Holden, P.C. Eklund, M.S. Dresselhaus, G. Dresselhaus, *Phys. Rev. B*, **48**, 2862 (1993)

11. L. Akselrod, H.J. Byrne, S. Donovan and S. Roth, *Chem. Physics*, **192**, 307 (1995).

12. M.S. Dresselhaus, G. Dresselhaus, P.C. Eklund, *Science of Fullerenes and Carbon Nanotubes*, Academic press inc., London (1995)

13. K.-A. Wang, A.M. Rao,P.C. Eklund, M.S. Dresshaus, G. Dresselhaus, *Phys. Rev. B*, **48**, 1375 (1993)

14. H. Kuzmany, M. Matus, T. Picher and J. Winter, in *Physics and Chemistry of Fullerenes*, K. Prassides ed., Klewer Academic, Dordrecht (1994)

15. J.E. Fisher, P.A Heiney, D.E. Luzzi and D.E. Cox, *Fullerenes: Synthesis, Properties, and Chemistry of Large Carbon Clusters*, from the American Chemical Society Symposium Series, **481**, 55 (1992)

16. P.H.M. van Loosdrecht, P.J.M. van Bentum, M. Verheijen and G. Meijer, *Chem. Phys. Lett.*, **198**, 587 (1992)

17. M. Braga, S. Larsson, A. Rosén and A. Volosov, *Astron. Astrophys.*, **245**, 232 (1991)

18. S. Leach, M. Vervloet, A Després, E. Bréheret, J.P. Hare, T.J. Dennis, H.W. Kroto, R. Taylor and D.R.M. Walton, *Chem. Phys.*, **160**, 451 (1992)

19. A. Kost, J.E. Jensen, M.B. Klein, J.C. Withers, R.O.Loufty, M.B. Haeri and M.E. Ehritz, *Fullerenes and Photonics*, Z.H. Kafafi ed., Proc. SPIE, **2284**, 208 (1994)

20. L. Akselrod, H.J. Byrne, J. Callaghan, A. Mittelbach and S. Roth, in *Electronic Properties of Fullerenes*, H. Kuzmany, J. Fink, M. Mehring and S. Roth eds., Springer Series in Solid State Sciences, Springer Verlag Heidelberg, **117**, 219 (1993)

21. S. Kazaoui, N. Minami, Y. Tanabe, H.J. Byrne, A. Eilmes and P.Petelenz, *Phys. Rev. B*, **12**, 7689 (1998)

22. L. Akselrod, H.J. Byrne, T.E. Sutto and S. Roth, *Chem .Phys. Lett.*, **233**, 436 (1995)

23. M. Kaiser, W.K. Maser, H.J. Byrne, A. Mittelbach and S. Roth, *Solid State Commun.*, **87**, 281 (1993)

24. G. Chambers, PhD dissertation, Dublin Institute of Technology. 2001

25. A.Casey, Final Year BSc. Project (FT225), Dublin Institute of Technology. Kevin St. 2003.

# Chapter 5.

## Optically Excited States and their Spectroscopy

### 5.1.    Introduction

A considerable understanding of the photophysical and photochemical properties of $C_{60}$ both in solution and solid has evolved over the past decade [1]. Interest in the electronic properties of the material was increased by the observation that when chemically doped with alkali metals [2,3] in a 1:1 stoichiometry, the films exhibited a metallic like conductivity and even furthermore by the observation that, when doped to a 3:1 stoichiometry, superconducting transition temperatures as high as 43 K [4] were attainable. It appears that addition of electrons to higher, unoccupied molecular orbitals dramatically increases the electronic interaction between the molecules.

Chapter 4 looked at the ground state optical properties of $C_{60}$. Vibrational spectroscopy provides strong evidence that the solid state environment exerts a minimum perturbation on the electronic structure of the fullerene molecule (solid state retains its molecular character). From this it seems that optically, the materials appear of little interest in both the molecular and solid state form. However a comparison between the absorption spectra in film and in solution shows the first sign of a notable deviation of the properties of the solid state to the isolated molecule; the feature at ~ 450nm. This feature is exclusive to the solid state and appears at an energy ~0.5eV higher than the molecular transition, which is attributed to an intermolecular charge transfer exciton [5], the presence of which indicates that the interaction between a ground state and a neighbouring optically excited state is significantly greater than between two ground states. This interaction needs to be examined further in order to elucidate this excited species.

At high intensities, the properties of fullerenes in the solid have been seen to change dramatically. At elevated intensities in single crystals a nonlinear luminescence is seen to emerge, with a cubic dependence on intensity [6]. The spectrum is broad and continuously red shifted. The emission lifetime similarly increases with the cube of the intensity. Photoconductivity studies [7] show a similar cubic dependence on intensity and the temperature dependence at elevated intensities suggests an optically induced insulator to metal phase transition, as a result of collective interaction

between neighboring excited states. The increased interaction between neighbouring optically excited species can be paralleled to that observed through chemical doping and justification can be drawn by the observation of a broadband visible electroluminescence emission from fullerene crystals upon electron injection [8]. The process has been likened to Mott transitions in indirect band gaps semiconductors [9], and a simple model suggests that such a transition may occur in fullerenes at an excitation density of ~40%. The transition at low temperatures is characterised [9] by a nonlinear evolution of the Raman mode at $1469cm^{-1}$ to $1463cm^{-1}$. The above observations are a strong indication that the metallic like form of a solid state fullerene can be reversibly induced both optically and by electron injection.

This chapter will deal with the optically induced excited states. Raman Spectroscopy has been seen to be a useful tool in the elucidation of several photoinduced processes in $C_{60}$. In solution, optical excitation leads to a population of the long lived triplet state, via a number of intermediate states [10]. The Raman spectroscopic signature of this molecular triplet in solution has recently been associated with a positioning of the $2A_g$ mode at $1466cm^{-1}$ at room temperature [11]. Similar measurements however at room temperature in the solid are hampered by the much documented photopolymerisation of $C_{60}$ [12], which occurs via a 2+2 cycloaddition. Previous work has proposed however [13] that below this phase transition temperature, it should be possible to isolate the intermediate excited states associated with the polymerisation and thereby identify the Raman signatures of the molecular triplet at $1466cm^{-1}$ and a second high intensity excited state at $1463cm^{-1}$.

## 5.2. Introduction to Excited Triplet State.

In chapter 4, the ground state optical properties of $C_{60}$ were discussed. The focus in ground state spectroscopy is essentially on the primary absorption of light by a molecule promoting an electron from the ground state ($S_0$) to the first excited state ($S_1$), referred to as the singlet state, which has an overall spin angular momentum of zero.
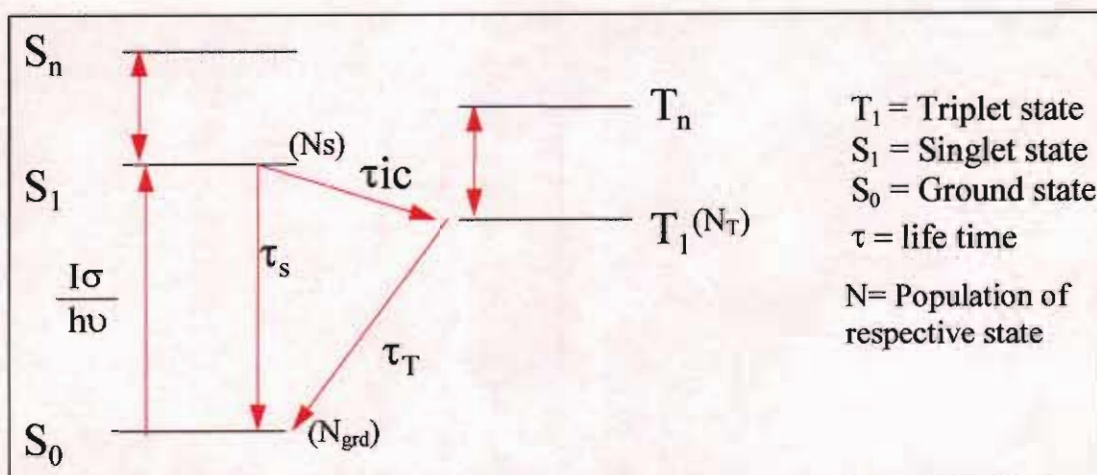
**Figure 5.1.** Jablonski level diagram showing optical transition to excited states.

Figure 5.1 shows an illustration of the stepwise proceedings of a molecule in its electronic states manifold. Once in the lowest excited singlet state the molecule can either fluoresce from $S_1$ to $S_0$ or pass from $S_1$ to the triplet manifold where it quickly reaches $T_1$. From there it can phosphoresce from $T_1$ to $S_0$. Kasha's Rules [14] differentiate between these two types of transitions, the one occurring between states of the same multiplicity, non-radiative e.g. $S_1$ to $S_0$, which is called internal conversion and the one which occurs between states of different multiplicity, e.g. $S_1$ and $T_1$, called intersystem crossing. The latter gives rise to the formation of the energetically lower lying triplet excited state ($T_1$) in accordance with Hund's rule [15].

The optical analysis of a molecule in these excited states (singlet/ triplet) is referred to as excited state spectroscopy. As in ground state spectroscopy, excited state spectroscopy optically examines the transitions from one energy level to another. In excited state spectroscopy one can have transitions from $S_1$ - $S_n$ or $T_1$ - $T_n$ depending upon the spin angular momentum of our excited state. The singlet -singlet absorption ($S_1$ - $S_n$ transition) of a molecule will yield a differential absorption which has a life-time, typically of the order of nano-seconds, governed by the decay of $S_1$. The triplet - triplet absorption in general is relatively long lived, typically around milli-seconds governed by the decay of $T_1$. This triplet-triplet absorption is origin of optical limiting behaviour in fullerene systems. Raman spectroscopy has been employed to characterise this state both in solution and solid.

## 5.3. Raman Spectroscopy of Molecular Triplet in $C_{60}$ Solution

As discussed in Chapter 4, Raman spectroscopy provides valuable information about the intra- and intermolecular bonding in $C_{60}$. The Raman spectrum of the isolated $C_{60}$ and the solid state $C_{60}$ are similar, due to the fact that the effect of the solid state on the vibrational spectrum is very weak.

$C_{60}$ shows 10 strong Raman lines the number of Raman allowed vibrational modes expected for the free molecule (figure 4.2). These spectral lines are therefore assigned to intramolecular modes, two with $A_g$ symmetry and 8 with $H_g$ symmetry. The $A_g$ "pentagonal pinch" mode at $1469cm^{-1}$, corresponds to breathing type tangential displacement of 5 carbon atoms around each of the 12 pentagons. The other $A_g$ mode is found at $492cm^{-1}$ and corresponds to a radial-breathing mode. It has been reported that an intensity dependent shifting of the pentagonal pinch mode from $1469cm^{-1}$ to $1458cm^{-1}$ has been observed in $C_{60}$ crystals [16]. For this reason this study shall concentrate on the characteristic pentagonal pinch mode at $1469cm^{-1}$, and its response to different optical and electronic conditions. Any decrease in symmetry changes the transfer of charge from the intramolecular bonds to the intermolecular ones, leading to a slight weaking of the former and thus to a small decrease in the frequency of the intermolecular phonon modes, in particular the well know $A_g(2)$ pentagonal pinch mode discussed above.

Studies have shown that this pentagonal pinch mode is seen to shift from $1469cm^{-1}$ to a new position of $1466cm^{-1}$, (see figure 5.2) with an increase in laser intensity [11]. These high intensities cause a high triplet state population in the solution, concluding that this feature at $1466cm^{-1}$ is a signature of the triplet state of molecular $C_{60}$, and an assignment of this shifting to the triplet state at $1466cm^{-1}$ is widely accepted. It should be noted that this shifting is fully reversible and cycleable.
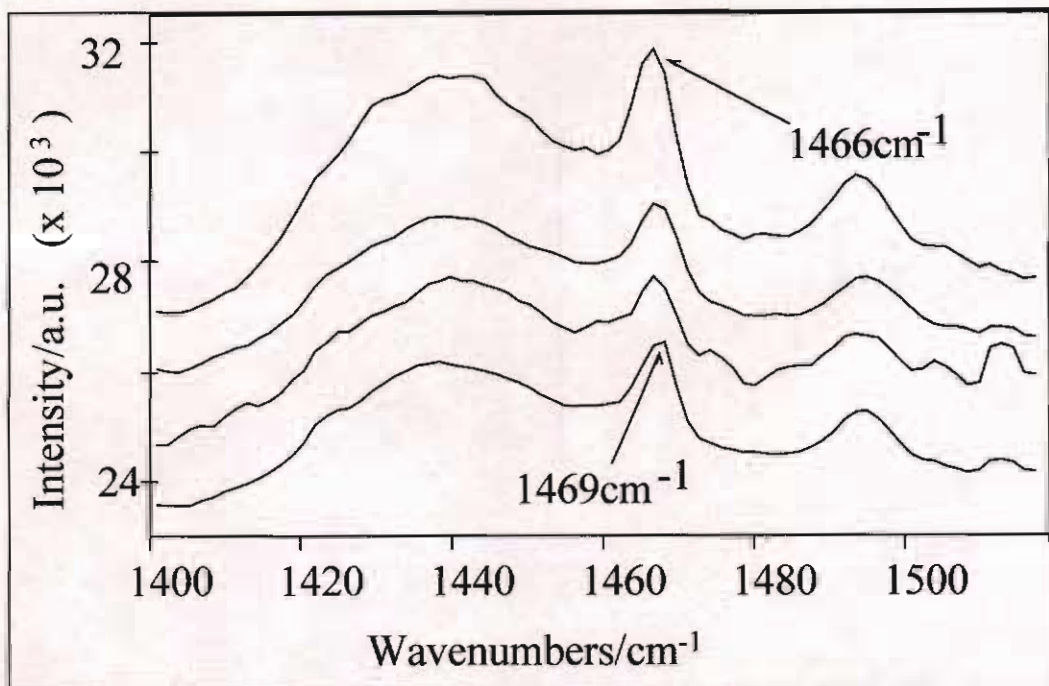
**Figure 5.2.** The Raman spectrum of the evolution of the molecular triplet of $C_{60}$ from $1469\text{cm}^{-1}$ to $1466\text{cm}^{-1}$

## 5.4. Observation and Identification of the Molecular Triplet in $C_{60}$ Films

The identification of the molecular triplet in the solid state is prohibited at temperatures above 243K, due to photopolymerisation as will be discussed in the next section. However, below the phase transition it is possible to isolate the excited states of $C_{60}$ in the solid, independent of the photopolymerisation. Van Loosdrecht et al [19], have indeed shown this to be true in $C_{60}$ crystals. At low temperatures the pentagonal pinch mode in the Raman spectrum of $C_{60}$ single crystals was seen to shift from $1469\text{cm}^{-1}$ to lower Raman frequencies as the laser intensity is increased. Recent work in $C_{60}$ thin films [13] has also shown two optically excited states with increased illumination, identified at $1466\text{cm}^{-1}$ and $1463\text{cm}^{-1}$. The evolution of these excited states is shown in figure 5.3.
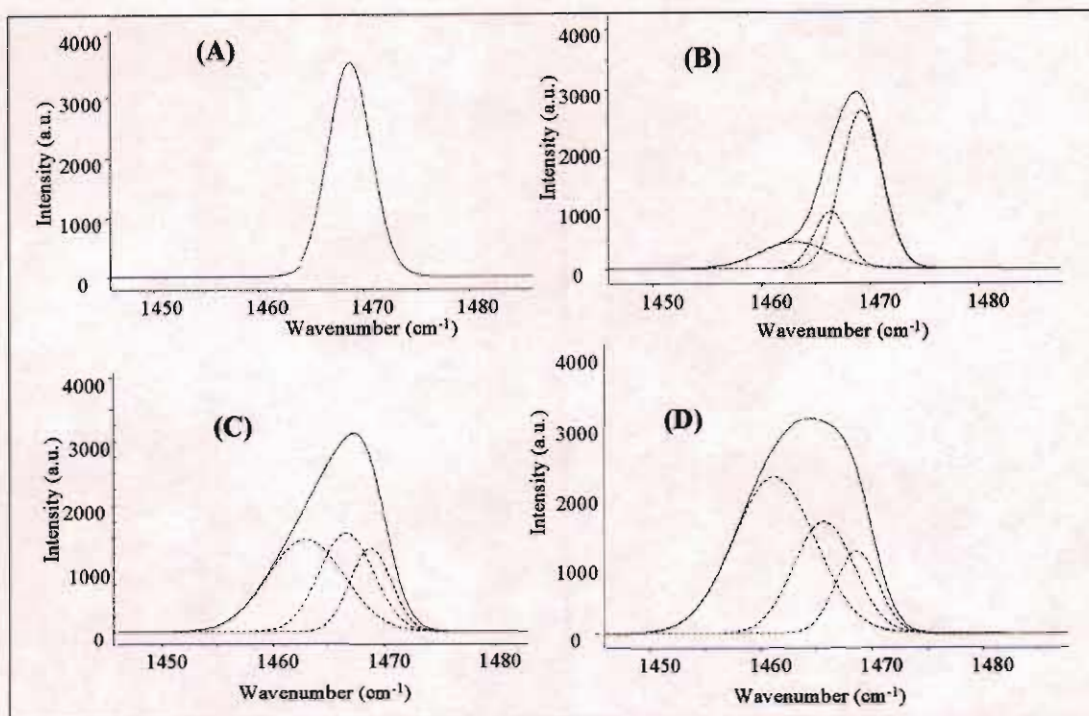
**Figure 5.3.** Raman spectra of the pentagonal pinch mode at 1469cm$^{-1}$ as the incident intensity at 514.5nm is increased. (A) The low irradance spectrum (>10$^4$Wcm$^{-2}$ ) of the pentagonal pinch mode is seen to be stable (B) At ~15000Wcm$^{-2}$ two new components appear in the spectrum at 1466cm$^{-1}$ and 1463cm$^{-1}$. (C) (25000Wcm$^{-2}$) and (D) the evolution of the three features is clearly evident with the feature at 1463cm$^{-1}$ becoming the dominant species at high laser intensities (35000Wcm$^{-2}$) in (D).

The data reported clearly shows the existence of two excited state species in solid thin films of C$_{60}$, the molecular triplet at 1466cm$^{-1}$ and an excited state specific to the solid positioned at 1463cm$^{-1}$. The second species has been reported to be intrinsic to C$_{60}$ at low temperatures and high intensities and an optically induced phase transition has been demonstrated [17]. The observation of electroluminescence from single crystals indicates that a comparable state may be induced by electron injection [18]. Therefore in this study the electrical properties of C$_{60}$ have been probed at room and low temperatures. In situ Raman spectroscopy has also been used to attempt to elucidate the various electrically produced species, by comparing them to already well characterised optically induced excited states, as will be discussed in chapter 6.

### 5.5. Photochemical processes in C$_{60}$

In chapter 2, the importance of the inter- and intramolecular processes in terms of their contribution to the electronic transport within the solid C$_{60}$ was highlighted. A

strong indication of an intermolecular interaction is the photochemical transformation of $C_{60}$ in the solid [19]. In the fcc lattice configuration solid state $C_{60}$ satisfies the topochemical and photophysical requirements necessary for the formation of a $C_{60}$ polymer via a number of intermediate excited states [19]. The change in the Raman pentagonal pinch mode of $C_{60}$, which is characteristically positioned at $1469 cm^{-1}$ for pristine $C_{60}$ [12], was seen to shift to a lower Raman frequency of $1459 cm^{-1}$, during the polymerisation, see figure 5.4 (e). However at low temperatures, the topochemical and photophysical requirements necessary for polymerisation are not satisfied, inhibiting the formation of the polymer [9], see figure 5.3.
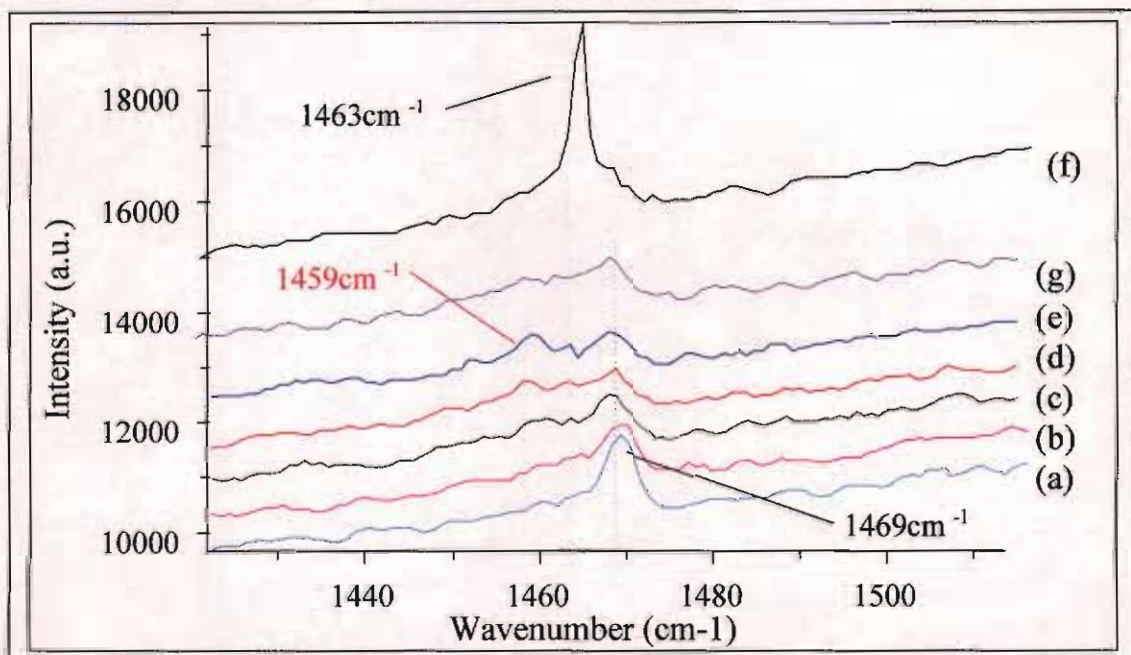


**Figure 5.4.** The evolution of the mode at $1469 cm^{-1}$ to $1459 cm^{-1}$ with respect to time. Prolonged illumination at low laser powers was seen to produce a peak at $1459 cm^{-1}$ (a) to (e). Then upon an abrupt increase of the laser power a peak at $1463 cm^{-1}$ appeared (f) and returning to the low laser powers regained the $1469 cm^{-1}$ (g) pentagonal pinch mode, indicating the cyclic nature of the processes

The photoproduct produced above 249K has been attributed to the formation of a $C_{60}$ polymer [19,20] and has been suggested to form via a 2+2 cycloaddition reaction, whereby the $\pi$ bonds of adjacent molecules open to form a covalent coupling between the molecules at room temperature [19]. Such reactions are commonly known in organic chemistry and involve the photoinduced coupling between the $\pi$-electrons of an excited triplet and those of a neighbouring ground state molecule. Figure 5.5 shows the general mechanism for a 2+2 cycloaddition in $C_{60}$. The 2+2 cycloaddition reaction is thermally forbidden but is one photon allowed when adjacent $\pi$ bonds are separated

by less than ~4.2Å. Additionally the reaction may proceed via injection of a charge into the lowest unoccupied triply degenerate molecular orbital (thus creating a state comparable to the optically excited triplet) or by the forcing together of the molecules under pressure [17].

Illumination with high intensities can reverse the polymerisation back to its pristine form via a high intensity metastable intermediate [18], figure 5.4.
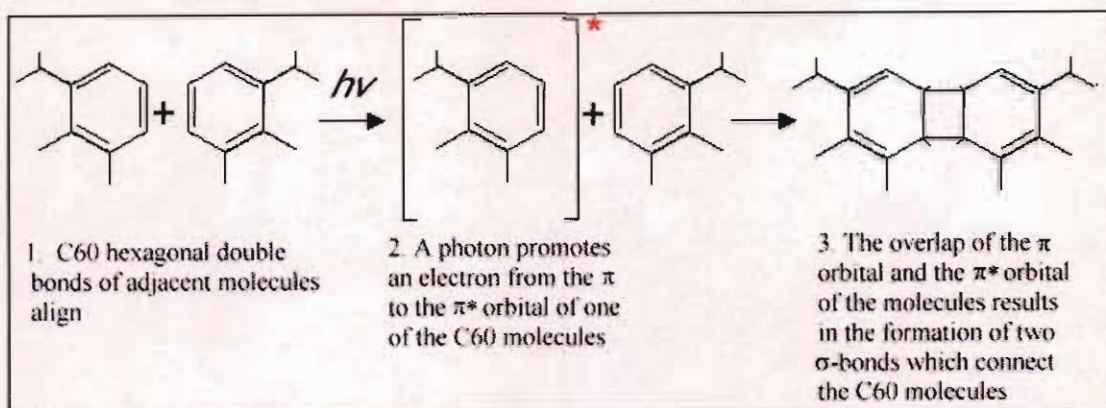


**Figure 5.5.** General reaction scheme of a 2+2 cycloaddition

## 5.6. Summary

Of the many electronically excited states of fullerene molecules, one holds special importance - $T_1$, the lowest lying triplet state. It is typically formed with substantial efficiency following light absorption and persists far longer than any other electronically excited states. These properties give triplet states key roles in most processes involving photochemistry or photophysics of $C_{60}$.

The Raman signature of the optically induced molecular triplet has been identified in both solution and solid, the pentagonal pinch mode for which has been assigned to a position of 1469cm$^{-1}$ shifts to a position of 1466cm$^{-1}$. Figure 5.6 summarises this and all other optically induced species produced in $C_{60}$ thin films. There has also been the identification of a second excited state specific to the solid, assigned with the Raman signature of 1463cm$^{-1}$, as similar measurements in solution show no Raman evolution beyond 1466cm$^{-1}$. This excited state intermediate occurs indirectly during the depolymerisation of $C_{60}$ at high intensities or directly at low temperatures and high intensity.

1. Two $C_{60}$ molecules line up with the hexagonal double bonds adjacent to each other

2. One of the $C_{60}$ molecules has an electron promoted from the $\pi$ to the $\pi*$. i.e. it is an excited state.

hυ

Relaxation

hυ

high intensity

hυ

high intensity

1469cm$^{-1}$

1463cm$^{-1}$  * *

1466cm$^{-1}$

1459cm$^{-1}$

*

4. Continued illumination with high intensities forms a high intensity excited state which is a metastable intermediate between the polymer and the ground state $C_{60}$ molecules

3. Formation of the polymer via the overlap of the $\pi$ orbital and the $\pi*$ orbital hence the 2+2 cycloaddition is completed.

**Figure 5.6.** Summary of the Optically Excited States produced in $C_{60}$ thin films and their Raman Modes. Blue and Red arrows denote the path possible below and above the phase transition temperature (249K) respectively. Multicolored arrows denote that the path is possible at both temperatures.

It has been proposed that the 1463cm$^{-1}$ state is equivalent to states produced by other means. Chemically such insulator to metal transitions can be induced by intersistial doping with alkali metals as discussed earlier. When solid state $C_{60}$ is doped 1:1 with an alkali metal (e.g. K) the complex behaves as a metallic conductor. Similarly when doped 3:1 with an alkali metal it has been shown to be superconducting e.g. $K_3C_{60}$ salts [2,3,4]. Raman spectroscopy of these charge transfer salts has shown that the pentagonal pinch mode (positioned at 1469cm$^{-1}$) down shifts by approximately 6cm$^{-1}$ per dopant ion/atom - species [21]. The charge transfer nature of these salts suggests that these doped systems (i.e. $KC_{60}$ and $K_3C_{60}$) are analogous to the ionic states $C_{60}^{-1}$ and $C_{60}^{-3}$ respectively. Therefore it may be speculated that the Raman signature of these anionic species would experience a similar down shift to those reported for the doped species. Indeed the monoanionic species have been reported to have a Raman signature that is down shifted by 6cm$^{-1}$ [22], leading to speculation that the ionic species $C_{60}^{-1}$ is similar to the optically excited co-operative state reported.

Electronically induced transitions from insulator to metal to superconductor in single $C_{60}$ crystals have been demonstrated recently [23,24], where in a FET geometry pristine fullerene crystals exhibited metallic behaviour at room temperature, as a result of charge induction at a semiconductor fullerene boundary by a gate voltage. At gate voltages sufficient to triply charge the molecules of the interface monolayer a superconducting state at a transition temperature of 11K was observed. $C_{60}$ single crystals intercalated with $CHCl_3$ and $CHBr_3$, in order to expand the lattice have increased this transition temperature further.

The results of the above cases indicate the feasibility of reversibly switching the properties of fullerenes from insulating to metallic to superconducting states by charge injection. Many disadvantages arise from working with crystals. Production of high quality single crystals and contacting on such small structures is difficult. Monitoring of the induced states is also hindered due to the optically thickness of the crystals. This project aims to examine these states in fullerene thin films. The states will be produced electronically and monitored as a function of electrical parameters and spectroscopic signatures particularly Raman. These results will be compared to the signatures of the optically induced states discussed in this chapter. Prior to analysing these results an understanding of the fundamentals of transport in molecular crystals is necessary and will be outlined in the next chapter.

## 5.7. References

1. H.J. Byrne, in *Physics and Chemistry of Fullerenes and Derivatives,* H. Kuzmany, J. Fink, M. Mehring and S. Roth eds., World Scientific Singapore, p183 (1995)

2. R.C. Haddon, A.F. Hebard, M.J. Rosseinsky, D.W. Murphy, S.J. Duclos, *Nature*, **350**, 320-322 (1991)

3. A.F. Hebard, M.J. Rosseinsky, R.C. Haddon, D.W. Murphy, S.H. Glarum, T.T.M. Palstra, A.P. Ramirez and A.R. Kortan, *Nature*, **350**, 600-601 (1991)

4. M.J. Rosseinsky, A.P. Ramirez, S.H. Glarum, D.W. Murphy, R.C. Haddon, A.F. Hebard, T.T.M. Palstra, A.R. Korton, *Am. Phys. Soc.,* **60**, 2830-2832 (1991)

5. S. Leach, M. Vervloet, A Després, E. Bréheret, J.P. Hare, T.J. Dennis, H.W. Kroto, R. Taylor and D.R.M. Walton, *Chem. Phys.,* **160**, 451 (1992)

6.    H.J. Byrne, W.K. Maser, W.W Rühle, Λ. Mittelbach, W. Hönle, H.G. von Schnering, B. Movaghar and S. Roth, *Chem. Phys. Lett.,* **204**, 461-466 (1993)

7.    H.J. Byrne, W.K. Maser, M. Kaiser, L. Akselrod, W.W. Rühle, X.Q. Zhou, A. Mittelbach and S.Roth, *Appl. Phys. A,* **57,** 81 (1993)

8.    A.T. Werner, J. Anders, H.J. Byrne, W.K. Maser, M. Kaiser, A. Mittelbach and S. Roth, *Appl. Phys. A.,* **57**, 157 (1993)

9.    H.J. Byrne, W.K. Maser, M. Kaiser, L. Akselrod, A.T. Werner, J. Anders, X.Q. Zhou, G. Mahler, T. Kuhn, A. Mittelbach and S. Roth, *Appl. Phys. A*, **57**, 303 (1993)

10.   H.Kuzmany, M. Matus, T. Pichler and J. Winter, in *Physics and Chemistry of Fullerenes,* K. Prassides ed., Klewer Academic, Dordrecht (1994)

11.   G. Chambers, H.J. Byrne, *Chem. Phys. Lett.,* **302**, 307-311 (1999)

12.   M.S. Dresselhaus, G. Dresselhaus and P.C. Eklund, *Science of Fullerenes and Carbon nanotubes,* Academic Press, London (1996)

13.   G. Chambers, A.B. Dalton, L.M. Evans, and H.J. Byrne, *Chem. Phys. Lett.,* **345**, 361-366 (2001)

14.   J.B. Birks, *Organic Molecular Photophysics,* John Wiley and Sons, London, (1975)

15.   P.W. Atkins, *Physical Chemistry,* 426-531 (oxford University Press 1990)

16.   P.H.M. van Loosdrecht, P.J.M van Bentum and G. Meijer, *Chem. Phys. Lett.,* **205**, 191, (1993)

17.   J, Shinar, Z.V. Vardeny, Z.H. Kafafi, *Optical and electronic properties of fullerenes and fullerene-based materilals,* Marcel Dekker Inc. New York (2000).

18.   L. Akselrod, H.J. Byrne, *Chem.Phys. Lett.,* **302**, 307 (1993)

19.   A.M. Rao, P. Zhou, K.A. Wang and P.C. Eklund, *Science,* **259,** 955, (1993).

20.   P.C. Eklund, A.M. Rao, Y. Wang, P. Zhou, M.J. Holden and K.A. Wang, in *Progress in Fullerene Research,* H. Kuzmany, J. Fink, M. Mehring and S. Roth eds, World Scientific Singapore 336, (1994).

21.   H. Kuzmany, M. Matus, B. Burger, J. Winter, *Adv. Mater.,* **10**, 731, (1994)

22.   C. Kvarstrom, H. Neugebauer, G. Matt, H. Sitter, N.S. Sariciftci, *Synthetic Metals,* **103**, 2430 (1999)

23.   J.H. Schön, Ch. Kloc and B. Batlogg, *Nature,* **408**, 549-552 (2000)

24.   J.H. Schön, Ch. Kloc and B. Batlogg, *Science,* **293**, 2432-2434 (2001)

# Chapter 6

## Transport Processes in Molecular Solids

### 6.1. Introduction

As discussed in chapter 1, $C_{60}$ is a molecular insulator but under certain circumstances it can change its properties in the solid state from insulating to conducting to even superconducting [1,2,3,]. Chapter 4 showed $C_{60}$ to be a molecular solid, as in it consists of molecules which are so stable that they retain much of their individuality when brought into close proximity. The spectroscopy of the fullerene molecule has been presented in previous chapters. Notably the departure from molecular behaviour in the solid form was of particular interest, indicating intermolecular electronic communication. In Chapter 7 the electronic properties of $C_{60}$ thin films under high voltages will be probed, so therefore in advance the electronic transport processes in solids must be outlined with particular attention paid to molecular solids.

### 6.2. Types of Solids

Solid state materials can be grouped into three classes, insulators, semiconductors and conductors depending on their conductivity, insulators having a very low conductivity and conductors having a very high conductivity. The conductivity of a semiconductor is between those of insulators and those of conductors, and is generally sensitive to temperature, illumination, magnetic field and minute amounts of impurity atoms. This sensitivity in conductivity makes semiconductors one of the most important materials for electrical applications.

In the gaseous state the average distance between molecules (or atoms) is large compared to the size of a molecule, so the molecules may be regarded as isolated from one another. Many substances, however, are in the solid state at ordinary temperatures and pressures. In that state the molecule can no longer be regarded as isolated. Their separation is comparable to the molecular size, and the strength of the forces binding them together is of a similar order of magnitude as the forces binding the atoms into the molecule. Hence, the properties of a molecule are altered by the presence of neighbouring molecules. Characteristic of crystalline solids is the regular arrangement of molecules; a recurrent or periodic pattern called a crystal lattice. In a

crystal, a molecule never strays far from a single fixed position. For a given material, there is a unit cell that is representative of the entire lattice. By repeating the unit cell throughout the crystal one can generate the entire lattice. The solid can be regarded as a large molecule, the forces between atoms being due to interaction between atomic electrons. Solids are classified according to the predominant type of binding, the principle being molecular, ionic, covalent and metallic.

Ionic solids consist of a close regular three-dimensional array of alternating positive and negative ions having a lower energy than the separated ions. The structure is stable because the binding energy due to the net electrostatic attraction exceeds the energy spent in transferring electrons to create the isolated ions from neutral atoms, just as for ionic binding in the molecules. The ions are arranged in close packed spheres and the crystal geometry depends on which arrangement minimises the energy, and in turn depends on the size of the ions involved. Because there are no free electrons to carry energy, or change from one part of the solid to another, such solids are poor conductors [4] e.g. NaCl.

Covalent solids contain atoms that are bound by shared valence electrons, as in covalent binding of molecules. The bonds are directional and determine the geometrical arrangement of atoms in the crystal structure. The rigidity of their electronic structure makes covalent solids hard and difficult to deform. Because there are no free electrons covalent solids are not good conductors e.g. diamond. However sometimes, as for silicon or germanium, they are semiconductors.

Metallic solids are materials in which the valence electrons are spatially delocalised throughout the solid and not confined to regions of high electron density and for which concomitantly the electrical conductivity is very high. An example of a metallic solid is a regular lattice of spherically symmetrical positive ions arranged like close packed spheres through which the electrons move. The electrons move in the combined potential of all the positive ions and are shared by all the atoms in the crystal. The atoms have vacancies in their outermost electron subshell and there are not enough valence electrons per atom to form tight covalent bonds, hence the electrons are shared by all the atoms and are free to wander through the crystal from atom to atom, there being many unoccupied electronic states.

Molecular solids consist of molecules that are so stable that they retain much of their individuality when brought into close proximity. The covalent bonds within the molecules are distinctly stronger than the intermolecular binding, and the constituents of the solid preserve their molecular character. The intermolecular binding force is the weak van der Waals attraction that is present between such molecules in the gaseous phase. Although the van der Waals interaction is ubiquitous, because it is so relatively weak, it is only important in those solids where other interactions (ionic, covalent, and metallic) are absent. The physical mechanism involved in van der Waals attraction is an interaction between electric dipoles. This attractive interaction arises for example from induced dipole – induced dipole interactions between two even closed shell molecules with spherically symmetric charge distributions, as a result of fluctuations in the charge distribution. In the solid, successive molecules have electric dipole moments which alternate in orientation so as to produce successive attractions. Many organic compounds, inert gases and ordinary gases such as oxygen, nitrogen and hydrogen form molecular solids [4].

## 6.3. Band Theory of Solids

### 6.3.1. Introduction

There is an enormous range of values of resistivity of solids. Properties of solids in general and metals in particular can be explained by the concept of band structures. This section will firstly show an overview of the early theories, which could explain some, but far from all the properties of solids. It will introduce some basic tools that are necessary for treating problems in periodic structures, and then will introduce Bloch's theorem, which is the cardinal theorem of solid state physics. This information provides the necessary machinery to define and discuss band structure.

### 6.3.2. Drude's Model

The first major step in understanding the electrical properties of solids was taken by Drude in 1905 [5]. The theory that Drude developed was naturally based on classical principles. The theory made an important assumption that is the 'independent electron approximation'. A metal contains a very large number of electrons. In principle the interaction of each electron with all others in the solid via the coulomb electrostatic interaction should be considered. This is clearly impossible to do in practice, so what

is done is to assume that each electron moves in an average potential created by all other electrons, as well as the positive ions in the crystal. Thus the motion of one electron can be treated independently, and simply add the contributions of the individual electrons to get the collective response.

In the classical free electron theories, including that formulated by Drude, there are the following assumptions in addition to the independent electron approximation.

1) Conduction is entirely by electrons
2) The sample defines a flat-bottomed potential well within which the electrons are constrained and within which they are free to move.
3) The electrons behave as a classical gas i.e.
   a) They are distinguishable.
   b) They are small and take up negligible volume.
   c) They have random motion.
   d) They are perfectly elastic.
4) There are no quantum restrictions on the electron energy i.e. the energy distribution of the electrons is a perfect combination.
5) A collision indicates the scattering of an electron by (and only by) an ionic core i.e. the electrons do not collide with anything else. These collisions occur at an average time $\tau$.
6) Collisions are instantaneous and result in a change in electron velocity.
7) An electron suffers a collision with the probability per unit time, $\tau^{-1}$ (the relaxation approximation) i.e. $\tau^{-1}$ is the scattering rate.
8) Electrons achieve thermal equilibrium with their surroundings only through collisions.

Drude used the concept of electron gas and applied assumptions similar to those of ideal gas theory. Accordingly, he set out that the particles (electrons and ions) only interact when colliding and that the volume of the particles are much less than the volume of the gas. The collisions between the electrons and the presumably fixed ions are regarded as elastic and the electron-electron and electron-ion interactions were neglected. The relaxation process after collisions was assumed to be independent of the state of the electrons prior to collision. This treatment made it possible to calculate properties of heated and electrical conductivites by simple mathematics. In addition

Drude's theory makes the assumption that all electrons have an average energy. It is seen that the application of statistical mechanics to a large ensemble of classical particles predicts a probability distribution for the electron energy known as the Boltzman distribution and the Drude assumption is clearly a very drastic approximation - this treatment had many shortcomings. The actual electron density in a solid can be at least 1000 times the density of an ideal gas and therefore suggests further interaction than mere elastic collisions. The ions are not fixed and do vibrate and thereby contribute themselves to the properties of a solid. Although Drude's theory has some false basic assumptions it did have some fortuitous successes. The probability of finding an electron at a certain velocity is governed by a so-called distribution function, which in the case of Drude was assumed to be a Maxwellian, a distribution function commonly found in thermodynamics [5].

### 6.3.3. Free Electron Model

Other models, for example the Sommerfeld model, refined Drude's theory by utilising the Fermi-Dirac distribution, which is widely used in quantum mechanics. Although Sommerfeld could explain more experimental results this model was also too simple. According to the free electron model (Sommerfeld model) the most weakly bound electrons of the constituent atoms move about freely through the volume of the metal. The valence electrons of the atoms become the conduction electrons. Forces between conduction electrons and ion cores are neglected in the free electron approximation. All calculations proceed as if the conduction electrons were free to move anywhere within the material. The total energy is all the kinetic energy; the potential energy is neglected. Even in metals for which the free electron model works well, the actual charge distribution of the conduction electrons is known to reflect the strong electrostatic potential of the ion cores.

Conduction electrons in all metals are observed to act very much like free electrons, except those metals where the d or f shell electrons overlap or fall close in energy to the conduction band. Electrons in the d shells tend to be more localised and less mobile than electrons in s and p shells. Conduction electrons in a simple metal originate from the valence electrons of the constituent atoms, e.g. in Na, the neutral atom has the electronic configuration $1s^2\ 2s^2\ 2p^6\ 3s^1$, and the valence electron in this case is the single 3s electron. Ionisation of the valence electron leaves behind the core

electrons, having an inert gas like configuration, and they remain tightly bound to the nucleus (in the case of $Na^+$ the core electrons are set $1s^2\ 2s^2\ 2p^6$). In the case of transition metal and rare-earth elements, the d- and f- electrons, even in partially filled shells are sufficiently tightly bound to the nucleus that they do not contribute to free electron gas. The model assumes that the ion cores (the atomic nuclei plus core electrons) have a negligible size (i.e. the valence-electron gas is free to explore all points in the volume). Another assumption underlying the free electron gas model is that the valence electrons experience everywhere in the solid a constant electrostatic potential. This is untrue in practice, since the ion cores will actually be the sites of deep minima in the potential, but nevertheless it is often a reasonably good approximation that the potential associated with the ion cores is constant between ionic sites.

In the simplest version of the free-electron-gas model, any 'graininess' associated with the individual atoms is smoothed out. Hence it is assumed that the net charge associated with the ion cores (as well as the rest of the valence electrons) is uniformly distributed throughout the volume of the solid. A valence electron experiences a constant potential everywhere, except at the surfaces of the solid where there is a potential barrier preventing escape of electrons out of the solid. The potential model is therefore that of the 3D square-well, particle-in-a box: an electron having a total energy. The scenario whereby all free electrons have the same average energy and the electrons are treated as classical distinguishable particles, as in a normal gas, is known as the Drude model as discussed earlier.

### 6.3.4. Motion of an Electron

Contrary to classical mechanics used in previous models, where the position of particles are described unambiguously by co ordinates in the 3D space, an electron in a microscopic structure is treated quantum mechanically and is thereby represented by a probability wave function. The allowed electronic states must be solutions of the Schrödinger equation which, in the general case where the potential energy V is a function of both space and time is,

$$\frac{-\eta^2}{2m_e}\nabla^2\Psi(r,t)+V(r,t)\Psi(r,t)=i\eta\frac{\partial}{\partial t}[\Psi(r,t)] \qquad\qquad \text{Eq.6.1}$$

where $m_e$ is the electron mass and $\Psi(r,t)$ is the electron wavefunction i.e. the wave-like solution of Eqn.6.1. For the case of a potential energy that is time-independent, $V(r,t)=V(r)$, the wave function can be separated into the product of a spatially varying and a time dependent part, via,

$$\Psi(r,t) = \psi(r)\phi(t)$$
Eq.6.2

To calculate the motion of the electrons the Schrödinger wave equation, which is the fundamental equation describing the state of microscopic particles in the same way as Newton's law is used for describing the motion of a classical body.

$$\frac{-\eta^2}{2m_e}\nabla^2\Psi(r) + V(\Psi)(r) = \xi\psi(r)$$
Eq.6.3

In this equation the first term accounts for the kinetic energy corresponding to the $1/2mv^2$ term in Newton's second law. $V(r)$ is a potential representing external influence on the motion of the electrons in question. In the case of free electrons, this potential is identically zero. Solving this equation for the free electron case gives a quadratic of the particle energy on the wave vector k (or momentum $\eta k$),

$$\xi(K) = \frac{\eta^2 k^2}{2m_e}$$
Eq.6.4

The relationship between the wave vector and the energy is called the dispersion and is the fundament for determining most of the properties of solids, including their transport properties, for example both thermal and electrical conductivities as well as information about optical properties.

### 6.3.5. Electrons in periodic solids

Although the Free Electron Model has virtues of being simple and capable of accounting for some physical properties of solids e.g. it gives a good insight into the heat capacity, thermal conductivity, electrical conductivity, magnetic susceptibility and electrodynamics of solids, nevertheless it has a number of severe limitations. The model fails to help with distinguishing between metals, semiconductors and insulators. The free electron gas theory ignores the fact that crystalline solids have a periodicity. It predicts that every solid containing elements with part filled electron

shells should exhibit metallic behaviour, this prediction fails spectacularly in the case of elements such as Si or Ge which have incomplete p-shells, but which are nevertheless electrical insulators at absolute zero [6]. The inconsistencies with the free electron model can be explained by taking into account the fact that the motion of the electrons is not free but is constrained by the spatial arrangement of the potentials associated with the ion cores.

As the electrons move in a solid there will be a non-negligible interaction between the electron and the ions in the solid. This interaction is expressed by adding a non-zero potential to Eq.6.3. As a result of the periodic arrangement of the ions, the potential will be periodic, i.e. it can be written $V(r)=V(r+R)$, (where R is a lattice vector). The dispersion will now look different from the free electron case because this potential enters the Schrödinger equation and leads to different solutions. The electrons obeying this modified Schrödinger equation are called Bloch electrons in contrast to free electrons. Their behaviour is summarised by the Bloch theorem that states that electrons in periodic potentials are described by plane waves multiplied by a function having the same periodicity as the lattice.

One form of the Bloch function is,

$$\psi_k(r+R) = e^{ik.R}\psi_k(r)$$
<div align="right">Eq.6.5</div>

An equivalent form for the Bloch function is that the wavefunction is the modulated plane wave,

$$\psi_k(r) = e^{ik.r}u_k(r)$$
<div align="right">Eq.6.6</div>

where $u_k(r)$ is a function with the same periodicity as that of a 3D lattice,

$$u_k(r+R) = u_k(r)$$
<div align="right">Eq.6.7</div>

The wave vector k associated with Bloch's theorem is not the electron momentum times the Planck's constant as would have been the case for a free electron described by plane waves. Instead it should be regarded as a quantum number just as the momentum p is the quantum number for motion in free space. This can be illustrated by letting the momentum operator act on the wave function, Eq.6.6. It follows that the

result is not in general a constant times the wave function and thus Eq.6.6 is not a momentum eigenstate. However, the similarity with the ordinary momentum leads us to define the crystal momentum as $\eta k$ where k is the wave vector of the Bloch wave function.

### 6.3.6. Energy bands

Using a result derived from the definition of the reciprocal lattice $e^{ikr}=1$, where k is a reciprocal lattice vector, leads to the fact that the eigenstates of Eq. 6.6 and their corresponding eigenvalues are periodic functions of the wave vector k in the reciprocal lattice. The eigen energies $e_n k(k)$ are thus continuous and periodic functions in k-space. These functions are referred to as the band structure of the solid.

It should be noted that a particular k-vector is not unique. An infinity of equivalent vectors may be generated. Each wave function is labelled with the smallest vectors in the set of wave vectors for that function. Therefore the k-vectors which are most significant are known. Any wave vector whose tip lies inside the perpendicular bisector of the reciprocal lattice vector is the smallest which can be generated, hence the first Brillouin zone, the smallest volume enclosed by the perpendicular bisectors (planes) of the reciprocal lattice vectors, contains all the most significant wave vectors. There are regions of energy for which no Bloch function solutions of the wave equation exist. These energies form forbidden regions in which the wavefunctions are damped in space and the values of the k's are complex.

Every solid contains electrons. The important question for electrical conductivity is how the electrons respond to an applied electric field. Electrons in crystals are arranged in energy bands separated by regions in energy for which no wavelike electron orbitals exist. Such forbidden regions are called energy gaps or band gaps, and result from the interaction of the conduction electron waves with the ion cores of the crystal. The crystal behaves as an insulator if the allowed energy bands are either filled or empty, for then no electrons can move in an electric field. The crystal behaves as a metal if one or more bands are partly filled. The crystal is a semiconductor or a semimetal if all bands are entirely filled except for one or two bands slightly filled or slightly empty. If an electric field is applied to the solid the electrons will acquire extra energy only if there are available empty levels within the

range of energy that the strength of the applied field allows the electron to gain. If there are no nearby empty levels, then the electron will not be able to gain any energy at all and the solid behaves like an insulator. What counts in determining the emptiness, or fullness, of the bands containing valence electrons is the valence of the atoms forming the solid, and the geometry of the crystal lattice into which they solidify. An isolated band will be full if a unit cell of the crystal lattice contains two valence electrons, one for each of the two possible values of the spin quantum number $m$.

A unit cell is the smallest geometrical arrangement of atoms that by periodic repetition can fully describe the geometrical arrangement of the atoms in the complete crystal. In a crystal lattice some or all of the degeneracy of the atomic valence electron levels with respect to the quantum number, $m$, is removed because these electrons are not in the spherically symmetrical potential of an atom in free space, but in a potential whose more complicated symmetry depends on the crystal geometry. For example the three degenerate levels from a p subshell of a single atom lead to three bands of N levels, each capable of holding two electrons of opposite spin, in a crystal containing N of these atoms. These bands may be completely nonoverlapping, partly overlapping, or completely overlapping in energy, depending on the crystal geometry. The term isolated band, used in expressing the condition of a full band, refers to a case in which these bands do not overlap each other or bands from another subshell.

When predicting whether a solid is an insulator or not the issue of band overlap is important, and this depends on the geometry of the crystal structure. If a completely filled band in terms of valence overlaps with a completely empty band, then there will be two partially filled bands, resulting in a solid that might have been an insulator actually been a conductor. However a solid cannot be an insulator unless one of its unit cells contains an even number of valence electrons, because an odd valence electron can never be in a filled band. At temperatures above absolute zero it is possible for some electrons to gain enough thermal energy to jump over the energy gap of a forbidden band of energy into a higher allowed band, thereby creating vacancies in the lower allowed band and making a new allowed band available. The nearly filled band is referred to as a valance band and the nearly empty band as the

conduction band. The probability of this happening increases with temperature, and it depends strongly on the width of the energy gap. Substances in which the width of the energy gap is small are called semiconductors, they become reasonably conductors at room temperatures though at low temperatures are insulators. Solids with a large energy gap will remain insulators even at relatively high temperature.

## 6.4. Sources of resistance

It was seen that even in the early models some sort of electron scattering mechanisms had to be invoked that gave a scattering rate by definition of $\tau^{-1}$. An obvious potential source of scattering is between electrons themselves especially if the electron density is very high, as it is in metals. According to the independent-electron approximation, such electron-electron interactions do not exist. Also the Bloch theorem shows that electron lattice interactions are critical in determining the electronic structure of a solid. The occurrence of electron-electron collisions and electron-lattice interactions are breakdowns of the one-electron approximation.

### 6.4.1. Electron-Defect and Electron-Phonon Scattering

When considering scattering mechanisms that occur, the obstacles with which the electrons collide, must be identified. The ions making up the crystal lattice is an immediate answer. The spacing between ions or atoms in all solids is of the order of 1Å, and the mean free path would be of a similar magnitude. While not apparent in the free electron model, it turns out that the conduction electrons are not scattered by the ions in a perfectly periodic lattice (Energy band theory explains this in terms of the electron wavefunction taking up the periodicity of the lattice). However, the lattice is not always perfectly periodic. This departure from periodicity can arise in two ways.

#### 6.4.1.1 Electron –Defect Scattering

The first is that the lattice may be imperfect. A real lattice may contain impurity atoms, which do not fit properly into the host lattice. It may also have a certain number of vacant sites, lattice sites where no ion is present. It may also have linear defects known as dislocations or planar defects such as stacking faults, boundaries where the sequential stacking of atomic planes are interrupted. Polycrystalline materials will have many boundaries between small crystallites oriented in different

directions. At low temperatures these crystal defects provide the dominant scattering mechanism. The mean free path is almost independent of temperature and varies with the perfection of the specimen. It is therefore a temperature independent contribution to the electrical resistivity.

### 6.4.1.2 Electron-Phonon Scattering

The second departure from periodicity occurs as the temperature rises and the crystal lattice begins to vibrate. Such vibration means that the conduction electrons will very often experience ions which are a long way from their equilibrium positions and this causes scattering of the conduction electrons. The lattice vibration is a collective effect because neighbouring ions interact strongly. These collective vibrations must be zero at the specimen boundary and the solution of the wave equation for the elastic wave leads to quantisation of the lattice vibrations. The quanta of elastic energy can be considered as quasi-particles and these are known as phonons. It is convenient to consider the scattering of electrons by the vibrating lattice in terms of particle-particle collisions between electrons and phonons. The lattice dynamics can show that the phonon density varies linearly with temperature at around room temperature. This implies that the mean free path varies inversely with temperature so therefore the electrical resistivity varies linearly with temperature at around room temperature.

The two types of scattering mechanism are defect and thermal, and the resistivity is the sum of a temperature independent part and a temperature dependent part. At temperatures well above absolute zero, the dominant cause of electron scattering is due to phonons: a phonon can always be emitted by an electron, thereby scattering the electron to another state or at elevated temperatures when the number of excited phonons is large, a phonon can be absorbed.

### 6.4.2. Electron-Electron Scattering

Due to the interaction of the conduction electrons with each other through their electrostatic interaction, the electrons suffer collisions. Also, a moving electron causes an inertial reaction in the surrounding electron gas, thereby increasing the effective mass of the electron. Electron–electron scattering does not give a direct contribution to the resistivity. However it has an indirect effect. It affects the occupation numbers of the electron states and therefore modifies the defect and phonon scattering.

In the conventional picture electrons are prohibited from scattering at low temperatures, as the temperature precisely determines the number of final states for a given electron to scatter into. Additional considerations following the Pauli exclusion principle add further constraints on the phase space for scattering. It was found that electron-electron scattering is in general negligible because of the influence of this principle. It is an astonishing property of solids, in particular metals, that conduction electrons, although crowded together only 2Å apart, travel long distances between collisions with each other [6]. The mean free paths for electron-electron collisions are longer than $10^4$Å at room temperature and longer than 10cm at 1K. Two factors are responsible for these long mean free paths, without which the free electron model would have little value: the most powerful being the Pauli exclusion factor as stated above and the second factor is the screening of the Coulomb interaction between two electrons.

At low concentrations, electrons in a semiconductor do not significantly influence the conductivity, their contribution is typically less than the phonon contribution thus the conductivity is much like an insulator, where the electron-phonon scattering and hence the conductivity is strongly temperature dependent. A semiconductor/insulator is thus characterised by an electrical conductivity which is strongly activated by increasing temperature. On the other hand, if semiconductors are heavily doped and the temperature is high, the Fermi level may enter a conduction or valence band and the material then behaves more "metallic like" [7]. In a metal, electrons are the primary carriers of energy and the electron contribution to the conductivity is dominant and independent of temperature [7].

## 6.5. Transport Properties in Molecular Materials

As opposed to covalent solids and atomic materials, molecular solids are made up of discrete units, weakly bound typically by van der Waals forces, in which electrons are localised. Within a conjugated system, the electrons can have high mobility but require energy to make the spatial transition to another molecule. Organic molecular systems can be either amorphous (as in the case of polymers) or crystalline (as in the case of fullerenes). The process of intermolecular transport can therefore be complex. In most cases the transport is a hopping-like process and can be thermally activated.

72

### 6.5.1. Thermally Activated Hopping

In systems where conductivity is dominated by thermally activated hopping, at low temperatures, the electrons which carry current through the material, are generally bound in potential wells resulting from defects, impurities, known collectively as traps or in the case of crystalline molecular materials the molecules themselves. For example, assuming that the potential wells are an energy, $\Delta$ deep; if the electrons are given a thermal energy, $\Delta$, they can escape and move through the substance (hence carrying a current) until they fall into another potential well. In such situations the electrical conductivity, $\sigma$, is roughly proportional to the probability that electrons can escape the traps. In a perfect molecular crystal, this trap energy is a single characteristic property of the molecule and the lattice packing and the conductivity is given by

$$\sigma \approx Ae\left(\frac{-\Delta}{K_B T}\right) \qquad\qquad \text{Eq.6.8}$$

where $A$ is a constant, $T$ is the temperature.

The localisation of the electronic wave function in these materials results in the transport of charge carriers via thermally activated hops with carrier mobility as a strong function of temperature and electric field. This hopping mobility is usually characterised by an increase in current with an increase in temperature.

### 6.5.2. Variable Range Hopping

In materials containing a large number of defects or with a disordered structure (non crystalline-molecular solids) the electrons which carry the current are in what is effectively a random potential (spatially the potential energy moves up and down randomly). The electrons gravitate to the potential wells (i.e. dips in the potential) at low temperatures; they can then move through the system by hopping to adjacent potential wells. As opposed to thermally activated hopping above there is no single activation energy which defines the system This is know as variable range hopping and the conductivity has a very distinctive temperature dependence,

$$\sigma = C \exp\left(\frac{D}{T^{\frac{1}{4}}}\right) \qquad\qquad\qquad \text{Eq.6.9}$$

where $C$ and $D$ are constants. It is the temperature exponent (1/4) that identifies this mechanism of conduction, typical of non crystalline molecular solids.

## 6.6. Fullerene conductivity

The electronic properties of solid state fullerenes are critically dependent on local environment and crystal packing [8], where thermal annealing has been shown to induce a transition from a thermally activated mechanism to a more "metallic-like" temperature independent behaviour.
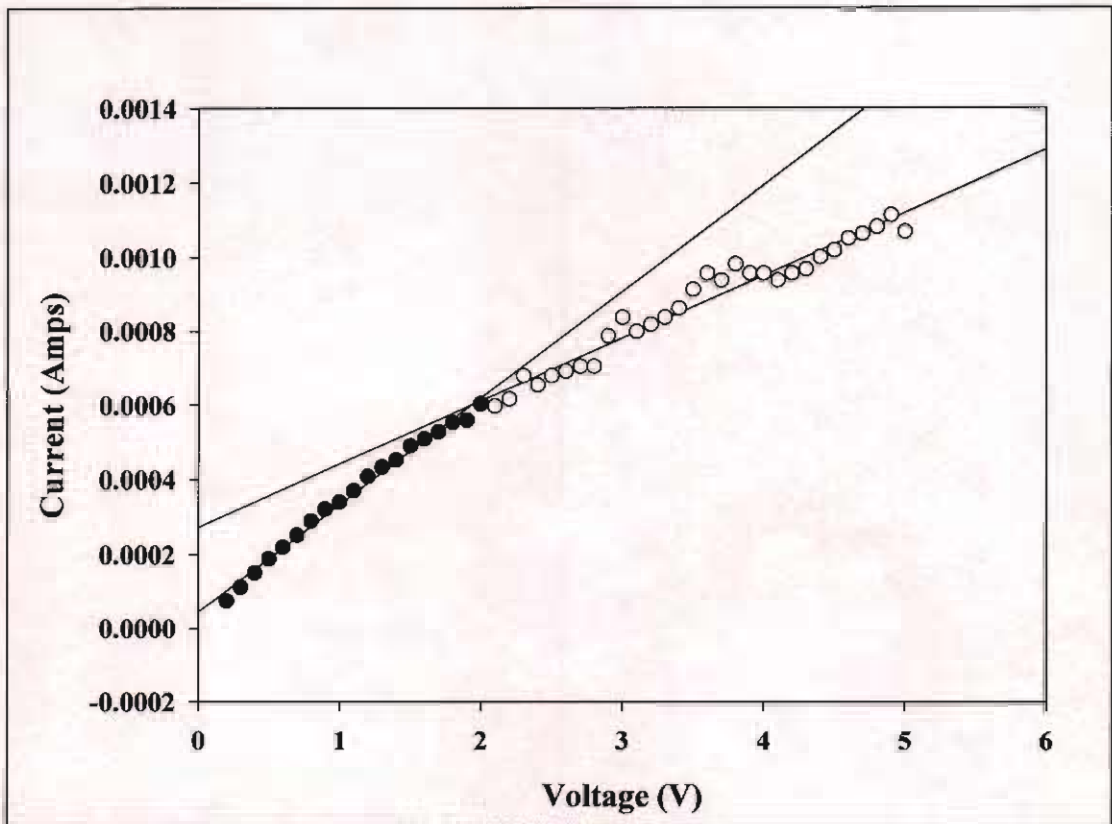


**Figure 6.1.** Current-voltage characteristics observed in low voltage region of pristine $C_{60}$ Film at room temperature.

Thin films of $C_{60}$ were made according to section 3.3, they were electrically contacted in a cryostat and the current voltage measurements were recorded with a Keithley 237 programmable electrometer were the voltage was varied while measuring current. Figure 6.1 shows the low voltage region of the current-voltage (IV) characterisation

of a $C_{60}$ film. The IV is initially ohmic with a conductivity of ~$6.0 \times 10^{-8} Scm^{-1}$, determined from the slope from the beginning of the graph of $2.9 \times 10^{-4} A/V$, film thickness of $1.0 \times 10^{-4} cm$, and film area of $0.48 cm^2$. As the voltage is increased the conductivity decreases to $3.5 \times 10^{-8} Scm^{-1}$ determined from the second half of the graph with a slope of $1.7 \times 10^{-4} A/V$. Values for conductivity measurements of $10^{-10} Scm^{-1}$ for untreated $C_{60}$ films have been previously reported [8]. The lower conductivity of these films may be due to fact that they were measured in a planar geometry where conductivity is limited by polycrystalline domain boundaries. The sandwich geometry $C_{60}$ film shows an insulating behaviour of low conductivity at low voltages and a temperature dependence study was carried out to investigate this behaviour. The results of this study are shown in figure 6.2.
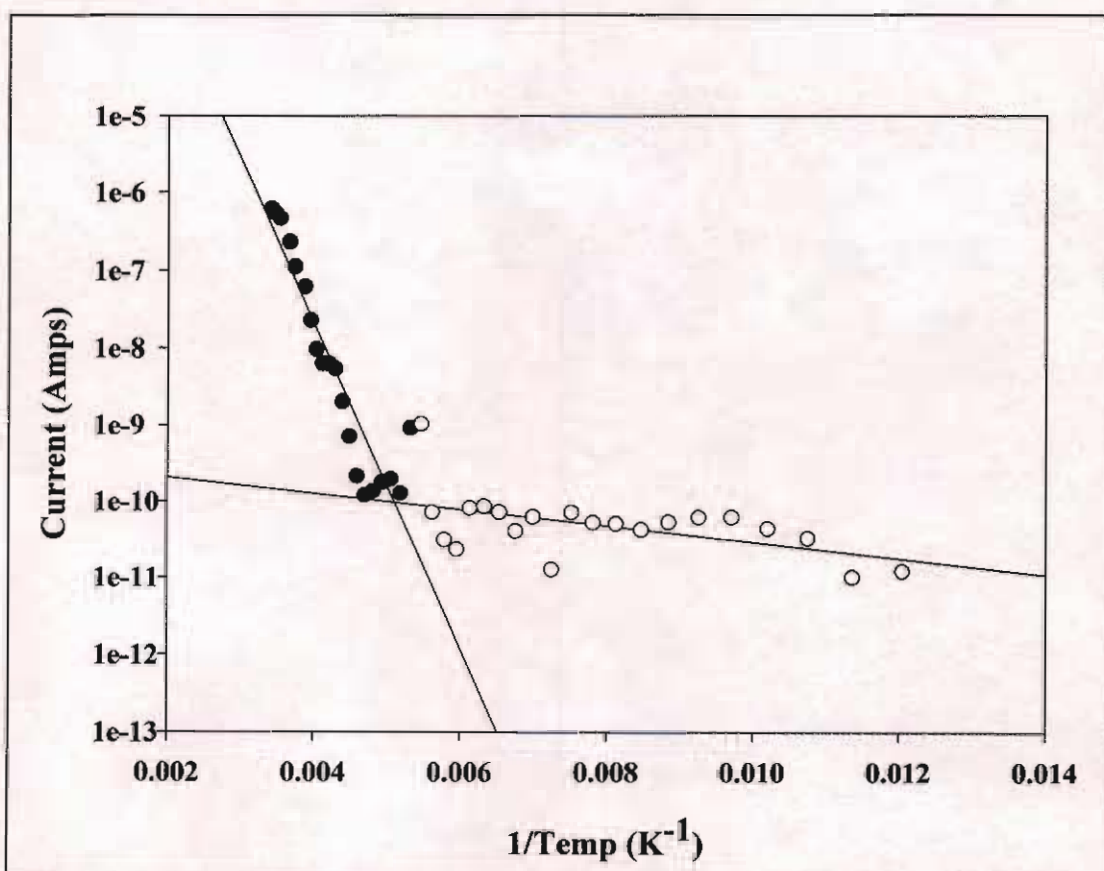


**Figure 6.2.** Temperature dependence of low conductivity of Pristine $C_{60}$ Film.

The temperature dependence of conductivity was performed by subjecting the $C_{60}$ sample to 1V, holding it at this voltage and noting the current as the temperature was decreased from 293K to 78K. If the samples were in an insulating state it would be expected that the current would decrease as the temperature was decreased, at these

low voltages. Normal behaviour of a molecular insulator is thermally activated hopping, characterised by Eq. 6.8. Figure 6.2 shows a decrease in current as the temperature is decreased as expected, however interestingly the rate of decrease of the current changes abruptly as it goes through the phase transition temperature. The activation energy above the transition temperature is very much higher than below. This implies that the intermolecular hopping energy is significantly increased above the transition temperature. This is consistent with decreased intermolecular mobility due to rotational motion [9].

## 6.7. Conductivity of annealed Fullerene films
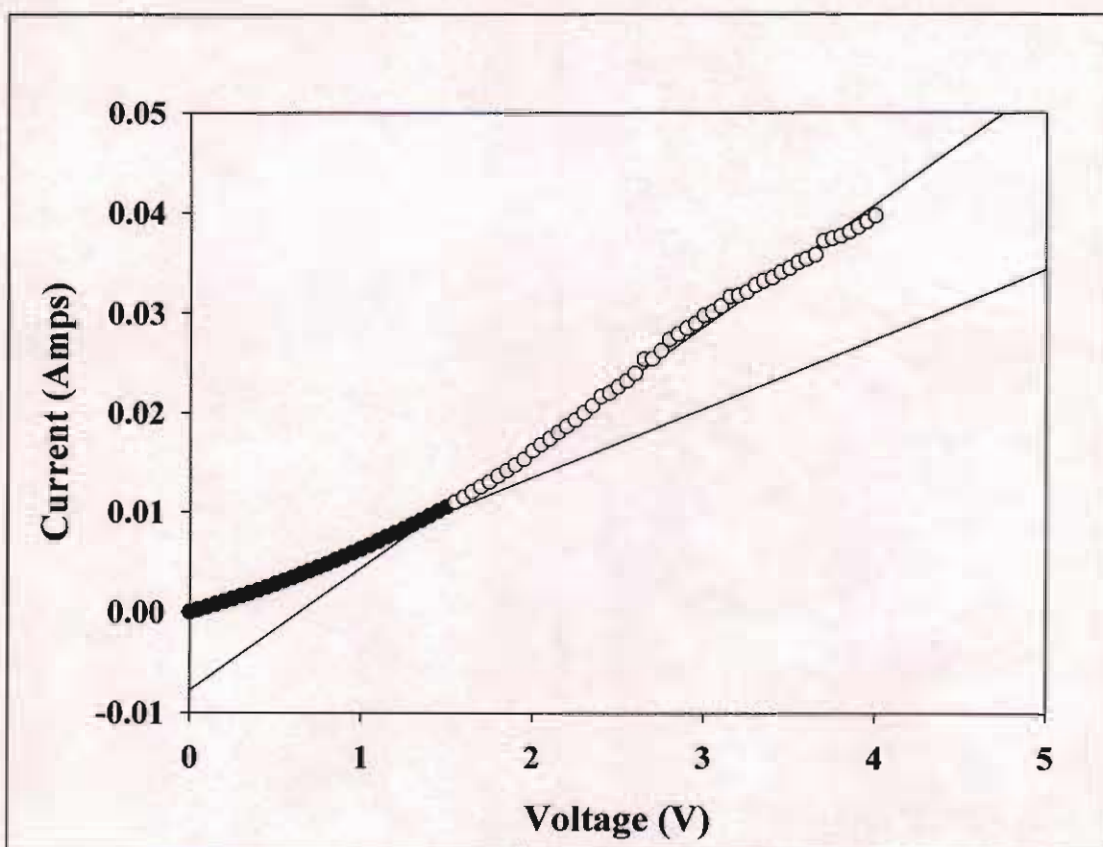


**Figure 6.3.** Current-voltage characteristics observed in low voltage region of Annealed $C_{60}$ Film at room temperature

The conductivity measurements of annealed $C_{60}$ films were also investigated. Annealed films of $C_{60}$ were made according to section 3.3.2, they were electrically contacted in a cryostat and the current voltage measurements were recorded with a Keithley 237 programmable electrometer were the voltage was varied while

measuring current. Figure 6.3 shows the low voltage region of the current-voltage (IV) characterisation of an annealed $C_{60}$ film.

The annealed film shows a higher conductivity at low voltages compared to the same region in the pristine film. The IV initially has a conductivity of $1.456 \times 10^{-6} Scm^{-1}$, determined from the slope from the beginning of the graph of $6.989 \times 10^{-3}$, film thickness of $1.0 \times 10^{-4} cm$, and film area of $0.48 cm^2$. As the voltage is increased the conductivity increases to $2.534 \times 10^{-6} Scm^{-1}$ determined from the second half of the graph with a slope of $1.216 \times 10^{-2}$. Annealing results in increased conductivity by a factor of ~42. Similar values for conductivity measurements of $10^{-6}$ $Scm^{-1}$ for annealed $C_{60}$ films have been previously reported [1]. A temperature dependence study was carried out to investigate the difference in the conductivity measurements between the pristine and annealed films.
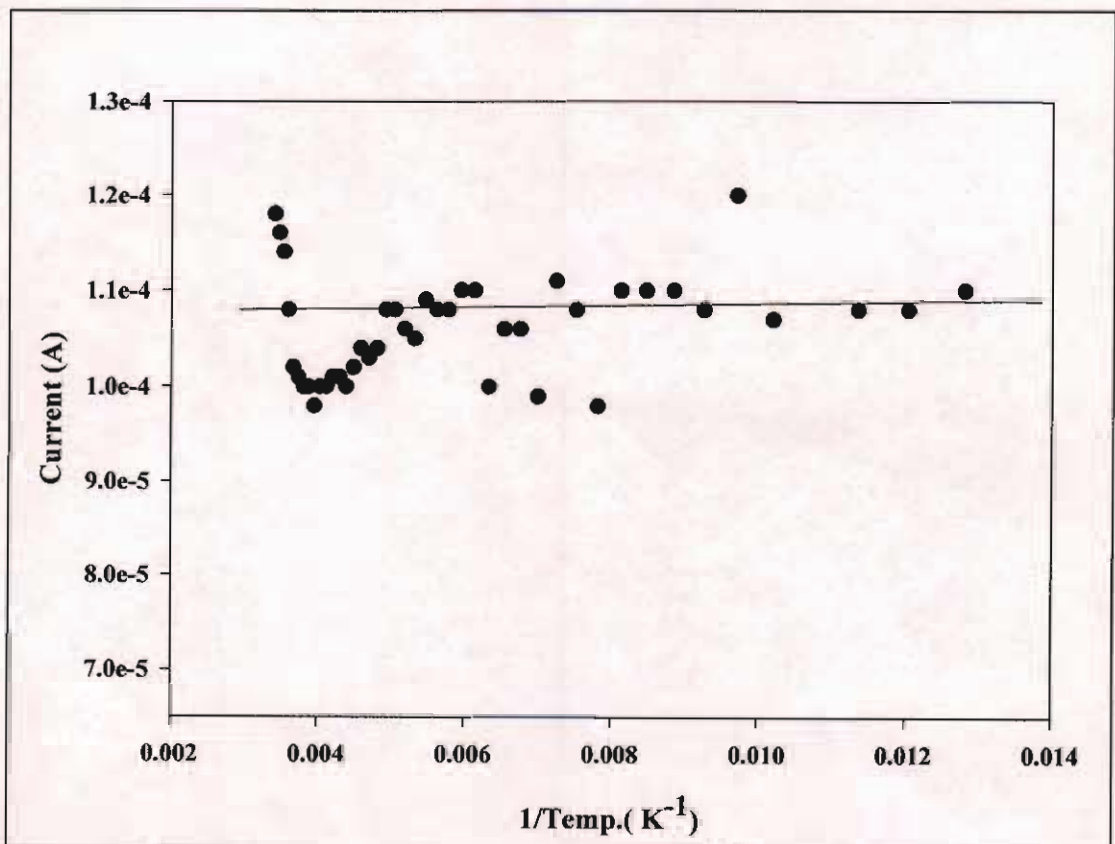


**Figure 6.4.** Temperature dependence of low conductivity of Annealed $C_{60}$ Film. Voltage held at 1V while decreasing temperature from 293K to 78K

Figure 6.4 shows the results of the temperature dependence study of the annealed film. The insulating characteristic of a decrease in current with a decrease in

temperature does not seem to be the case in this situation. Although the current changes abruptly as it goes through the phase transition temperature, it seems to remain approximately constant down to 78K. Such a temperature independence of conductivity may be characteristic of a metallic like behaviour and an insulator to metal transition is inferred to have happened.

## 6.8. Summary

In this chapter the transport mechanisms of organic molecular semiconductors were investigated and in particular the transport processes in solid $C_{60}$. The various types of solids were described, highlighting $C_{60}$ as being a molecular solid. The covalent bonds within the molecules are distinctly stronger than the intermolecular binding and hence the constituents preserve their molecular character. Transport in fullerenes has been shown to be largely dominated by intermolecular hopping processes. Temperature dependence studies have shown the transport process to be thermally activated, characteristic of a molecular insulator or semiconductor. The transition temperature seems to have a strong influence on this hopping process and thermally annealing the films increases the conductivity of the films to a more metallic like state. Further investigation is necessary into the transport processes of electrically or optically induced excited states.

## 6.9. References

1     M. Kaiser, M.K. Maser, H.J. Byrne, A. Mittelbach and S. Roth, *Solid State Commun.*, **87**, 281, (1993)

2     R.C. Haddon, A.F. Hebard, M.J.Rosseinsky, D.W. Murphy and S.J. Duclos, *Nature*, **350**, 320-322 (1991)

3     A.F. Hebard, M.J. Rosseinsky, R.C. Haddon, D.W. Murphy, S.H. Glarum, T.T.M. Palstra, A.P. Ramirez and A.R. Kortan, *Nature*, **350**, 600-601 (1991).

4     R. Eisberg, R. Resnick, *Quantum Physics of atoms, molecules, solids, nuclei and particles*, 2nd Edition, John Wiley and Sons, New York. (1985)

5     B.K. Tanner, *Introduction to the physics of Electrons in Solids*, Cambridge University Press (1995)

6     C. Kittel, *Introduction to Solid State Physics*, 5th Edition, John Wiley and Sons, New York (1976)

7    J.R. Christman, *'Fundamentals of Solid State Physics'*, Wiley Europe Publishers (1988)

8    M. Kaiser, W.K. Maser, H.J. Byrne, A. Mittelbach and S. Roth, *Solid State Commun.*, **87**, 281 (1993)

9    P.H.M. van Loosdrecht, P.J.M. van Bentum, M. Verheijen and G. Meijer, *Chem. Phys. Lett.*, **198**, 587 (1992)

# Chapter 7

## Insulator to Metal Transitions

### 7.1. Insulator to Metal Transitions in Fullerenes.

Much of the interesting physics of the conducting and superconducting states of fullerenes arises from the population of the lowest unoccupied molecular orbital (LUMO), by electron transfer from dopant metals [1]. In the solid state, 100% single population of the LUMO, (of figure 2.3), results in the formation of a metallic -like state [2]. Such a population is also obtainable without doping via optical excitation or by electron injection [3]. When produced by electron injection a broad intense luminescence is produced with the additional interest that the current characteristics of the material became highly non-linear [4]. Similarly when the population of the state is obtained by optical excitation from the ground state, the metastable metallic state is highly luminescent and non-linear, with an apparent threshold behaviour [5].

The transport properties of the system under illumination [5] showed that at low intensities the photoconductive response of fullerene crystals has a square root dependence, (figure 7.1), and the temperature dependence (figure 7.2) shows the transport process to be thermally activated, as in the case for the conductivity measurements in chapter 6, characteristic of a molecular insulator or semiconductor [5,6]. In figure 7.1, above approximately $100Wcm^{-1}$ the photocurrent becomes cubicly dependent on the input intensity.

The increase in photoconductive response is indicative of a significant change in the characteristics of the transport processes. Measurement of these changes was performed by sweeping the temperature and monitoring the high and low intensity response at each temperature, figure 7.2, [5]. Whereas the low intensity the photoconductive response decreases by three orders of magnitude over the temperature range measured, the high intensity response remains constant within an order of magnitude below the transition temperature. Such a temperature independence of the conductivity may be characteristic of a metallic-like behaviour and a Mott-like insulator to metal transition is inferred. This high intensity state is characterised by a Raman signature of the pentagonal pinch mode of $1463cm^{-1}$ as discussed in chapter 5.

The non-linear behaviour of the transport properties of $C_{60}$ under high intensity illumination is indicative of a transition between a phase which is dominated by molecular processes at low intensities, to one which is more metallic in nature at high excitation densities [5]. The onset of the cubic dependence of the photoconductive response is consistent with an increased delocalisation of the $\pi$-electrons between the balls [7], consistent with a Mott- transition. These effects exhibited by fullerenes under high intensity illumination point towards a departure from the molecular like behaviour of the weakly excited state through the influence of the interaction of molecules in the excited state, where these insulator to metal transitions are reversible.
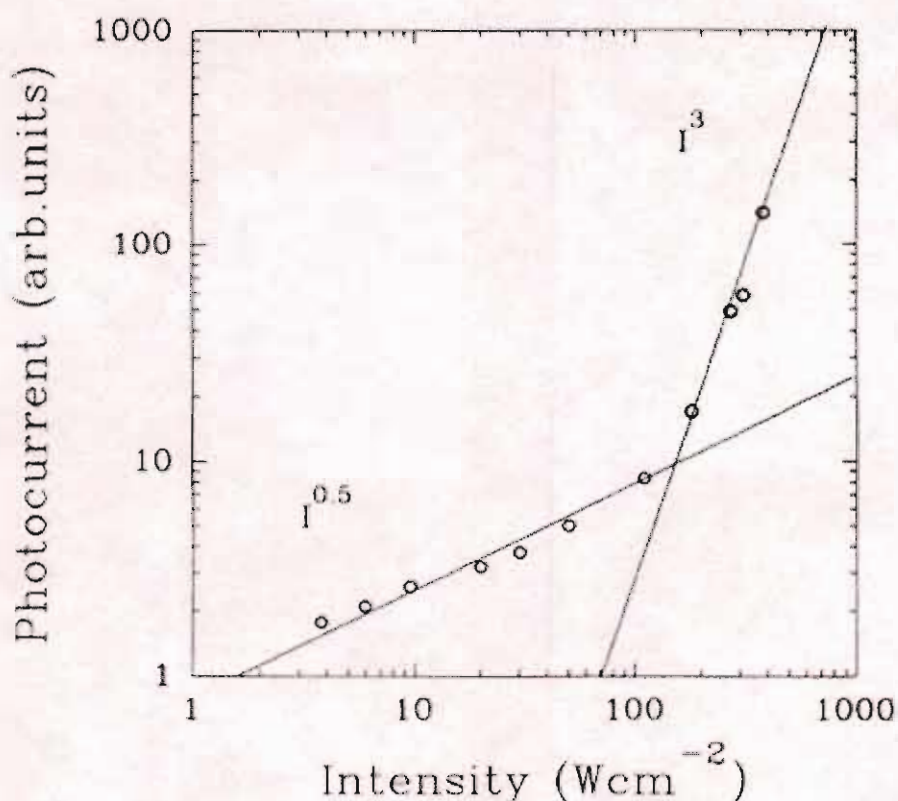


**Figure 7.1.** Intensity dependence of the photocurrent in fullerene crystal in the region of the intensity threshold associated with the onset of nonlinear luminescence [5].

Electrically induced transitions from insulator to metal to superconductor in single crystals of $C_{60}$ have also been demonstrated [8,9]. In this chapter it will be investigated whether equivalent states can be produced by charge injection in thin films. Characterisation of these insulator to metal transitions will be attempted spectroscopically with comparisons made to the already well characterised optically induced excited species.
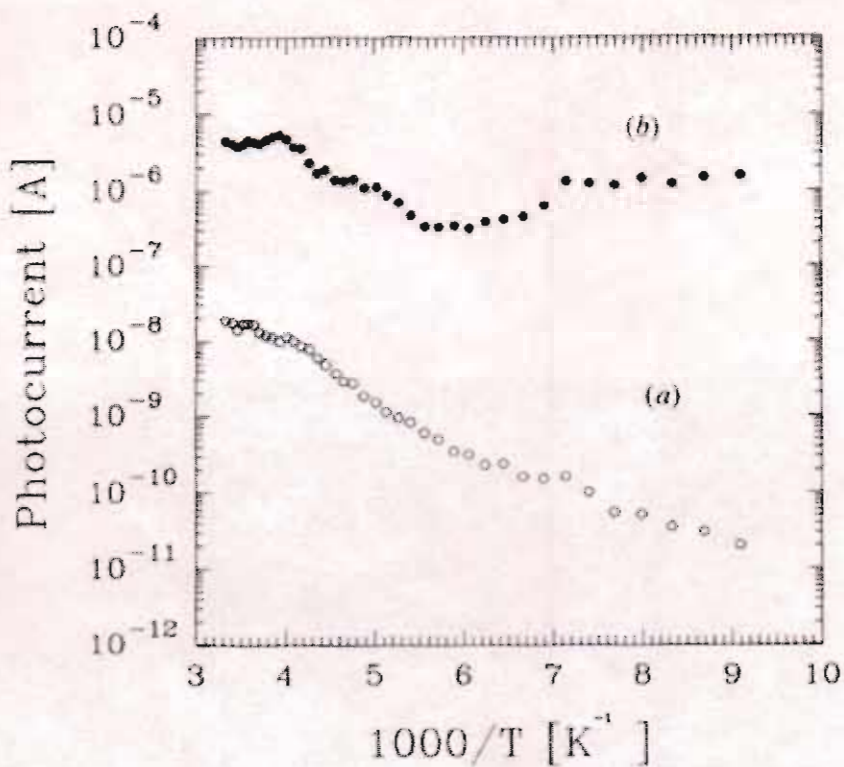
**Figure 7.2.** Temperature dependence of the photoconductive response (a) low illumination conditions, (b) high illumination conditions [5].

## 7.2. Current Voltage Characterisation of Pristine $C_{60}$ Films at room temperature.

Conductivity measurements at room temperature and low voltages (<6V), on undoped $C_{60}$ films show initially, the sample to be weakly conducting, as discussed in chapter 6. As the voltage was increased in the positive direction with respect to the aluminium electrode there was a sharp increase in current, at approximately 9.5V. Further increases in voltage result in little or no change in current until about 10.5V where there is a sharp reduction in current observed. As the voltage was increased the characteristics were seen to be irreversible indicating a structural or chemical change in the material. However reversal of the polarity results in similar sharp features, after which the positive bias characteristics can be reproduced. The relative instability of the highly conducting species observed in Figure 7.3 may be similar to the lattice collapse reported by Smie and Heinze [10], for the electrochemical reduction of $C_{60}$ films. Solid state cyclic voltammetery measurements were combined with both in situ conductivity and ESR measurement. In their study they found that the onset of the first reduction peak coincided with a strong increase in conductivity although at the

point of maximum reduction, the conductivity values were substantially reduced. This reduction in conductivity was attributed to structural rearrangements due to cationic inclusion into the lattice, and was also strongly supported by the peak ESR signal, which corresponded to the peak in the conductivity rather than in the voltammogram. ESR indicates 50% charging at collapse.
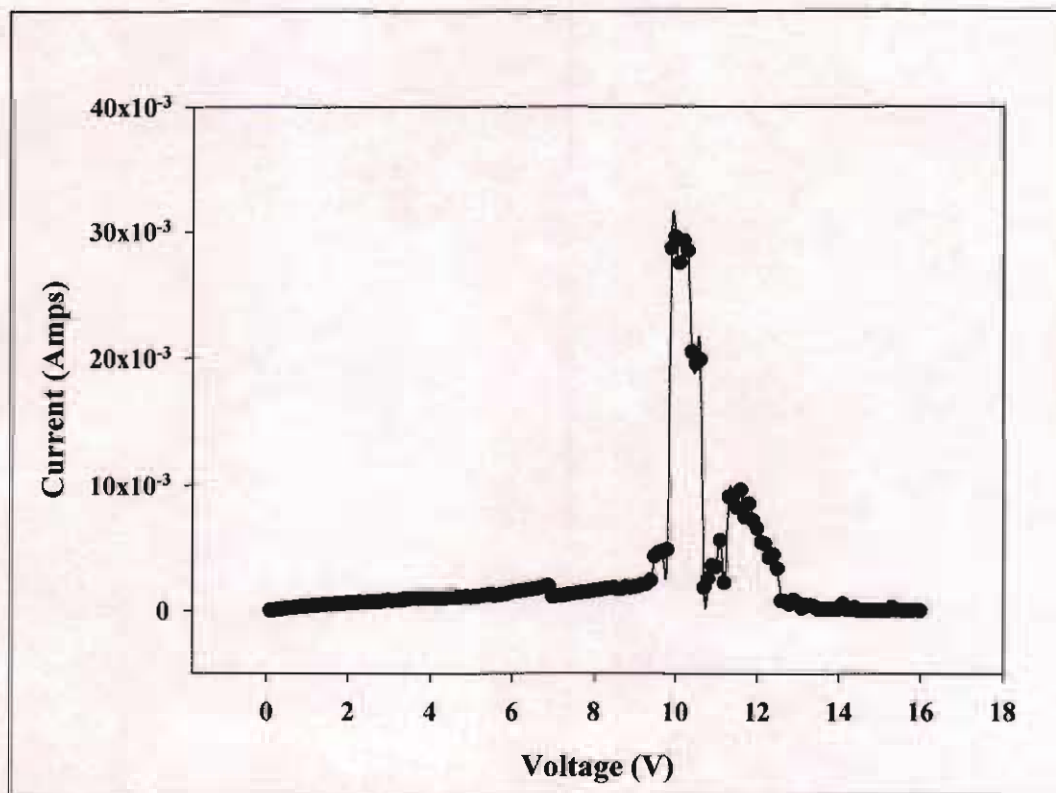


**Figure 7.3.** Current-Voltage characteristics observed for Pristine ITO/$C_{60}$/Al structure at 300K

In Figure 7.3 a similar process can be seen where at a well-defined voltage a sharp increase in the conductance results. The relative stability for this highly conducting species may be due to the absence of any charge balancing cation in the sandwich type structure. However further increasing the voltage results in a sharp reduction with a second maximum. The cyclic voltammagram reported by Smie and Heinze also displays a second reduction maximum [10], which was attributed to the formation of dimeric dianions. The presence of a second maximum in Figure 7.3 may thus suggest that the $C_{60}$ lattice is unstable to the addition of electrons and can collapse to a polymeric-like species with or without the presence of charge balancing cations

Similar conductivity measurements of $C_{60}$ films at room temperature have been demonstrated in past studies [11]. Comparison of these measurements show similar behaviour to those shown in this study. Previous studies again show that as the voltage is increased in the positive direction with respect to the aluminium electrode, there is a sharp increase in current. It was noted that the current increase in previous studies reached only $\mu$A, compared to currents of mA in this study, which may be due to different sample thickness. Again with further increasing of voltage, a sharp reduction in current was observed with a second maximum, showing the relative instability of the conducting species and the absolute values of these maxima seem to be in good agreement with this study.

## 7.3. Current Voltage Characterisation of Annealed $C_{60}$ Films at room temperature
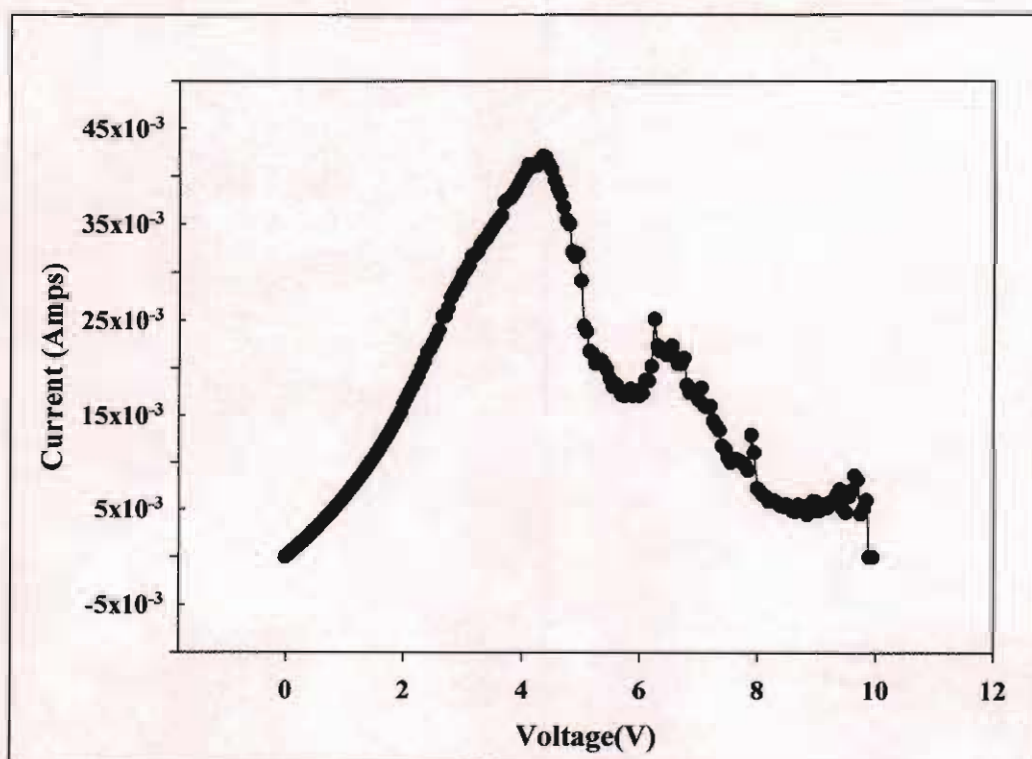


**Figure 7.4.** Current- voltage characteristics observed for annealed ITO/$C_{60}$/Al structure at 300K.

Measurement of the current-voltage characteristics were repeated at room temperature for annealed films, figure 7.4. Comparison of these results to that of the pristine film show similar behaviour. It was shown that the voltage increased in the positive direction with respect to the aluminium electrode, again with a sharp increase in

current. However differences are seen in the low voltage regions of the two graphs. In figure 7.3 at low voltages the sample is seen to be weakly conducting, and in figure 7.4 this behaviour is not seen with an immediate increase in current. The temperature dependence study completed in chapter 6 discussed this difference. It was shown that the temperature independence of the conductivity in the annealed films was characteristic of a "metallic like" behaviour. Due to thermal annealing during the production of the film an insulator to metal transition occurred, accounting for the insulating state not been observed during the IV characterisation of the annealed films.

In both films a high conducting state is generated. From results presented in figures 7.3 and 7.4 it appears that this state occurs at lower voltages in annealed films because a higher critical current density is achieved at lower voltages in more conductive annealed films. Once this high conductive state is reached, then both forms of films behave in the same way. It appears therefore that the principle effect of annealing is ease of achieving this high conducting state. The collapse of the IV and the stabilisation of this high conducting state is discussed in the following sections.

## 7.4.    In –situ Raman at Room Temperature

In order to identify the different states produced during electronic injection of these annealed $C_{60}$ films in-situ Raman spectroscopy was taken at a range of voltages at room temperature. In the low voltage region of figure 7.4 the well-characterised pentagonal pinch mode at 1469cm$^{-1}$ was identified, figure 7.5(a). In the high voltage region of figure 7.4 after the lattice collapse, in-situ Raman spectroscopy shows two additional peaks present, figure 7.5(b). The first additional peak has a Raman position analogous to that reported for the $C_{60}$ photo-polymer [12] at 1458cm$^{-1}$, discussed in chapter 5. Indeed $C_{60}$ is known to form a polymer electrically [10]. The second feature at 1452cm$^{-1}$ has in the past been associated with polymer chain branching [13].
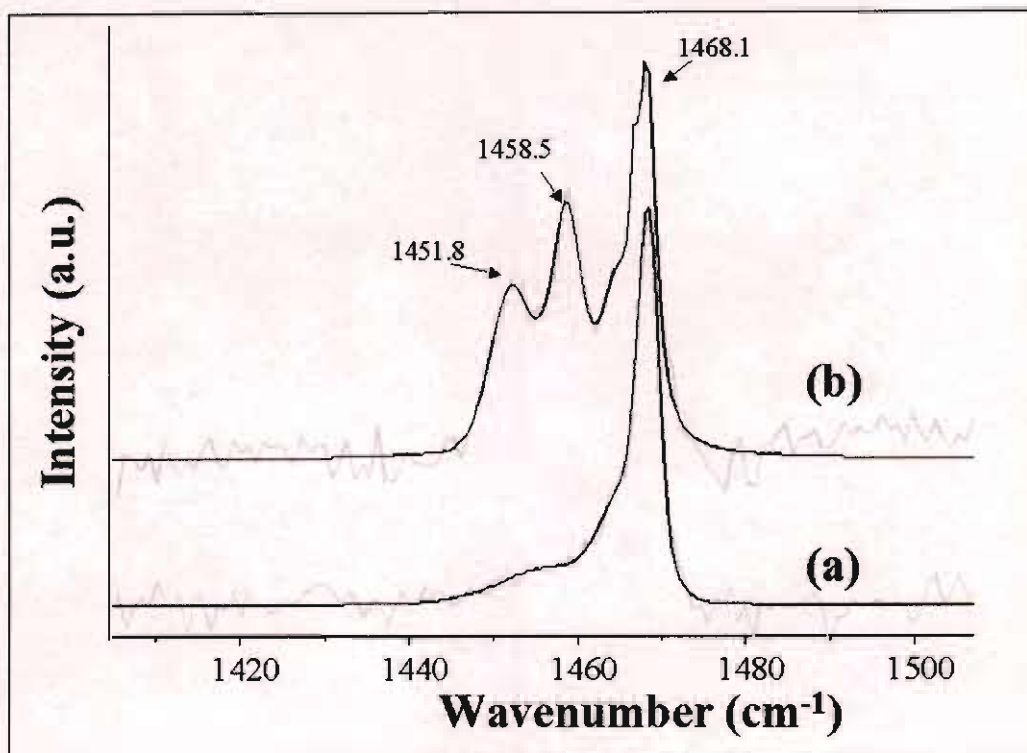
**Figure 7.5.** Raman Spectra of $C_{60}$ film showing the pentagonal pinch mode at 1469cm$^{-1}$ and after breakdown of the excited state showing two new peaks at 1458cm$^{-1}$ and 1452cm$^{-1}$. The Raman signature returns to the 1469cm$^{-1}$ position after electroluminescence.

## 7.5. Electroluminescence at Room Temperature



**Figure 7.6.** Contacted $C_{60}$ Film in Linkam Cooling Stage, before and during Electroluminescence

At high voltages (~6V) the film is seen to emit sporadic white flashes at randomly localized points on the surface. Figure 7.6 shows frames from a video showing this observation. This white light emission can be associated with the electroluminescence previously reported in $C_{60}$ crystals [14]. It was noted after the white light emission that the surface electrode interface had deteriorated considerably, as shown in Figure 7.7.

As aforementioned at room temperatures, Raman spectra recorded in the low voltage region of IV curve, figure 7.4, shows the characteristic pentagonal pinch mode of $C_{60}$ at $1469cm^{-1}$, figure 7.5(a). In the dark regions of figure 7.7(b), produced after prolonged time at high voltages, this mode is also present suggesting the material centered in these regions is pristine $C_{60}$. On the other hand the smooth region shown in figure 7.7(b), has a Raman signature the same as that of Figure 7.5(b) where the polymer peak at $1458cm^{-1}$ is present.



(a)                                        (b)
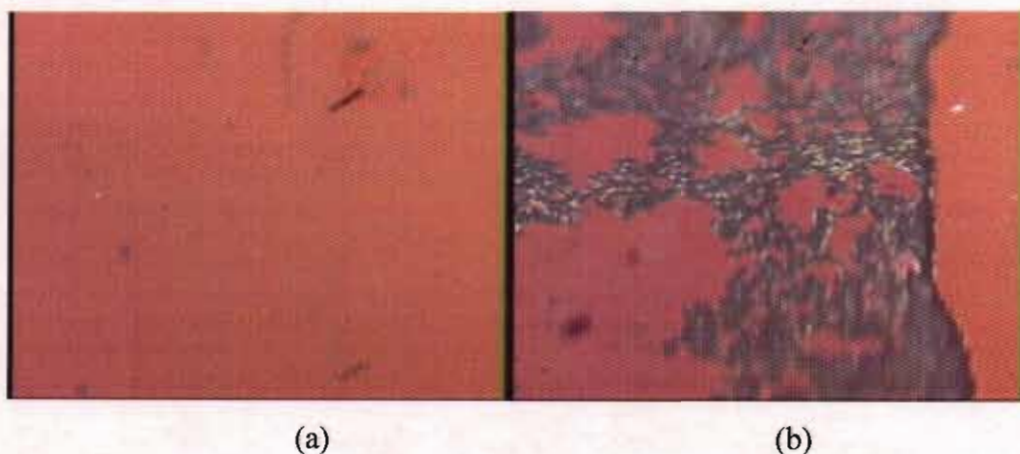
**Figure 7.7.** Images of $C_{60}$ films (a) before electronic injection and (b) after electroluminescence.

Photochemically the polymer is formed by prolonged illumination. However, high intensity illumination is known to reverse this process [15]. It is proposed here that a similar reversible polymerisation can occur electrically. That is, the reduction of current above ~5V is due to the lattice collapsing to a polymer phase which compensates for charge induction and the observed white emission is due to local high current densities producing a state equivalent to a high current state which can restore the collapsed lattice to its pristine structure.

## 7.6. Current Voltage Characterisation of $C_{60}$ Films at Low temperatures.

The polymerisation of $C_{60}$ has been extensively studied [15,16], and the molecular dynamics and photochemical properties of $C_{60}$ are seen to be strongly temperature dependent, due mainly to the orientational phase transition at 249K. The molecular triplet state at $1466cm^{-1}$ is not observed at room temperature due to the formation of the polymer. Below this temperature the lattice is frozen and structural modification is inhibited [17]. As a result the experiment was repeated at low temperature (20K) in order to prevent this lattice collapse.
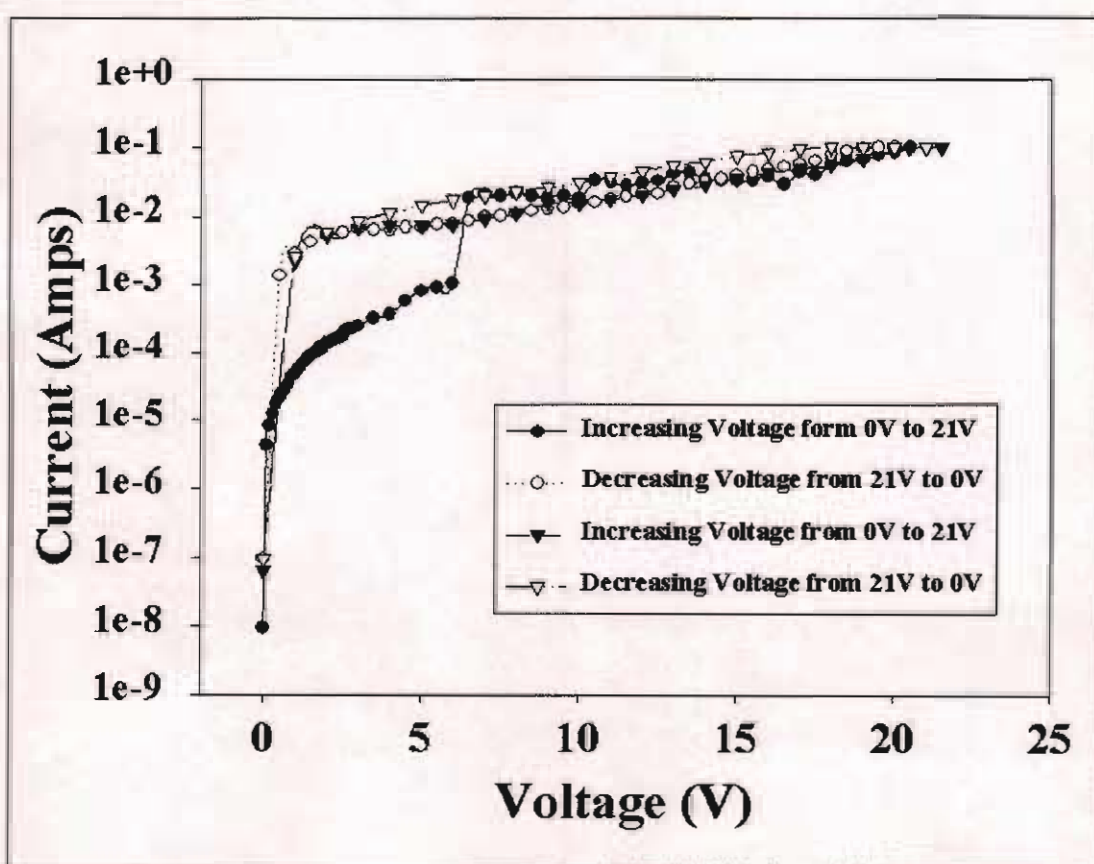


**Figure 7.8.** Current voltage characteristics observed for ITO/$C_{60}$/Al sandwich structure at 30K

Figure 7.8 shows results of the I-V characteristics of the $C_{60}$ films at low temperatures. Note that the current is plotted logarithmically. As in the case at room temperature, increasing the voltage results in a dramatic increase in the current. However, whereas at room temperature further increases in voltage results in a substantial drop in conductance, at low temperatures the current continues to increase,

suggesting that the polymerisation process is inhibited. Reduction of the voltage reproduces the initial curve until a certain point were it does not revert to its initial low conductance but continues to decrease linearly. This current is stable for long periods and the curve is reproducible *ad infinitum*. Further reduction results in an abrupt switch to low current, while increasing the voltage again rapidly increases the current. This process is completely cycleable and reproducible.

Similar results of these conductivity measurements at low temperatures have previously been reported [11], and it was seen again that while increasing voltage the current was seen to increase dramatically without the substantial drop in conductance at high voltages, confirming that the polymerisation process is inhibited.

## 7.7. Raman Spectroscopy at Low temperatures
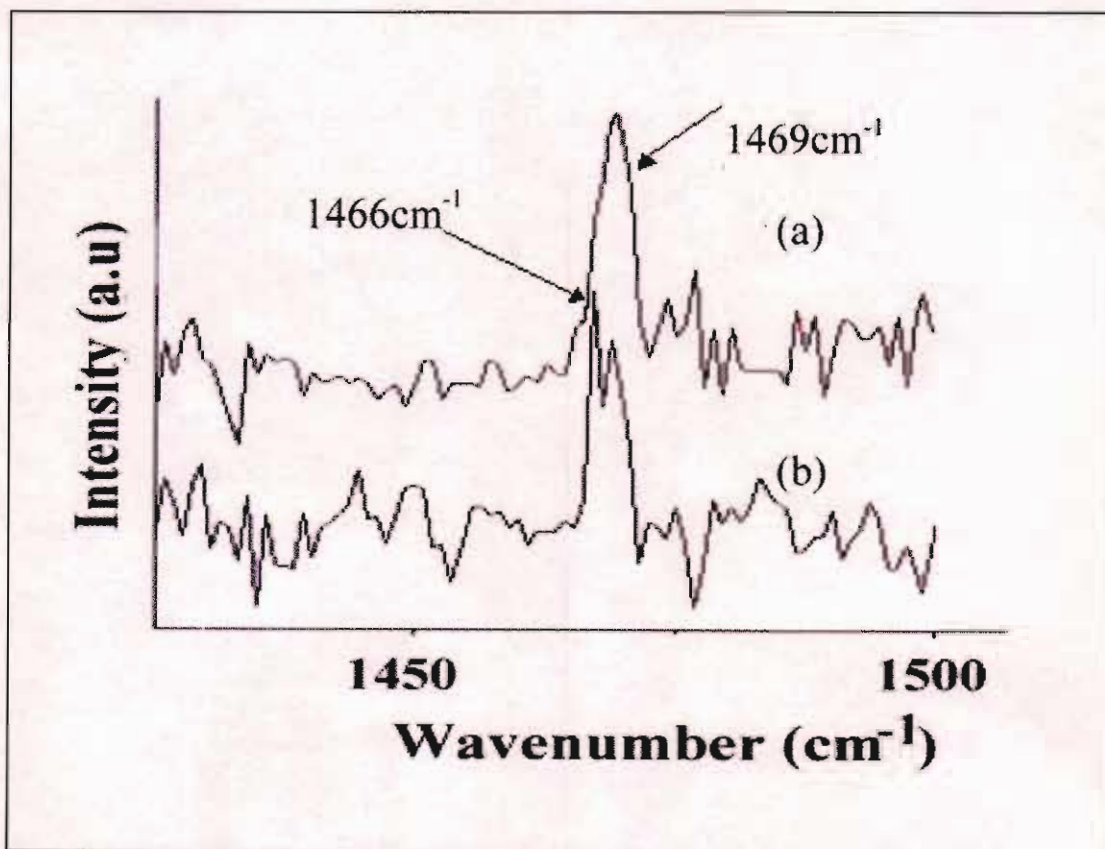


**Figure 7.9.** Raman Spectra of $C_{60}$ film at low temperatures (77K) showing (a) the characteristic pentagonal pinch mode of pristine $C_{60}$ at1469cm$^{-1}$ and (b) an additional peak emerging at 1466cm$^{-1}$ at 3V, analogous to the molecular excited triplet state.

The conduction process in these polycrystalline thin films appears not to be uniform through the film, increasing the difficulty in capturing the spectroscopic signature of

these highly conducting states. However Raman spectra recorded at low temperatures showed the observation of the triplet excited state at $1466cm^{-1}$ beginning to emerge. Spectra recorded at low temperatures are shown in figure 7.9. In the low voltage region of figure 7.8 the Raman shows as with room temperature the characteristic pentagonal pinch mode at $1469cm^{-1}$, Figure 7.9(a). This mode is present until approximately 3V, at this voltage there is a sudden increase in current and the Raman shows the appearance of an additional peak at $1466cm^{-1}$ emerging. This additional peak has a Raman position analogous to that reported for the photo induced molecular triplet excited state in $C_{60}$ thin films [18], suggesting that this state can be produced electrically as well. The Raman signal was extremely noisy, and an improved signal would need to be obtained to prove it is the molecular excited triplet state conclusively.

## 7.8. Electroluminescence at Low Temperatures

In some films, as at room temperatures, the application of high voltages showed electroluminescence. Images of the electrode interface before and after electroluminescence at these low temperatures again show marked deterioration similar to that shown in figure 7.7(b). Raman spectroscopy of the deteriorated regions exhibits the characteristic pentagonal pinch mode of $1469cm^{-1}$ but notably, the smooth regions also show the characteristics of the pristine material. This suggests that there is no collapse of the lattice structure, and that the deterioration shown in Figure 7.7(b) may be due to high local densities in the $C_{60}$ film, causing the actually damage to the top aluminium electrode and not to the $C_{60}$ film itself.

Nonlinear conductivity and electroluminescence have previously been reported in fullerene crystals [14]. The spectrum of the emission is broad and evolves nonlinearly and although it does not match with the molecular energy it matches the nonlinear photoluminescence in fullerene crystals [19], which has been attributed to an optically induced insulator to metal transition in the highly excited state. The nonlinear conductivity measurements at low temperatures are consistent with an insulator to metal transition by electron injection. That it does not occur at room temperature is consistent with the instability of the fullerene lattice to charge injection [10]. In polycrystalline thin films, it would appear that this conduction process is sporadic

through the film and the challenge remains to improve the crystallinity of fullerene films such that the high conducting state can be spectroscopically characterised.

## 7.9. Summary

Carriers injected into molecular like states hop through the crystal lattice under the influence of the field. However at high excitation densities, as a result of optical pumping, chemical doping or electrical pumping, there is seen to be a dramatic non-linear phenomena which has been associated with a Mott-like transition. Under high intensity illumination, both the optical and electronic properties of the solid state of fullerenes undergo non-linear changes. The temperature independence of the photoconductive response clearly indicates these changes are due to a metallic like phase at high excitation densities. The results shown here demonstrate that similar effects are observable through electron injection.

1.Noninteracting Ground State

2.One of the molecules has an electron promoted from the $\pi$ to the $\pi*$ i.e. it is in an excited state

Electronic injection

Relaxation

Low Temp.

No collapse

Electronic injection

$1469cm^{-1}$

$1469cm^{-1}$?

$1466cm^{-1}$

$1459cm^{-1}$

4.Polymerisation reversed via this hich current density metastable intermediate

3.Formation of the polymer via the overlap of the $\pi$ orbital and the $\pi*$ orbital hance the 2+2 cycloaddition is completed

**Figure 7.10.** Summary of Electronically produced states in $C_{60}$ thin films and their Raman Modes. Blue and Red arrows denote the path possible below and above the phase transition temperature (249K) respectively. Multicolored arrows denote that the path is possible at both temperatures.

Figure 7.10 summarises the main details of this chapter. It has been shown that $C_{60}$ films can undergo a reversible and cycleable transition to a highly conducting state that can be readily produced by the application of a moderate voltage at low temperatures. The observed Raman spectroscopy has been proven to be a valuable probe in identifying the electronic processes at a molecular level and should help elucidate the true nature of these conducting species. It clearly demonstrated that the reduction in sample conductivity at room temperature is material in origin, suggesting the formation of a polymeric phase. It has also shown that prolonged high voltages restored the film to its pristine structure, analogous to the photopolymer being reversed by high illumination. The conduction process in these thin films is sporadic in nature and if it was possible to record the Raman signature of the high current electroluminescent state it is believed that the pentagonal pinch mode would be situated at $1463 cm^{-1}$, analogous to the photoinduced excited state discussed in chapter 5.

## 7.10. References

1. R.M. Fleming, A.P. Ramirez, M.J. Rosseinsky, D.W. Murphy, R.C. Haddon, *Nature*, **352**, 787 (1991)

2. R.C. Haddon, A.F. Hebard, M.J.Rosseinsky, D.W. Murphy and S.J. Duclos, *Nature*, **350**, 320-322 (1991)

3. R.C. Haddon, L.E. Brus and K. Kaghavachari, *Chem. Phys. Lett.*, **125**, 459 (1986).

4. A.T. Werner, H.J. Byrne, D. O'Brien and S. Roth, *J. Mol. Crys. Liq. Crys.*, **256**, 795 (1994)

5. H.J. Byrne, A.T. Werner, J. Anders, W.K. Maser, M. Kaiser, L. Akselrod, W.W Rühle, A. Mittelbach J. Anders, X.Q. Zhou, G. Mahler, T. Kuhn and S. Roth, *Appl. Phys. A.*, **597**, 303 (1993).

6. J. Kaiser, J. Reichenbach, H.J. Byrne, J. Anders, W. Maser, S. Roth, A. Zahab and P. Bernier, *Solid-St Commun.*, **81**, 261 (1992).

7. H. Yonehara and C. Pac., *Appl. Phys. Lett.*, **61**, 575 (1992).

8. J.H. Schön, Ch. Kloc and B. Batlogg, *Nature*, **408**, 549-552 (2000)

9. J.H. Schön, Ch. Kloc and B. Batlogg, *Science*, **293**, 2432-2434 (2001)

10. A. Smie and J. Heinze, *Physics and Chemistry of Fullerenes and Derivatives*, World Scientific Singapore (1995)

11.     G. Chambers and H.J. Byrne, *Mol. Materials*, **13**, 193-200 (2000).

12.     H. Kuzmany, M. Matus, T. Picher and J. Winter, *Physics and Chemistry of the Fullerenes,* K. Prassides ed., **443**, 287-309, Kluwer Academic, Dordrecht. (1994)

13.     T. Wågberg, P. Jacobsson, B. Sundqvist, *Phy. Rev. B.*, **60**, 4535. (1999)

14.     A.T. Werner, J. Anders, H.J. Byrne, W.K. Maser, M. Kaiser, A. Mittelbach and S. Roth. *Appl. Phys. A,* **57**, 157 (1992)

15.     L. Akselrod, H.J. Byrne. *Chem. Phys. Lett.*, **215**, 131. (1993)

16.     G. Chambers and H.J Byrne , *Chem. Phys. Lett.*, **302**, 307. (1999)

17.     M.S. Dresselhaus, G. Dresselhaus and P.C. Eklund. *Science of Fullerenes and Carbon Nanotubes.* Academic Press, London (1996)

18.     G.Chambers, A.B. Dalton, L.M.Evans, H.J. Byrne. *Chem. Phys. Lett.,* **345**, 361-366 (2001)

19.     H.J. Byrne W.K.Maser, M. Kaiser, W.W. Rühle, L. Akselrod, A.t. Werner, J. Anders, X.-Q. Zhou, G. Mahler, T. Kuhn, A Mittelbach and S. Roth, *Appl. Phys. A,* **57**, 303 (1993).

# Chapter 8

## Conclusions

### 8.1. Introduction

Most studies have concentrated on the non-linear behaviour observed in single $C_{60}$ crystals. However such crystals do not easily lend themselves to in situ characterisation. This study has been devoted to reproducing this behaviour in thin film form. This project has centred on examining transitions from insulating to metallic states in Fullerene thin film structures in a sandwich type geometry. It was shown that $C_{60}$ films undergo a reversible and cycleable transistion from insulating to a highly conducting state induced by charge injection. The states produced where monitored as a function of electrical parameters and spectroscopic signatures and were compared to the documented signatures of chemically and optically induced states. Non-linear evolution of the Raman spectrum of thin films has been observed and current–voltage characteristics indicating an abrupt insulator to metal transition have been observed in thin film sandwich structures, indicating that the phenomenon is not exclusive to single crystals.

### 8.1. General Conclusions

$C_{60}$ is a closed caged carbon molecule that is highly symmetrical, with an icosahedral point group $I_h$ [1]. The sixty carbon atoms are arranged at the vertices of twenty hexagonal and twelve pentagonal rings. Each carbon molecule is in a $sp^2$ hybridised bonding arrangement, which gives rise to sixty delocalised $\pi$ electrons and it is these electrons that are of particular interest when considering the electronic and optical properties of $C_{60}$. Of particular interest is the degree of intermolecular interaction in the solid state, basically how do these molecules communicate with each other.

In the solid state the molecules spin freely around their lattice positions, but this rotation is frozen out at temperatures below 249K and the molecules that had been in the fcc arrangement change to that of a sc arrangement [2]. This complicating factor has effects on the optical and electronic properties.

Vibrational spectroscopy reveals that $C_{60}$ mostly retains its molecular character in the solid state [2], confirming the importance of the icosahedral symmetry. Electronic spectroscopy reveals features that are specific to the solid state [3]. Intermolecular charge transfer excitons is an important process in fullerene solids showing the first indication of an intermolecular interaction. Spectroscopic analysis of annealed films leads to the conclusion that a structural reordering of the $C_{60}$ lattice has occurred [4,5,6].

Raman spectroscopy has been proven to be a valuable probe in identifying optically induced excited states. The Raman signature of the molecular triplet state of $C_{60}$ in both the solution and solid state has been assigned to the positioning of the pentagonal pinch mode at $1466 cm^{-1}$ [7,8,9]. $C_{60}$ is stable under ambient conditions however when it is exposed to high intensity illumination above 149K it can form a number of polymeric states [10]. These polymeric states have been suggested to form via a 2+2 cycloaddition reaction, whereby the $\pi$ bonds of adjacent molecules open to form a covalent coupling between the molecules at room temperature. Illumination with high intensities can reverse the polymerisation back to its pristine form via a high intensity metastable intermediate [11]. This second excited species has been identified is specific to the solid, and been assigned with the Raman signature of $1463 cm^{-1}$ [9]. This state occurs indirectly during depolymerisation of $C_{60}$ at high intensities or directly at low temperatures and high intensities.

Comparable studies show that these photoinduced excited states can be achieved by other means. Chemically by intersistal doping [12,2,13] where Raman spectroscopy showed the pentagonal pinch mode shifting down by $6 cm^{-1}$ per dopent molecule. Electronically induced transitions were demonstrated in $C_{60}$ crystals [14,15]. These electronically induced states where attempted to be produced in $C_{60}$ thin films and compared to well characterised optically induced states.

To do this thin films of $C_{60}$ were prepared in a sandwich type geometry with indium tin oxide (ITO) as the bottom electrode and aluminium as the top electrode. Current-Voltage characterisation was carried out firstly at room temperature, which showed that as the voltage is increased there was a sharp increase in current. Further increases in voltage

result in a sharp reduction in current. These characteristics were seen to be irreversible by increased voltage indicating a structural or chemical change in the material. Upon examination of the temperature dependence of the sample conductance it was observed that the films did not show true thermally activated transport, characteristic of a molecular insulator, but rather one of a partially annealed material. It is proposed that this process can occur during the deposition procedure. It is a controllable factor and the effects of the heat treatment can be varied independently and systematically during the film deposition procedure.

In situ Raman spectroscopy demonstrated that the reduction in sample conductivity at room temperature is material in origin suggesting the formation of a polymer. This is the first time that the polymer has been formed electronically and spectroscopically characterised in $C_{60}$ thin films. At high voltages the film is seen to emit sporadic white flashes at randomly localised points on the surface, and this can be associated with the electroluminescence previously reported in $C_{60}$ crystals [16]. It was shown spectroscopically that prolonged high voltages restored the film from the electronically induced polymer to its pristine form structure, analogous to the photoploymer being reversed by high illumination [17].

At low temperatures, as in the case of the room temperature results, as the voltage was increased there was a dramatic increase in the current. However there is no drop in conductance at further increased voltages suggesting that the polymerisation process is inhibited at low temperatures. Raman spectroscopy also backs up this statement with spectroscopic evidence to show there is no collapse in the lattice structure. Again, as with the room temperature studies, the application of high voltages showed electroluminescence, and this may be one sign of the highly excited state is been produced electrically. This is the first time electroluminescene has been observed in $C_{60}$ films. However the conduction process in these polycrystalline films appears not to be uniform throughout the film, increasing the difficulty of capturing the spectroscopic signatures of the highly conductive states. The crystallinity of the fullerene films needs to be improved as not to hinder the spectroscopic characterisation of these conducting species. It has been shown that thermal annealing [5,6] and solvent inclusion [18,19]

improve the crystallinity of $C_{60}$ films. It is suggested that some of these possibilities be investigated for future projects. Initially in this work it was shown that there was some evidence to suggest that annealing of the thin films shows improvement in its conductivity. The temperature dependence study in chapter 6 shows that through partial annealing during deposition the film switches form a insulating to a metallic like material, and with further systematic and quantitative studies may build on this knowledge to further improve on film preparation techniques. Hopefully this will enable the Raman signature of the electrically excited states to be identified by making the conduction process more uniform throughout the film.

## 8.3.    Overview

$C_{60}$ films undergo a reversible and cycleable transition to a highly conducting state. Reduction of sample conductivity at room temperature is due to formation of polymer. At low temperatures Raman evidence suggests that molecular triplet can be formed electrically as well as optically. Prolonged high voltages restore film to pristine structure via a high current density metastable intermediate which is high luminescent.

## 8.4.    References

1.    H.W. Kroto, J.R. Heath, S.C. O'Brien, R.F. Curl, and R.E. Smalley, *Nature* **318**, 162-163 (1985).

2.    H.Kuzmany, M.Matus, B. Burger, J. Winter, *Adv. Mater.* **10**, 731-745. **(1994)**

3.    S. Leach, M. Vervloet, A Després, E. Bréheret, J.P. Hare, T.J. Dennis, H.W. Kroto, R. Taylor and D.R.M. Walton, *Chem. Phys.,* **160**, 451 (1992)

4.    L. Akselrod, H.J. Byrne, T.E. Sutto and  S. Roth, *Chem .Phys. Lett.,* **233**, 436 (1995)

5.    M. Kaiser, W.K. Maser, H.J. Byrne, A. Mittelbach and S. Roth, *Solid State Commun.,* **87**, 281 (1993)

6.    G. Chambers, PhD dissertation, Dublin Institute of Technology. 2001

7.    G. Chambers, H.J. Byrne, *Chem. Phys. Lett.,* **302**, 307-311 (1999)

8.    P.H.M. van Loosdrecht, P.J.M van Bentum and G. Meijer, *Chem. Phys. Lett.,* **205**, 191, (1993)

9.	G. Chambers, A.B. Dalton, L.M. Evans, and H.J. Byrne, *Chem. Phys. Lett.*, **345**, 361-366 (2001)

10.	A.M. Rao, P. Zhou, K.A. Wang and P.C. Eklund, *Science*, **259**, 955, (1993).

11.	L. Akselrod, H.J. Byrne, *Chem.Phys. Lett.*, **302**, 307 (1993)

12.	R.C. Haddon, A.F. Hebard, M.J. Rosseinsky, D.W. Murphy, S.J. Duclos, *Nature*, **350**, 320-322 (1991)

13.	C. Kvarstrom, H. Neugebauer, G. Matt, H. Sitter, N.S. Sariciftci, *Synthetic Metals*, **103**, 2430 (1999)

14.	J.H. Schön, Ch. Kloc and B. Batlogg, *Nature*, **408**, 549-552 (2000)

15.	J.H. Schön, Ch. Kloc and B. Batlogg, *Science*, **293**, 2432-2434 (2001)

16.	A.T. Werner, J. Anders, H.J. Byrne, W.K. Maser, M. Kaiser, A. Mittelbach and S. Roth. *Appl. Phys. A*, **57**, 157 (1992)

17.	L. Akselrod, H.J. Byrne. *Chem. Phys. Lett.*, **215**, 131. (1993)

18.	M.S. Dresselhaus, P.C Eklund, *Science of Fullerenes and Carbon Nanotubes*, Academic press inc. (1995)

19.	A.M. Rao, P. Zhou, K.A. Wang and P.C. Eklund. *Science*, **259**, 955. (1993)

## Appendix 1

### Presentations and Journals

### Oral Presentations

- "In –Situ Raman Spectroscopy of Electronic Processes in Fullerene Thin Films" S.B. Phelan, G. Chambers, G. Farrell, B. O'Connell and H.J. Byrne, presented at The Materials Research Society (MRS) spring seminars, San Francisco, USA. April 2002.

### Poster Presentations

- "In –Situ Raman Spectroscopy of Electronic Processes in Fullerene Thin Films" S.B. Phelan, G. Chambers, G. Farrell, B. O'Connell and H.J. Byrne, FOCAS Conference, June 2002.

- "In situ spectroscopy of electronic processes in fullerene thin films",
  S.B. Phelan, G.F. Farrell, B.S. O'Connell, G. Chambers and H.J. Byrne,
  "Opto-Ireland 2002, Optics and Photonics Technologies and Applications", W.J. Blau, J.F. Donegan, A.F. Duke, B.D. MacCraith, J. A. McLaughlin, N.D. McMillan, G.M. O'Connor, E. O'Mongain and V. Toal eds., SPIE Proceedings Volume 4876, (2003) pp704.

- "Excited state properties of $C_{60}$ revisited :a Raman study", G. Chambers, S.B. Phelan, G. Farrell and H.J. Byrne, "Opto-Ireland 2002, Optics and Photonics Technologies and Applications", W.J. Blau, J.F. Donegan, A.F. Duke, B.D. MacCraith, J. A. McLaughlin, N.D. McMillan, G.M. O'Connor, E. O'Mongain and V. Toal eds., SPIE Proceedings Volume 4876, (2003), pp.732

### Journals

- "A Raman study of the Temperature Dependence of excited states in $C_{60}$ Thin Films.", G.Chambers, S.B. Phelan, and H.J. Byrne, Chem Phys Lett. (To be submitted 2004)

- "Nonlinear transport processes in Fullerene thin films", S.B. Phelan, G.Chambers and H.J. Byrne, Applied Physics A, (to be submitted 2004).

- "Photophysical and Photophysical properties of Fullerenes", G.Chambers, S.B. Phelan, G. Farrell and H.J. Byrne, invited review in "Recent Research Developments in Physical Chemistry" (to be submitted 2004).